JRC Scientific and Technical Reports

EU-PEMS PM EVALUATION PROGRAM - Second Report - Study on Post DPF PM/PN Emissions

A. Mamakos, M. Carriero, P. Bonnel,

H. Demircioglu, K. Douglas,

S. Alessandrini, F. Forni, F. Montigny, D. Lesueur

EUR 24793 EN - 2011

JRC
EUROPEAN COMMISSION

Institute for Energy

The mission of the JRC-IE is to provide support to Community policies related to both nuclear and non-nuclear energy in order to ensure sustainable, secure and efficient energy production, distribution and use.

European Commission
Joint Research Centre
Institute for Energy

Contact information
Pierre Bonnel, Massimo Carriero
Address: Joint Research Center, Via Enrico Fermi 2749, 21027 Ispra (VA), Italy
E-mail: pierre.bonnel@jrc.ec.europa.eu, massimo.carriero@jrc.ec.europa.eu
Tel.: +39 0332 785301, +39 0332 786354
Fax: +39 0332 785236

http://ie.jrc.ec.europa.eu/
http://www.jrc.ec.europa.eu/

Legal Notice
Neither the European Commission nor any person acting on behalf of the Commission is responsible for the use which might be made of this publication.

Europe Direct is a service to help you find answers
to your questions about the European Union

Freephone number (*):
00 800 6 7 8 9 10 11

(*) Certain mobile telephone operators do not allow access to 00 800 numbers or these calls may be billed.

A great deal of additional information on the European Union is available on the Internet.
It can be accessed through the Europa server http://europa.eu/

JRC 64214

EUR 24793 EN
ISBN 978-92-79-19931-8 (print)
ISBN 978-92-79-19932-5 (online)

ISSN 1018-5593 (print)
ISSN 1831-9424 (online)

doi:10.2788/95192

Luxembourg: Publications Office of the European Union

© European Union, 2011

Reproduction is authorised provided the source is acknowledged

Printed in Italy

TABLE OF CONTENTS

ACKNOWLEDGMENTS

The present work was conducted in co-operation with the experts of the companies as listed below. The European Commission expresses its gratefulness for their co-operation and the provision of the equipment used during this program.

MM. Les Hill, Daniel Scheder (HORIBA)

M. Cesare Bassoli, Daniele Testa (CONTROL SISTEM)

MM. Oliver Franken, Lauretta Rubino, David Booker (SENSORS EUROPE, SENSORS INC)

MM. Karl Obergugenberger, Wolfgang Schindler (AVL)

MM. Ville Niemela, Erkki Lamminen (DEKATI)

The authors would also like to gratefully acknowledge Carsten Gruening and Sebastiao Martin Dos Santos for providing the nebulizer and PSL samples used for the calibration of our DMA unit. We would also like to thank the following companies and persons for the supply of instruments/products and for the technical support provided:

- INEOS Oligomers for supplying us with Poly-alpha olefin employed in the calibration experiments
- Rosanna Passarella for providing purified and deionized water (Milli-Q) for the preparation of the PSL aqueous solutions.

1 INTRODUCTION

1.1 BACKGROUND

The present work was conducted in the frame of the EU-PEMS PM evaluation programme. The program was launched in 2008 by the European Commission to assess the potential of portable instruments to measure particulate emissions on-board of vehicles. The EU-PEMS program is a voluntary program, receiving contributions from the European Joint Research Center (JRC), some portable emissions equipment manufacturers (AVL, Dekati, Control Sistem, Horiba, Sensors Inc.) and the European association of heavy-duty engines manufacturers (ACEA).

The text of the call underlined the objectives of the program and defined the list of the basic technical requirements to be met by the instruments to be valid candidates.

The candidate instruments had to fulfil a few basic requirements:

- To measure the total PM mass over a long sampling period, either following the standard method or using a method proven to be equivalent to the standard method;
- To provide a second-by second (“real-time”) information on the emitted PM mass at any time during the test. This is a necessary pre-requisite for evaluating the data according to the moving average window (MAW) method (work or CO_2 based);
- To be ready for on-vehicle tests and in particular to include a solution to transport the raw or the diluted exhaust, to allow for an installation of the system within a few meters from the vehicle tailpipe.

Measurement principles that were not fully in line with the laboratory standard methods to measure PM mass were also accepted for evaluation, either with variations of the dilution method (e.g. constant dilution) or with alternative physical principles (e.g. measurement of the soot instead of total PM).

Upon the conclusions of the study, the main conclusions of the project were to recommend the candidate principle(s) and to discuss whether the corresponding technological progress of the instruments was sufficient to foresee a short term introduction in the legislation.

1.2 PREVIOUS FINDINGS AND OUTLINE OF THE PRESENT WORK

The figure below shows the different phases of the program, spread between 2009 and 2010 and how each phase of the evaluation has addressed different topics. The first phase main objective focused on the identification of instrumentation principles. Five in total candidate systems were evaluated on the Heavy Duty Engine (HDE) test bench of the Vehicle Emissions LAboratories (VELA) of the Joint Research Centre (JRC), using the exhaust of three HDEs. These included a 10 l Cursor Euro III engine equipped with an EMITEC Partial Flow Deep Bed Filter, a 10 l Man Euro V engine equipped with a Selective Catalytic Reduction (SCR) after-treatment system and a 15 l Cummins US07 engine equipped with an active regeneration Diesel Particulate Filter (DPF).

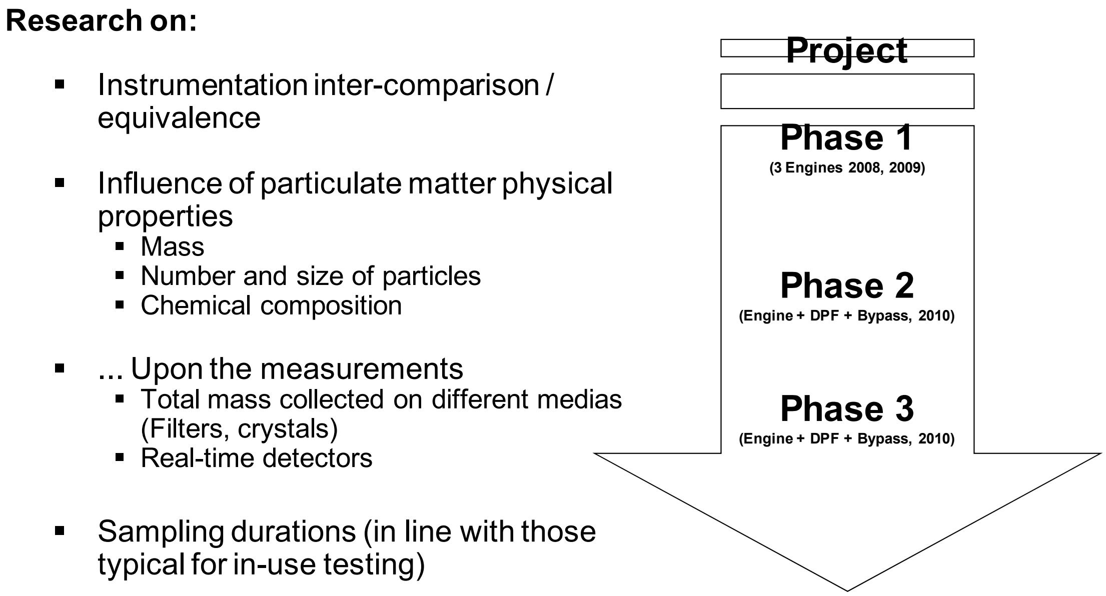

Figure 1: Evolution of the PEMS-PM programme

This experimental phase has now completed, with the final report published in 2010 (Bonnel et al. 2010) and extended data analyses published in the scientific literature (Rubino et al. 2009, Giechaskiel et al. 2011). The general conclusions are summarised below:

- Portable Proportional Partial Flow Sampling (PPFS) systems were found to comply with the laboratory requirements in terms of proportionality and temperature control of the dilution and sampling system.
- A good correlation was generally observed between the PM results obtained with the portable PPFS systems and the laboratory reference equipment. Relative larger inconsistencies were observed at post DPF levels however.
- Some of the real time sensors exhibited a satisfactory sensitivity, even at post-DPF levels, offering at the same time a sufficient level of information that would allow determination of PM mass accumulation rates.

Based on these findings, a reference measurement principle was proposed that should consist of:

- An exhaust PPFS and a filter mass based method, following the design and performance requirements applicable to laboratory equipment.
- A complementary real-time detector on diluted and temperature controlled exhaust, to estimate the PM mass accumulation rate.

It was agreed though that, alternative dilution approaches (i.e. constant dilution) and weighting methods (like Quart Crystal Microbalances - QCM and Tapered Element Oscillating Microbalances - TEOM) will also be accepted as long as they yield equivalent results.

However the study also identified some open issues that required additional investigation. The major concern was the observed deterioration in the correlation between the PM results of the portable and the reference systems at current PM levels and below. At these emission levels, some inconsistencies were also observed in the responses of the different real time sensors.

In an attempt to address these issues and better understand the properties of PM at such low emission levels, a follow-up activity was undertaken. Two diesel HDEs were employed in with a Continuously Regenerating Trap (CRT) / Bypass configuration that allowed an adjustment of the emission levels from Euro V (20 mg/km) to CRT out. The study was carried out in two phases (Phase 2 and Phase 3).

Phase 2 focused on the contribution of background and adsorbed material on PM. To this end, the PM emissions at four in total different levels were quantified using Teflo, TX40 and Quartz filters. The latter provided the means to quantify the Elemental Carbon (EC) content of PM. Calibrated reference aerosol instrumentation was also employed in parallel and the collected data analyzed to estimate the mass of airborne particles in real time. This served as an additional benchmark (complimentary to EC and PM) against which the different real time sensors were evaluated. The study also investigated cross-sensitivities of the different sensors to non-PM sources (like humidity and other gaseous pollutants).

The results of these investigations were communicated to the manufacturers most of whom undertook some remedy measures. After these modifications, the different candidate systems were tested again in a third stage using another diesel HDE. One particular issue addressed in this second phase was the consistency of the PM results with respect to the sampling time.

This report summarizes the results of the second phase of the program. The work conducted during the third phase will be reported in a follow-up document.

2 EXPERIMENTAL

2.1 CANDIDATE INSTRUMENTS

Five in total candidate PEMS-PM systems were employed in this study, namely:

- Micro Particulate Sampling System (m-PSS) by Control Sistem
- Micro Soot Sensor (MSS) with Gravimetric Filter Box (GFB) by AVL
- Dekati Mass Monitor (DMM)
- On Board System with Transient PM measurement (OBS-TRPM, abbreviated as OBS hereinafter) by Horiba
- Portable Particle Measurement Device (PPMD) by Horiba

This was the same equipment that was tested in the main campaign (Bonnel et al. 2010) with the exception of two systems that were modified to comply with the proposed reference specifications. In particular, the system from AVL was modified to incorporate a prototype Gravimetric Filter Box (GFB) that allows PM sampling at a constant dilution in parallel to the MSS. The m-PSS was also modified to incorporate a particle sensor sampling diluted and temperature controlled exhaust. The five candidate systems are described briefly in the following sections.

2.1.1 HORIBA's OBS

Horiba's OBS is an on-board proportional partial flow system that collects mass on 47 mm filters at a total flowrate of 30 lpm (Wei et al. 2009). A schematic of the OBS is given in Figure 2. Dilution takes place at the sampling probe where the sample is drawn at a flowrate proportional to the exhaust flow. The diluted exhaust is then transported to the filter cabinet with a 4 m heated (at 47 °C) line. The cabinet, which also incorporates a cyclone to remove large particles (cut point at 6 um), is also maintained at a temperature of 47 °C by means of direct surface heating.

A small amount of the diluted exhaust is bypassed to a TSI's Electrical Aerosol Detector (EAD), also referred to as Diffusion Charge Sensor (DCS), measuring the total particle length in real time (Frank et al. 2008). The operation principle of the EAD is based on diffusion charging of the aerosol, followed by detection of the charged particles via a sensitive electrometer. Part of the sampled flow (1 lpm from the total 2.5 lpm) is passing through an absolute filter and then through a corona charger producing the air ions. This flow of ions is reunited with the remaining air flow in a mixing chamber bringing particles into a well defined charge state. The charged aerosol then passes through an ion trap that removes any excess ions before being detected in the electrometer. The number of elementary units of charge acquired in this counter flow diffusion charger is found to be linearly related to the diameter of the particles. Therefore the total current measured in the electrometer is proportional to the total length of the sampled aerosol.

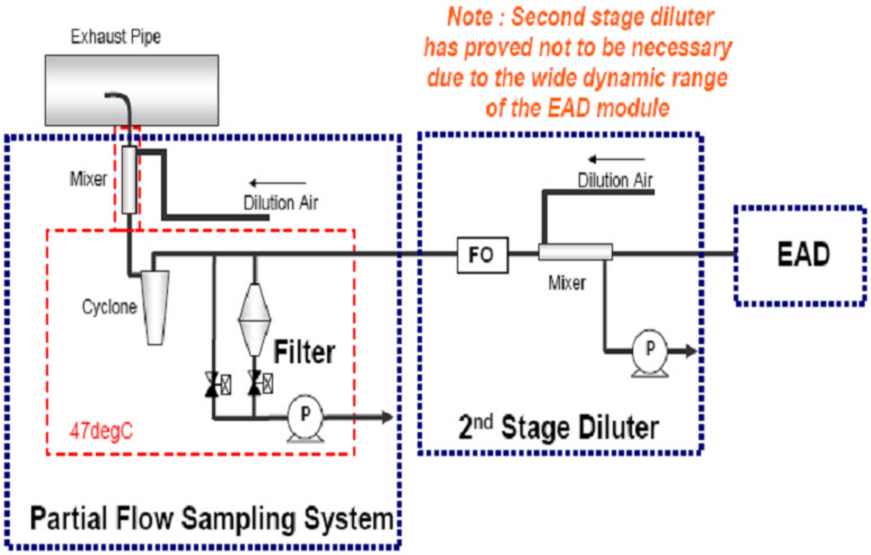

Figure 2: Horiba's OBS: Schematic of its principle of operation

2.1.2 AVL PM PEMS 494

The system from AVL utilizes a constant dilution partial flow system sampling exhaust at a constant flowrate. The dilution system, referred to as AVL's conditioning unit, allows for a dilution of up to 12 and a temperature and pressure conditioning of the diluted exhaust (temperature below 60 °C and pressure at ambient ±50 mbar). The exhaust gas is diluted in a dilution cell mounted directly at the sample point to minimize particle losses. The diluted exhaust gas is sampled in parallel through the MSS measuring cell and over the measurement filter inside the GFB. Therefore one heated line which is connected to the GFB box is used. The MSS and GFB box is connected via an insolated hose. The flowrates are 2 lpm for the MSS and 5 lpm for the GFB The GFB is externally heated by direct surface heating to control the filter face temperature to 47°C (±5°C). This prototype GFB did not incorporate a cyclone.

The MSS operates on the photoacoustic principle (Schindler et al. 2004). The exhaust aerosol passes through a resonator cell were it is exposed to an intensity modulated 808 nm laser beam. This "chopped" light beam is absorbed by the soot particles leading in a periodic heating and cooling of the air surrounding the particles (Figure 3). This is manifested as a periodic pressure wave which is measured by a sensitive microphone and the signal amplified in a "lock-in" amplifier. The 808 nm wavelength was selected in order to minimize interferences from other exhaust gas components and any volatile compounds of PM. The microphone signal is proportional to the mass of soot particles.

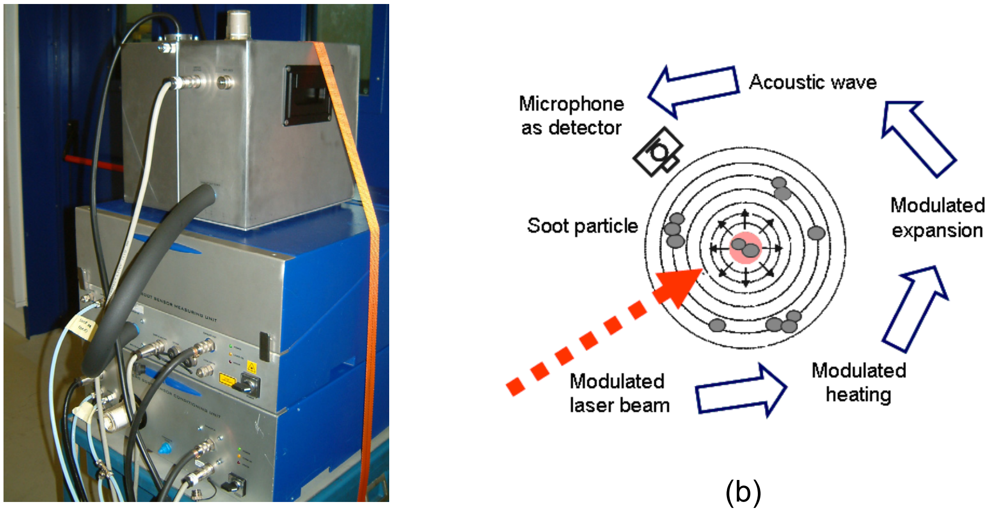

(b)

(a)

Figure 3: AVL 483 MSS (a) and a schematic of its principle of operation (b)

2.1.3 Control Sistem's m-PSS

The Micro Particulate Sampling Sistem (m-PSS) (Control Sistem) is as a proportional partial flow system (the on-board version of PSS-20) that does not require compressed air or cooled water. PM samples are collected on 47 mm filters at a flowrate of 30 lpm. The filter temperature is kept at 47±5°C by means of heating the dilution air. The system does not incorporate a cyclone.

The particular unit was equipped with a prototype particle sensor developed by Pegasor Ltd. The operation principle of the Pegasor Particle Sensor (PSS) is based on the electrostatic charging of particles and the subsequent measurement of current induced as the charged aerosol passes through the sensor. This flow through design does not require collection of particles for the measurement of their charge and therefore the extracted flow is returned in the mPSS at a point upstream of the filter. The PSS also incorporates an ejector diluter to protect the corona needle from getting contaminated. The necessary pressurised dilution air was provided by a pump located in the m-PSS. This additional dilution air was taken into account for the control of the total diluted flowrate.

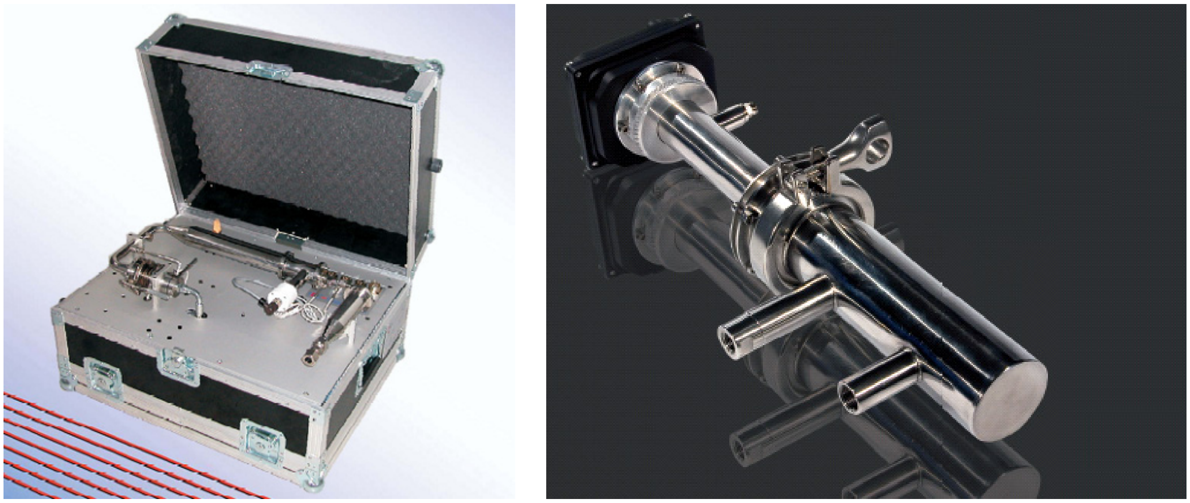

(a) (b)

Figure 4: Control Sistem's m-PSS (a) and Pegasor's Particle Sensor (b).

2.1.4 Sensors PPMD

The Portable Proportional Particulate Mass Measuring Device (PPMD) by Sensors Inc. is a partial and proportional flow sampling system combined with a carousel Quartz Crystal Microbalance (QCM). The proportional partial flow system utilizes a two stage dilution referred as micro proportional sampling system (MPS). Exhaust is extracted through a capillary tube and immediately mixed with a small amount of dilution air. In order to increase response time the exhaust is brought to the sampling capillary at an excess flow that is then bypassed. The secondary dilution air flow passes through a venturi creating an underpressure that draws the sample from the primary dilution stage. The air required for dilution is sampled from ambient and is conditioned inside the PPMD. The dilution air flow is controlled using a multi-bit parallel solenoid array. The PPMD device incorporates two MPS systems in series. The second MPS, which allows for additional dilution when high emitting engines are tested, was not employed in this study.

The Carousel QCM consists of eight QCM sampling units each equipped with a heated inlet, an electrostatic precipitator and a quartz piezoelectric crystal. One crystal (user selected) serves as a reference monitoring changes in the ambient conditions, while the remaining 7 are sampling sequentially diluted aerosol at a user preset sampling period (typically between 1 and 2 min). The sample is drawn from the MPS at a flowrate of 4 lpm but from this stream only 0.5 lpm are passing from the active QCM sampling unit. A corona discharge produced in a needle electrode located upstream the quartz crystal charges the particles and the developed electric field results in a uniform precipitation of the charged particles on the surface of the crystal. The piezoelectric crystal is excited in each natural frequency by means of an electronic oscillator attached to the two metal plates placed on the two sides of the quartz crystal. As particulates are deposited on the surface of the crystal their natural frequency decreases. The particulate mass collected on the filter is then determined by measuring the change in the natural frequency after the sampling period. In that respect the PPMD does not provide a real time signal but rather the mass increase on each crystal after a predefined sampling period. A sampling period of 120 s was employed in all tests. This sampling period (which is 4 times the minimum duration of valid Not To Exceed (NTE) events) was selected in order to allow for a sufficient mass to be collected on the crystals and at the same time give some info on the evolution of PM emissions over the cycle.

Sensors have also supplied a prototype Laser Aerosol Monitor (LAM) to be employed in the measurements. The LAM operates on a laser light scattering and provides the mass of soot in real time. It utilizes its own micro proportional sampling system (MPS) to sample exhaust aerosol from the tailpipe in parallel to the PPMD.

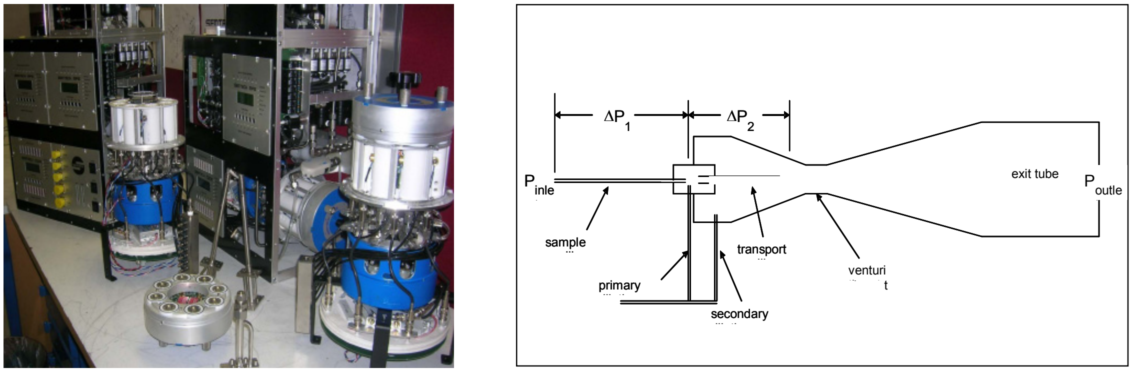

(a) (b)

Figure 5: PPMD (a) and Schematic of the micro proportional sampling system (b)

2.1.5 DMM

The Dekati Mass Monitor (DMM) is an instrument which measures the mass concentration of airborne particles in real time by combining aerodynamic and mobility size particle classification (Figure 6). DMM samples exhaust aerosol at a flowrate of 8.75 lpm, downstream of an inlet preseparator with an aerodynamic diameter (AD) cutpoint at 1.3 um. The sample then enters a triode corona charger where a positive ion flux charges particles. A small flow of HEPA filtered sheath air (1.5 lpm) protects the corona charger from getting in direct contact with particles. A weak electric field downstream of the charger deflects particles having high electrical mobility onto an electrometer (mobility electrode), which measures the current produced by the deflected charged aerosol stream. Particles with lower electrical mobility exit the electric field and are aerodynamically classified in a six-stage cascade impactor. Each impactor stage is connected to an electrometer that measures the current produced as particles release their charge. The recorded signals from the cascade impactor and the mobility electrometer are combined in order to calculate the effective particle density profile, which is required for the conversion of the measured impactor currents to particle number and mass concentrations.

The DMM did not incorporate any dilution system and in most of the tests was connected to the CVS tunnel either directly or through a Dekati's ThermoDenuder (TD) operating at 300°C. A limited number of tests have been conducted with the DMM sampling from the laboratories partial flow system (AVL's Smart Sampler – SPC). Due to the relatively high sample flowrate of the DMM, that might affect the sample exhaust gas flowrate (Giechaskiel et al. 2010), only 3.2 lpm were sampled from the SPC. A mass flow controller provided the additional 5.55 lpm conditioned make up air from the lab's compressed air line.

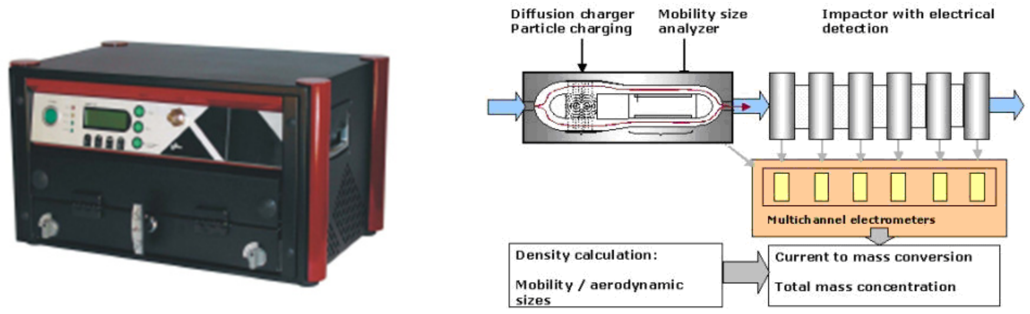

(a)

(b)

Figure 6: DMM (a) and schematic of its operating principle (b)

2.2 EXPERIMENTAL FACILITIES

2.2.1 Test Engine

The engine used in this study (Figure 7a) was the PMP “Golden Engine”, i.e. an IVECO Cursor 8 Euro III engine (Table 1) with a CRT. The CRT employed in the test programme was a cordierite wallflow filter of approximately 24 litres volume and originally supplied by Johnson-Matthey. The CRT is preceded in the exhaust system by a close-canned Pt-based oxidation catalyst (Eminox) of approximately 4.25 litres volume.

In order to evaluate the performance of the instrumentation at different emission levels, a by-pass line (160 cm in length and 89 mm in diameter) was employed, connected in parallel to the CRT system. The amount of exhaust bypassing the CRT system (and in that respect the particle emission levels) was controlled by means of a valve. In the tests of the CRT out levels, the by-pass line was plugged with a stainless steel disc plate to ensure that no exhaust is passing through the bypass line. The engine exhaust configuration with this bypass system is illustrated in Figure 7b. The distance between the engine and the “golden” after-treatment device was 250 cm (internal diameter 25 cm) and it was not insulated.

The engine was mounted on the test bench of the VELA-5 laboratory (Motor AFA-TL 510/1.9-4, 500 kW, 2500 Nm, 3500 rpm). Exhaust gas temperatures and pressures were recorded upstream and downstream of the after treatment device. Engine coolant and intercooler temperatures were controlled respectively at 75 and 40-45°C.

Table 1: Golden Engine Information

Make and model	IVECO Cursor 8 (Euro 3)
Engine configuration and capacity	7.8 l, 6 cylinder, 4 valves/cylinder
Compression ratio	17:1
Maximum power	260 kW @ 1900 to 2400 rpm
Maximum torque	1280 Nm @ 1000 to 1900 rpm
After-treatment	Continuous Regenerating Trap (CRT)

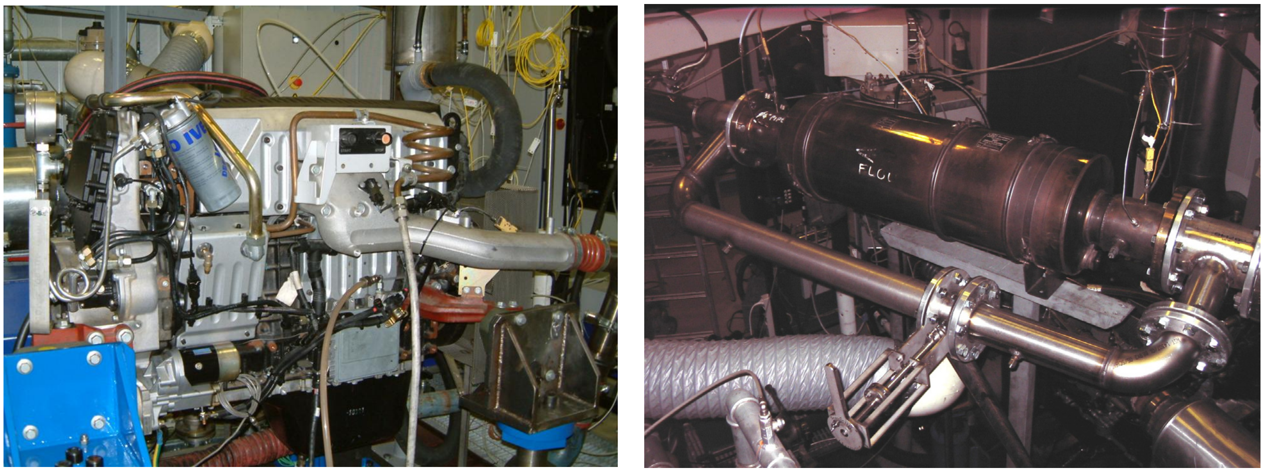

(a) (b)

Figure 7: Golden Engine (IVECO CURSOR 8) (a) and exhaust configuration with the by-pass pipe and valve (b).

2.2.2 Fuel and Lubricating Oil

The engine was running on the lubricating oil used during the PMP validation exercise tests which preceded this measurement campaign. The test lubricant was a BP Vanellus E8 fully synthetic, 5W/30 PAO (polyalphaolefin) based oil with <0.2% sulfur content (Table 2). The tests were conducted immediately after the PMP validation exercise without changing the oil.

The fuel employed was a certified CEC reference fuel complying also with Annexes 3 and 4 of Directive 2003/17/EC describing fuel specifications to be employed after 1st January 2009 (i.e. sulphur content of lower than 10 ppm). The most important properties can be seen in Table 3 and the detailed specifications in Annex A.

Table 2: Lubricating oil specifications.

<table>
<tr><th><i>Properties</i></th><th><i>Method</i></th><th><i>Units</i></th><th><i>Value</i></th></tr>
<tr><td>Density @15 °C</td><td>ASTM D4052</td><td>g/ml</td><td>0.860</td></tr>
<tr><td>Cinematic Viscosity @100 °C</td><td>ASTM D445</td><td>mm^2/s</td><td>12.03</td></tr>
<tr><td>Viscosity Index</td><td>ASTM D2270</td><td>°</td><td>163</td></tr>
<tr><td>Viscosity CCS @ -30 °C</td><td>ASTM D2602</td><td>cP</td><td>5260</td></tr>
<tr><td>Total Base Number</td><td>ASTM D2896</td><td>Mg KOH/g</td><td>15.9</td></tr>
<tr><td>Sulphated Ash</td><td>ASTM D874</td><td>°C</td><td>1.9</td></tr>
<tr><td colspan="4"><i>Specifications:</i>
SAE 5W-30
ACEA E4/E5/E7
MB approval 228.5
20072/77
MAN M3277
Volvo VDS-2
Scania LDF
RVI RXD
Cummins CES
MTU Type 3
Mack EO-M Plus
DAF HP1/HP2</td></tr>
</table>

Table 3:Fuel specifications.

Properties	*Method*	*Units*	*Value*
Density @ 15 °C	EN ISO 3675-98	[kg/m^3]	836.5
Viscosity @ 40 °C	ASTM D445	cSt	3.666
IBP °C	ASTM D86	°C	171
FBP	ASTM D86	°C	364
10% vol	ASTM D86	°C	208
50% vol	ASTM D86	°C	282
95% vol	ASTM D86	°C	360
Cetane Number	ISO 5165-98	[-]	52
Polycyclic aromatics	IP391	[%] by mass	4
Sulphur	ISO 4260 / ISO 8754	[ppm] or [mg/kg]	5.9
Water content	EN ISO 12937	mg/kg	90
Biodiesel Content	EN 14078:2003	% v/v	<7

2.2.3 Reference Sampling Instrumentation

2.2.3.1 Primary Full Dilution Tunnel

The exhaust was transported to the primary full dilution tunnel (CVS tunnel) through a 9.5 m long (the first 3 and last 3 m were insulated) stainless steel tube. The exhaust gas was introduced along the tunnel axis, near an orifice plate that ensured rapid mixing with the dilution air. The dilution air line had highly efficient dilution air filters for particles and hydrocarbons to reduce the contribution of dilution air to PM (H13 of EN 1822). The flow rate of diluted exhaust gas through the tunnel was controlled by a critical orifice venturi. A flow rate of 80 m^3/min at normal reference conditions (0 °C and 1 bar) was used in all tests. The tunnel operated in the turbulent flow regime (Re = 25000 depending on the diluted gas temperature). The residence time of the exhaust in the dilution tunnel was in the order of 0.5 s.

Three probes (of 12 mm inner diameter) were used for sampling, placed at the same cross section of the tunnel and facing upstream the flow. These probes were installed 10 tunnel diameters downstream of the mixing point to ensure complete mixing of the dilution air and the exhaust gas. One probe was used for the secondary dilution tunnel and the particulate mass (PM) measurements and the other two for aerosol instrumentation. A flow splitter (a 1.5 m tube having 4 sampling points equally distributed along its length) was connected to one of these probes allowing for a concurrent connection of 4 instruments. The flow splitter was connected to the probe through a URG-2000-EP cyclone having a cutpoint at 2.5 nm at the flowrate employed (see Annex B). The necessary flow to achieve this cut off size was provided through a high volume pump (operating at a flowrate of 90 lpm).

The secondary dilution tunnel fulfils the requirements laid down in the Heavy-Duty Engine regulations (Reg. 49). In addition, it was equipped with a cyclone pre-classifier (URG-2000-30EP) to limit the contribution of re-entrained and wear materials to the filter mass. The samples were drawn from the primary dilution tunnel at a flowrate of 30 lpm without employing any additional dilution. The particular operating conditions were selected in order to establish the same PM sampling conditions (filter face velocity and concentrations) with the different candidate systems investigated. The cyclone, the secondary tunnel and the filter holder were externally heated by direct surface heating to permit aerosol stabilization of >0.2 s prior to sampling and to ensure close control of the filter face temperature to 47 °C (±5 °C). The temperature was measured 20 cm upstream of the filter.

PM samples were collected on 47 mm Teflon-coated glass-fiber Pallflex® TX40H120-WW filters (TX40), 2 um pore size 47 mm Teflo filters (R2PJ047 - Pall Corp.) or 47 nm non-heat treated Quartz filters (2500QAO-UP – Pall Corp.). The latter allowed for the quantification of the Elemental Carbon (EC) content of PM. One single 47 mm filter was used rather than primary and a back-up filters to minimize weighing errors and the volatile artefacts of the back-up filter (Chase et al. 2004).

2.2.3.2 AVL's Smart Sampler

The SPC-472 Smart Sampler (AVL Inc.) was used as a "reference" proportional partial flow system (Silvis et al. 2002). The sampling point of the SPC system at the tailpipe was positioned 5 m downstream of the CRT. The sampling probe was sharp-edged and open ended, facing directly into the direction of flow. The dilution took place within 20 cm from the exhaust tube using filtered air. In order to achieve extremely low particle number background (<10 cm^{-3}) HEPA and Carbon filters were added at the dilution air line. Downstream of the mixing tunnel, a URG-2000-30EP cyclone was installed with a 50% cutpoint at approximately 6 µm at the flowrate employed. The transfer tubing between the cyclone and the filter was heated to permit aerosol stabilization prior to sampling and to ensure close control of the filter face temperature to 47 °C (±5 °C). PM samples were collected on 47 mm Teflon-coated glass-fiber Pallflex® TX40H120-WW filters or 2 um pore size 47 mm Teflo filters (R2PJ047 - Pall Corp.) at a flowrate of 30 lpm. The split ration was set at 0.0375%. A PMP compliant solid particle number measurement system (see section 2.2.4.1) was connected downstream of the cyclone. The extracted flow (0.65 g/s) for the particle number measurements was taken into account from the SPC control software. The exhaust flowrate signal (required for the control of the sample flowrate) was provided by the test bench control software and was determined by means of real time measurements of the intake air flow and the fuel consumption.

2.2.4 Reference Aerosol Instrumentation

2.2.4.1 Horiba's Solid Particle Counting System

Two prototype Horiba's Solid Particle Counting Systems (SPCS) units were employed in parallel for the measurement of the solid particle number emissions from the primary dilution tunnel and the SPC. These were the golden PMP Particle Number systems (PN) employed in the Heavy Duty PMP validation exercise (Andersson et al. 2010). However in the current study the positioning of the two units was interchanged. In that respect the SPCS unit that was sampling from the CVS tunnel (SPCS19) in the PMP campaign, was installed in the SPC and vice versa (SPCS20 was now sampling from the CVS).

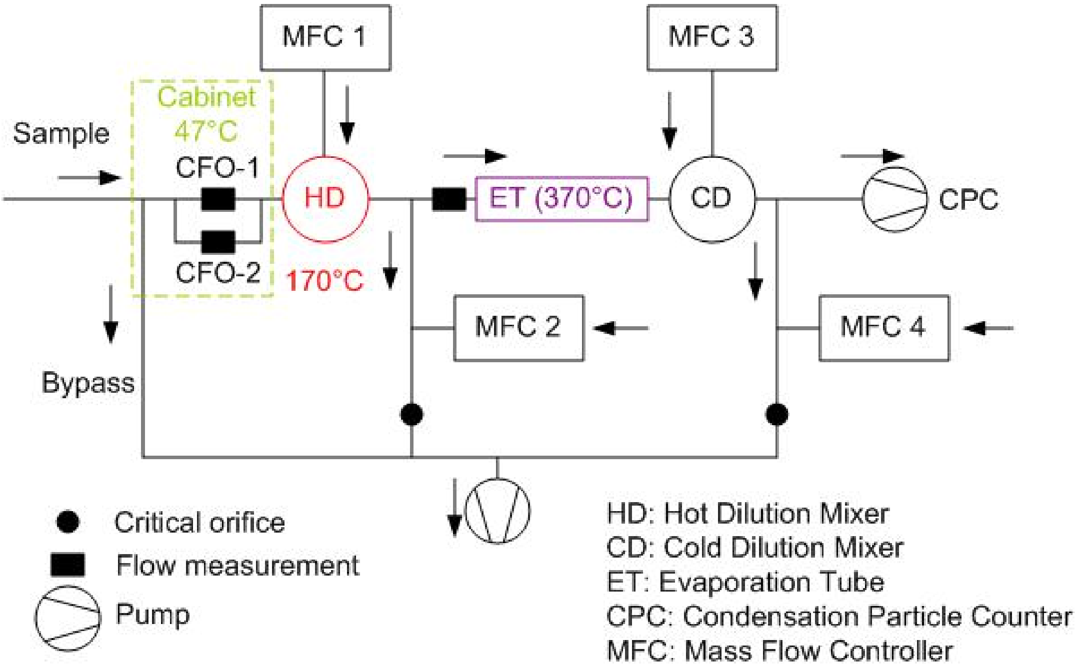

Figure 8: Flow schematic of the SPCS unit.

The SPCS unit consists of a Hot-Diluter (HD), an Evaporation Tube (ET), a Cold Diluter (CD) and a TSI's 3010D Condensation Particle Counter (CPC). A flow schematic of the SPCS unit is shown in Figure 8. The aerosol first enters a temperature controlled cabinet where it is diverged into a bypass flow, the sole purpose of which is the decrease of the residence time in the sampling line, and the sample flow. The sample mass flowrate is measured in real time by an orifice flowmeter, taking into account the temperature and the pressure of the sample as determined with a thermocouple and a pressure transducer, respectively. The sample is then diluted in a temperature controlled mixer (HD) with heated – filter dilution air supplied at an adjustable flowrate by means of a mass flow controller (MFC1).

A small fraction of the diluted aerosol exiting the HD passes through a orifice flowmeter and then enters an externally heated ET whose wall temperature is controlled in the range of 300 to 400 °C. During the ~0.5 s residence of the aerosol inside the ET, the volatile particles are vapourized to gas phase. Immediately after exiting the ET the thermally treated aerosol enters a mixer (CD) where it is cooled by filtered-dilution air supplied at an adjustable flowrate by means of another mass flow controller (MFC3). The concentration of the aerosol exiting this secondary diluter is then measured in real time with a TSI's 3010D CPC.

The excess flow from the two dilution stages is sampled with a pump. The dilution ratio of the two diluters is kept constant by supplying make-up air in the two excess lines. Two mass flow controllers (MFC2 and MFC4) continuously adjust the make up air to account for small fluctuations of the sample flowrates measured in real time with the two flowmeters.

In these prototype units, the user has to specify the desired dilution ratio of each diluter as well as the dilution air flowrates and the bypass flow. The values employed in this measurement campaign were:

- Primary dilution ratio (HD): 10
- Primary dilution air flowrate (MFC1): 11.5 lpm

- Secondary dilution ratio (CD): 15
- Secondary dilution air flowrate (MFC3): 10.5 lpm
- Bypass flowrate: 2 lpm

The results obtained with the two instruments were corrected for the CPC slopes and the average Particle Concentration Reduction Factors (PCRF) at 30, 50 and 100 nm (in accordance to the legislation) as determined during the PMP Heavy Duty Validation Exercise (Giechaskiel et al. 2008, Giechaskiel et al. 2009b).

2.2.4.2 TSI's 3936L10 Scanning Mobility Particle Sizer

A TSI's 3936L10 Scanning Mobility Particle Sizer (SMPS) was employed for the measurement of the number weighted mobility size distributions. The particular SMPS unit consists of a TSI's 3077 neutralizer (employing a 2 mCi activity ^{85}Kr source) for particle charging, a TSI's 3081 cylindrical Differential Mobility Analyzer (DMA) for size classification and a TSI's 3010 CPC for particle detection. An impactor having a cut-off size above 1 μm (0.071 cm nozzle – TSI part number 1508111) was employed to remove very large particles but also to monitor the sample flowrate through the measurement of the induced pressure drop. The neutralizer was almost 10 years old and therefore the actual activity levels were about 1 mCi. The operating flowrates were regularly checked during the measurement campaign with a bubble flowmeter (Gillian Gillibrator – 2). The measured sample flow rate (which was consistently measured to be 0.96 lpm), was employed for the data inversion.

The SMPS operated on a sheath over sample flow rate setting of 10 lpm over 1 lpm and a scan time of 90 s in all engine tests. These settings allows for the determination of the size distribution in the size range of 7.5 nm to 294.3 nm. The size distributions were acquired using TSI's software (AIM 8.1.0.0), which takes into account particle losses inside the instrument. Over transient tests, the voltage of the DMA was fixed to transmit particles of a given size. A different particle size was employed at each repetition of the transient cycle (section 2.2.4.2). Four such time traces at fixed sizes (35 nm, 55 nm, 74 nm and 108 nm) were collected providing some information on the real time size distributions. The sizes were selected in a way that would cover the size range around the peak of the size distribution (as determined over the steady states) and at the same time would allow a correction for the presence of doubly charged particles (Maricq et al. 2004).

The SMPS unit was also employed in some tests with PolyStyrene Latex (PSL) and PAO particles, aiming at the calibration of the different real time sensors. In these tests the SMPS operated at a flow rate setting of 3/0.3 lpm and a scan time of 300 s. These settings allowed for the determination of the size distribution in the 14 to 750 nm size range. More details on the exact settings employed will be given on the following relevant sections.

The performance of the SMPS unit was checked at the end of the engine testing. The results of these investigations (presented in Annex C) verified that both the neutralizer and the Differential Mobility Analyzer (DMA) column operated according to their specifications. The CPC was found to constantly underestimate the number concentration by approximately 15%. Accordingly the SMPS results obtained in the measurement campaign were corrected for this offset.

2.2.4.3 Sunset Laboratory OC-EC Aerosol Analyzer

The Laboratory OC-EC Aerosol Analyzer by Sunset Laboratory was used to analyze aerosol particles collected on quartz-fiber filters for the quantification of the organic and elemental carbon content of PM (Birch et al. 1996). This instrument uses a thermal-optical method to analyze the EC and OC collected on quartz filters. Samples are thermally desorbed from the filter medium under an inert helium atmosphere followed by an oxidizing atmosphere using carefully controlled heating ramps. By careful system control and continuous monitoring of the optical absorbance of the sample during analysis, this method is able to both prevent any undesired oxidation of original elemental carbon and make corrections for the inevitable generation of carbon char produced by the pyrolitic conversion of organics into elemental carbon.

47 mm Quartz-fiber filters were employed. The punch used for the analysis was 1.0 by 1.5 cm in size. The stain area, required for the deduction of PM emissions, was measured to be 11.34 cm^2 for the filter holder employed. The detection limit of the method is 0.2 $\mu g/cm^2$ which corresponds to a PM level of ~0.5 mg/kWh. Due to the very small background level of the filters employed (2500QAO-UP – Pall Corp.), it was not necessary to pre-bake the filters. The background levels, measured by analyzing a blank filter coming from the same batch, were determined to be 0.43 $\mu g/cm^2$ OC and 0.00 $\mu g/cm^2$. Results presented in this report have been corrected for this background.

2.2.5 Aerosol Generators

2.2.5.1 JRC's Homemade Oil Particle Generator

A JRC prototype oil particle generator generator was employed for the production of Poly(Alpha) Olephin (PAO) particles used for the calibration of the aerosol instrumentation (Figure 9). The operation principle is based on the evapouration condensation technique. The PAO oil is placed in a metal crucible in which is heated through an electric Bunsen near its boiling point. A small flow of nitrogen is introduced into the crucible to displace vapour from the surface of the bulk material to a cooler region of the generator where it mixes with carrier gas flow and condenses. The size and concentration of the produced aerosol can be varied by means of controlling the rate of vapour transport from the crucible (via the nitrogen flow) and/or the subsequent cooling rate of the vapour (via the carrier air flow). The nitrogen and carrier air flowrates employed in these tests were 10 lpm and 1 lpm, respectively.

Figure 9: JRC's homemade oil particle generator

2.2.5.2 CETAC U5000AT+ Ultrasonic Nebulizer

An Ultrasonic nebulizer (Figure 10) was employed to re-suspend NIST traceable polystyrene spherical particles (Thermo Scientific 3500A – 498 nm ± 5 nm) for the calibration of the Differential Mobility Analyzer (DMA). A peristaltic pump introduces diluted aqueous suspensions of PSL spheres across an oscillating piezoelectric transducer. The oscillations disperses the sample into a fine aerosol, which is swept out of a spray chamber by conditioned (dehumidified, carbon & HEPA filtered) air. The produced aerosol then passes through a temperature controlled heated tube and an electrothermally cooled condenser. An integrated drain pump removed the condensed sample and any excess sample liquid from the spray chamber. The carrier air flowrate employed in this study was 1.5 lpm. The temperatures of the heated tube and the condenser were set at 140°C and -4°C, respectively.

Figure 10: CETAC U5000AT+ ultrasonic nebulizer

2.3 GENERAL OUTLINE OF THE EXPERIMENTAL SETUP

2.3.1 Engine Testing

Unless a breakdown or technical problem occurred on an instrument, the candidate instruments were tested simultaneously during the engine tests. Figure 11 gives the general layout of the instrumentation employed during the engine tests.

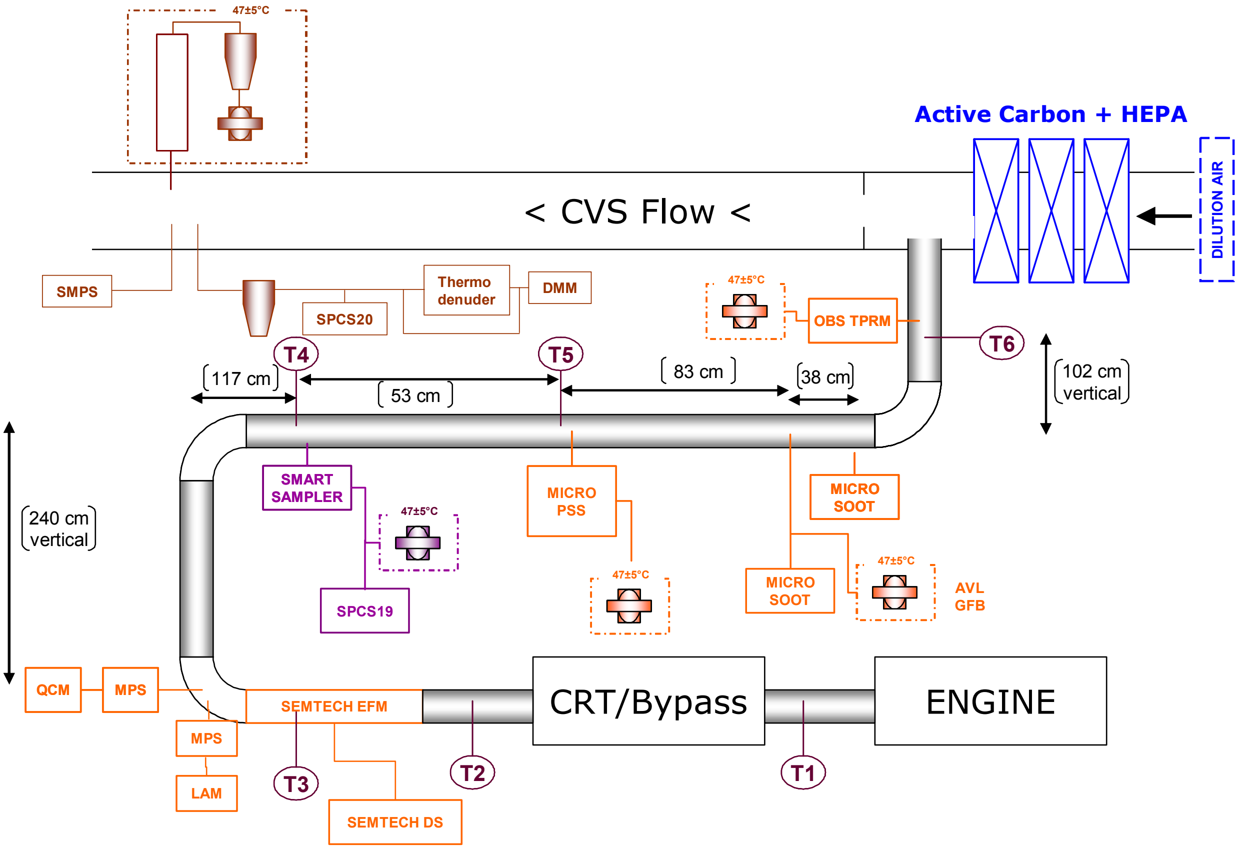

Figure 11: Layout of the instrumentation employed in the engine tests.

All candidate systems were sampling from the tailpipe sharp edged and open ended probes, phasing directly into the direction of flow. The only exception was the DMM which was sampling from the CVS tunnel, using the flow splitter described in section 2.1.5. In the case of the OBS and MSS, dilution took place within 20 cm from the tailpipe, and then the diluted samples were transferred to the filter cabinets using heated lines (of 3 m and 2 m, respectively). The m-PSS was connected to the tailpipe through a 1 m heated line (at 47°C). The PPMD was connected to the tailpipe through a very short (20 cm length) unheated metal tube.

The necessary dilution air for the OBS and MSS was supplied externally through the laboratories compressed air line which included high efficiency HEPA and charcoal filters. The Sensors micro proportional sampling system (MPS) and the Control Sistem's m-PSS units utilized ambient air that was conditioned internally.

The necessary exhaust flow signal was provided by the test bench control software and was determined by combining the real time measurement of engine intake air flow and fuel consumption. This was not however the case for the Sensors PPMD system which employed its own exhaust flowmeter component, installed into the tailpipe right upstream of the sampling probe. This is a real time, velocity based flowmeter that utilizes a multipoint averaging Pitot tube.

One additional MSS was employed in parallel sampling from the tailpipe through a separate probe using its own conditioning unit. Most of the tests were performed using a constant dilution ratio of 6 in both units. In some tests, focusing on the investigation of possible cross sensitivities to non soot compounds, a lower dilution ratio of 2 was employed. For the same reason, the second MSS unit was sampling exhaust through an HEPA filter in some tests.

2.3.2 Calibration Experiments

The general outline of the setup employed for the calibration of the aerosol instrumentation with PAO particles is given in Figure 12. Aerosols were generated with the JRC's homemade oil particle generator. The particle number concentration of the produced polydisperse aerosol was recorded with a TSI's 3790 CPC sampling through a TOPAS DDS 560 diluter in order to examine the stability of the generator. The TSI's 3081 DMA was used together with the TSI's 3080 classifier platform to generate monodisperse particles. A 10 mCi ^{85}Kr neutralizer was employed inside the 3080 classifier platform to charge the particles. The classified aerosol then passed through a ^{241}Am neutralizer or a dummy replica of it containing no radioactive source, and then mixed with conditioned make up air supplied from the compressed air line through a mass flow controller. The diluted sample was then fed to the TSI's 3010 CPC and the instrument under calibration through a 1 m tube (of ¾ in internal diameter) which also served as a static mixer. The flowrates (SMPS sheath & sample, 3010 CPC, 3790 CPC and the sample flowrate of the instrument evaluated) were measured before and after the tests with a bubble flowmeter (Gillian Gilibrator-2).

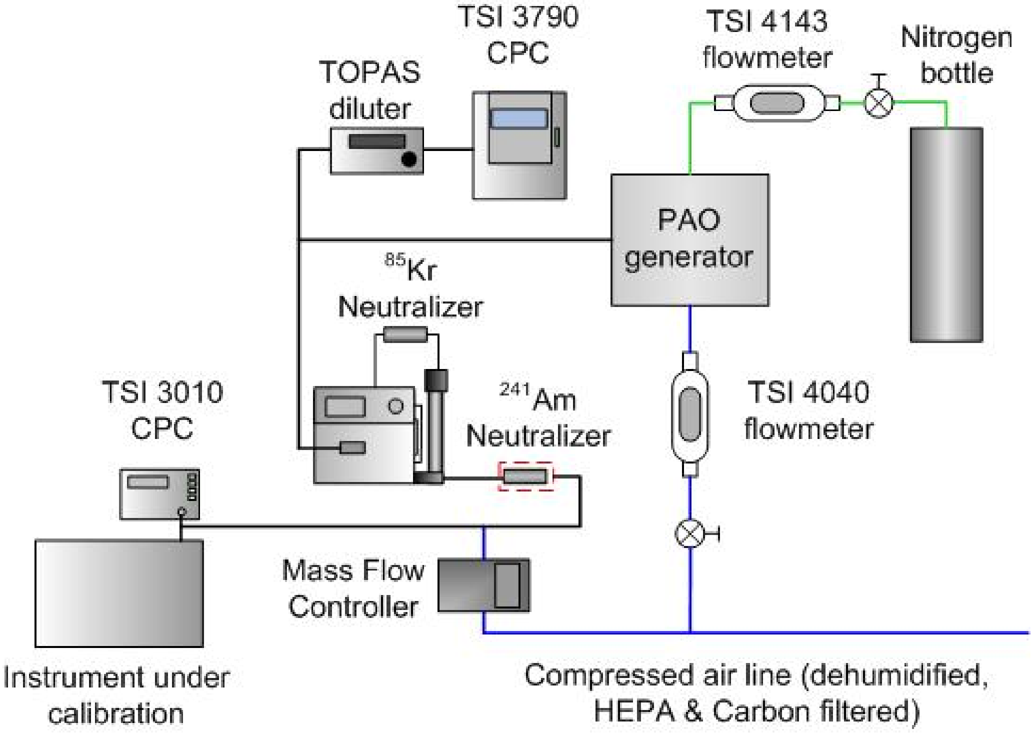

Figure 12: Setup employed for the calibration of the aerosol instrumentation with PAO particles.

2.4 TEST PROCEDURES

The daily engine measurement protocol included a PM background test, followed by the World Harmonized Transient Cycle test procedure (which includes a cold start cycle followed by hot start repetition). At the end of each measuring day, two steady state measurements at ESC mode 12 (2120 rpm / 860 Nm) and ESC mode 7 (1380 rpm / 320 Nm) were performed which also served as a conditioning of the CRT system. During the background tests, the engine was not dismounted from the primary dilution tunnel and the proportional partial flow systems operated in a flush mode (that is only dilution air was sampled).

Measurements have been conducted at four different particulate emission levels corresponding to CRT out (no bypass), and 3 different bypass valve positions resulting in PM emission levels at a Euro V level (40% valve opening), a Euro VI level (10% valve opening) and an intermediate level between the Euro VI and CRT out levels (2% valve opening). The daily test procedure was repeated 4 times at each configuration in order to establish the repeatability of each candidate PEMS system results but also investigate the effect of filter media and sampling duration on PM. The four PM sampling approaches investigated were:

- Use of Teflo filters and a sampling period of 10 min over ESC mode 12 and 15 min over ESC mode 7 and background tests.
- Use of Quartz filters in the CVS tunnel and TX40 on the all partial flow systems and a sampling period of 10 min over ESC mode 12 and 15 min over ESC mode 7 and background tests.
- Use of TX40 filters and a sampling period of 10 min over ESC mode 12 and 15 min over ESC mode 7 and background tests.
- Use of TX40 filters and a sampling period of 20 min over ESC mode 12 and 30 min over ESC mode 7 and background tests.

During the test day were Teflo filters were employed, PPMD measurements were conducted without greasing the crystals in order to investigate any possible interference of grease in the QCM response. In half of the tests at each valve position the DMM was sampling through a Dekati's thermodenuder and in the remaining directly from the CVS tunnel.

3 EXPERIMENTAL RESULTS

3.1 REFERENCE LABORATORY INSTRUMENTATION

This section describes in some detail the results obtained with the reference laboratory instrumentation, in order to get some insight on the emission levels and the nature of PM at the different aftertreatment configurations employed. Exceptionally, the effect of background is investigated using also information from the different candidate systems, in order to better understand its origin.

3.1.1 PM Background

One of the concerns regarding the characterization of PM emissions at such low levels pertains to the capability of the regulated methodology to discriminate the true emissions from background. Testing of the particular engine with the CRT installed, in the framework of the PMP Heavy Duty Validation Exercise (Andersson et al. 2010), resulted in significant inconsistencies between labs. These differences were attributed to the different background levels in the dilution systems (both CVS and PFSS) of the different labs. Most importantly, the two laboratories that regularly performed background measurements, found similar filter loadings during engine and background testing, even if the background levels differed by almost an order of magnitude. It is therefore very important to investigate the contribution of background in order to better asses the performance of the different candidate PEMS PM systems.

Two sources of background can be identified: a) the dilution air and b) deposits in the exhaust and the sampling system. In addition to solid and volatile airborne particles, adsorbed gaseous compounds may also contribute to background PM. Therefore the background PM levels might be strongly affected by the sampling conditions and especially the temperature of the exhaust and sampling system. It is therefore difficult to accurately quantify the background PM levels and there is no sound way to back correct the PM results for this. Regardless of the uncertainty associated with the quantification of background, it is very important to quantify it and take this information into account when assessing the different candidate PEMS-PM systems.

Figure 13 summarizes the background PM levels (expressed as mass emission rates at engine exhaust levels) measured in the CVS tunnel and the reference PFSS (SPC) but also the three candidate PEMS-PM systems that utilize a filter for total PM characterization (AVL's GFB, OBS and m-PSS). The results are plotted separately for the different filter media and, in the case of TX40 filters, for the different sampling durations.

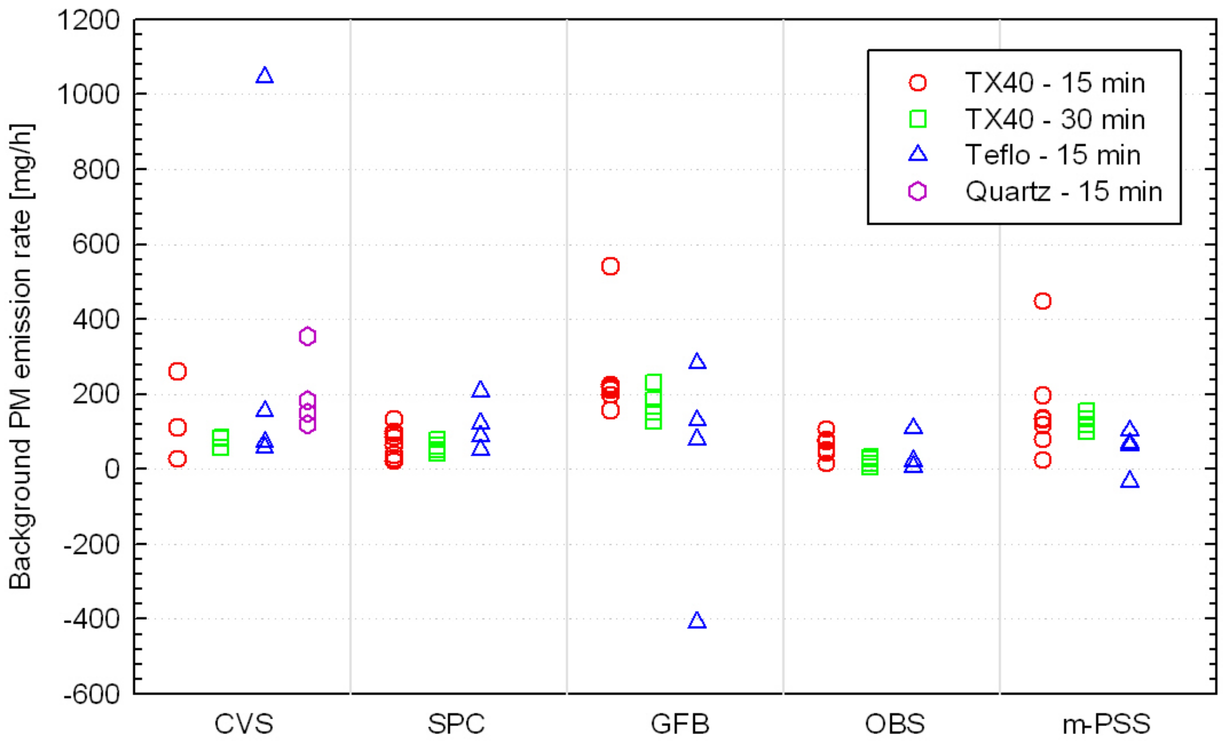

Figure 13: Background PM levels measured in the CVS, the reference PFSS (SPC) and the different candidate PEMS-PM systems, with different filter media / sampling times.

Background PM generally ranged from 0 mg/h to approximately 200 mg/h, with some extreme values as high as 1000 mg/h. This corresponds to an equivalent PM emission of 0 to 4.3 mg/kWh over WHTC. This means that background can reach up to half the Euro VI emission standard, highlighting the difficulties associated with the PM measurements of low emitting engines. It should be stressed at this point that JRC was found to be the laboratory with lowest background levels in the PMP Heavy Duty validation exercise, and therefore the situation might be more severe under average laboratory conditions.

A relatively higher background level was determined for the GFB, ranging from 80 to 280 mg/h, that corresponds to an equivalent 1.7 to 6.1 mg/kWh emission over WHTC. This relatively higher background is related to the lower sampling flowrate employing the GFB.

The data also suggest that the variability of the results improves when increasing the sampling time from 15 to 30 min, at least for TX40 filters for which there is available information. The minimum duration of an In-Service Conformity test is five times a WHTC or European Transient Cycle (i.e. 150 min) and it is expected that this will further reduce the variability of the results.

Prolonged sampling period also results in an apparent decrease of the background levels. On average the calculated background emission rates decreased by 14% (SPC) to 90% (GFB). This suggests that some of the PM background is adsorbed gaseous material the amount of which does not increase proportionally with sampling time. In line with this, the thermo-gravimetric analysis suggested that the entire content of PM is OC. The mechanism by which gaseous compounds adsorb onto the filter is more complicated (Mader et al. 2001) and there exists a saturation level that depends on a number of parameters (filter medium, chemical composition and concentrations, relative humidity and temperature) some of which vary during actual engine testing (Chase et al. 2004). In typical PEMS-PM applications the sampling period can be several hours and this is expected to effectively reduce the contribution of background.

Teflo filters resulted some times in unrealistically high or even negative background levels. This points towards some handling difficulties associated with these particular type of filters. However, by excluding these outliers, similar levels of background and variability were observed.

It is worth noting that the m-PSS gave systematically higher background PM in all tests with TX40 filters. On average the background determined with the m-PSS was two to three times higher, even though this is not that clear in the chart due to the large day to day variability. Interestingly, the m-PSS was the only system (from those utilizing filter holders for the determination of the total PM) that was not supplied with laboratory conditioned dilution air. This is an indication that the dilution air might be the major contributor to background PM and raises concerns regarding the capability of the PEMS-PM systems to efficiently control background levels on board. It is worth noting though that when Teflo filters were employed, similar levels of background were determined. Teflo filters are known to be less prone to adsorption artefacts, so this might indicate larger adsorption artefacts. Perhaps more importantly, this indicates that it might be preferable to employ Teflo filters in PEMS applications.

3.1.2 PM emissions

Figure 14 summarizes the PM emission results determined from the CVS (left-hand panels) and SPC (right-hand panels). Each bar corresponds to the cycle-average emissions, with the horizontal line inside each bar indicating the estimated contribution of background (top part of the bar). The error-bars stand for ±1 standard deviation of the PM results (top error bars) and the background measurements (lower error bars). The contribution of background on the PM samples was calculated by means of simply scaling up (or down) the filter mass collected over the background tests to account the different sample time employed in the various tests. The results presented in the previous section suggest that this is not strictly valid, and therefore the indicated background contribution should only serve as an eye-guide.

At 40% bypass valve position, the PM emission levels are generally found to be just below the Euro V emission standard of 20 mg/kWh. CVS data suggest an average PM value of 15 mg/kWh over both the cold start and the hot start WHTC. PM decreased to approximately 11 mg/kWh over the high power ESC mode 12 and increased to 25.5 mg/kWh over ESC mode 7. The thermo-gravimetric analysis of the Quartz filters suggested that the PM emissions at this configuration were relatively dry with the OC content ranging from 30 to 35%. Similar levels of PM were determined with both Teflo and TX 40 filters. SPC results were also found to be in very good agreement with CVS data suggesting a PM emission level of ~13 mg/kWh over the two WHTC cycles and ~9 mg/kWh over ESC mode 12. Systematically lower PM levels of around 13 mg/kWh were obtained though over ESC mode 7. The reason for this discrepancy is not clear as it was not observed at other bypass valve positions. Finally, the background PM was found to be at about 10% of the actual PM emission levels, with more than 99.9% of it being OC.

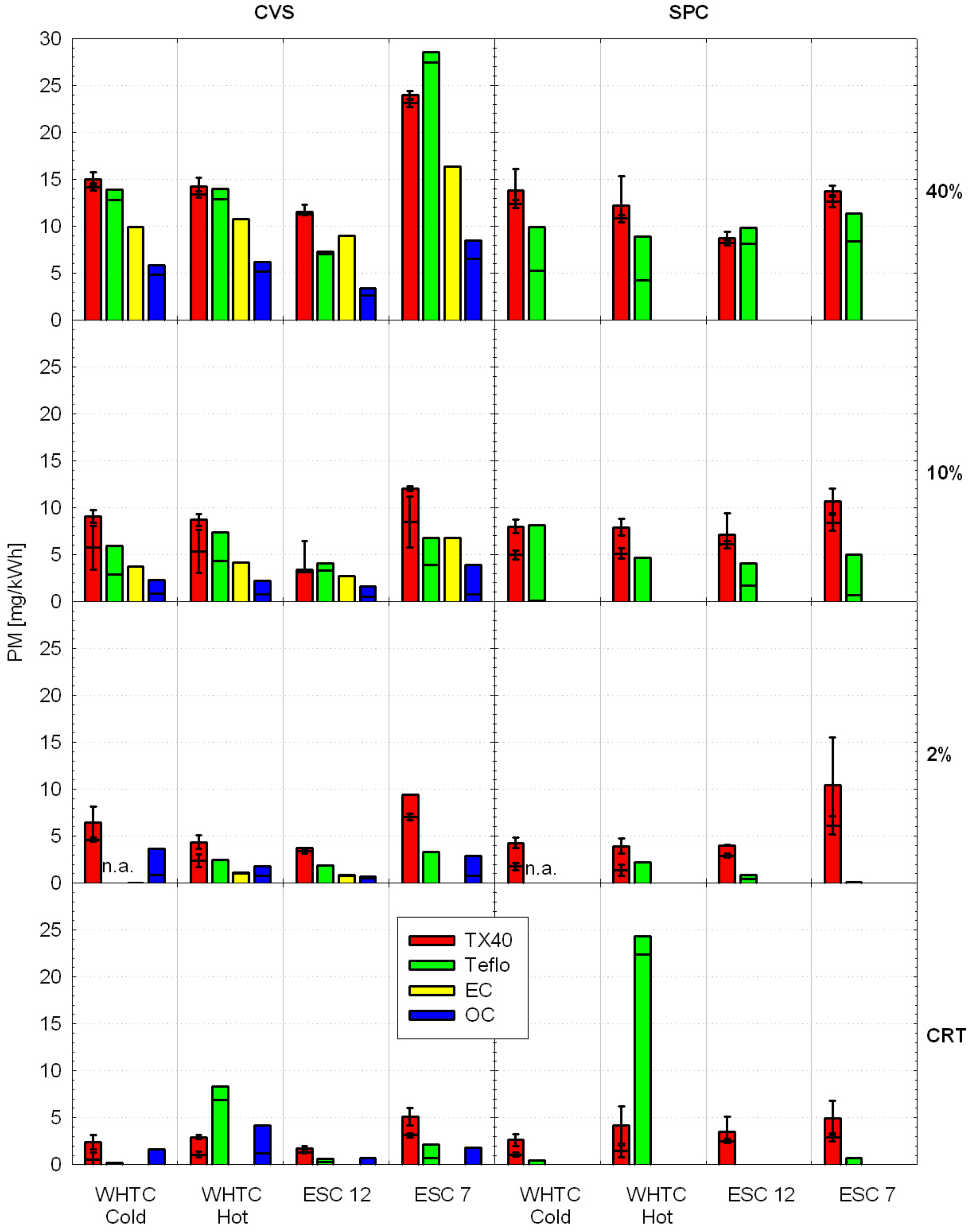

Figure 14: PM emissions at the different bypass valve positions as determined in the CVS (left-side panel) and the SPC (right-side panel). The horizontal line in each bar shows the estimated background contribution (upper part of the bars). Error bars correspond to ±1 standard deviation of the PM results (top error bars) and the background PM (lower error bars).

PM emissions at 10% opening of the bypass valve were found to be around the Euro VI limit value of 10 mg/kWh. Again no differences were observed between the cold start and hot start WHTC with the PM averaging at ~8 mg/kWh for both SPC and CVS. PM levels were slightly lower over ESC mode 12 (~5.5 mg/kWh) and slightly higher over ESC mode 7 (~10 mg/kWh) but the differences were much smaller compared to the 40% valve position tests. The thermo gravimetric analysis suggested again a 30% contribution of OC in the PM over all test cycles. Some discrepancies were observed between TX40 and Teflo filters at this emission level with the latter yielding in general lower PM emissions by 15% to 55%. The PM background was found to be at ~30% of the PM levels at this valve position. Again more than 99% of the background PM was OC.

At 2% valve opening, the PM emissions averaged at 5.8 mg/kWh when TX40 filters were employed. The use of Teflo filters resulted in systematically lower PM emissions averaging at ~2 mg/kWh. No clear cycle effect could be identified. The thermo gravimetric analysis of the quartz filters revealed very small amounts of EC mainly emitted over the hot start WHTC (1.1 mg/kWh) and the high power ESC mode 12 (0.8 mg/kWh). Over the cold start WHTC and ESC mode 7, the OC constituted more than 99 % of the emitted PM. Background PM was found to be anywhere between 10% and 100% of the PM emissions.

With the bypass pipe completely sealed, the PM emissions decreased even further averaging at 3.5 mg/kWh when TX40 filters were employed. Use of Teflo filters suggested even smaller PM emissions of ~0.7 mg/kWh, if the two unrealistically high results at hot WHTC are excluded as outliers. Thermo gravimetric analysis of the quartz filters suggest that practically all of the PM is OC. At those very low emission levels, background PM was sometimes found to exceed that measured with the engine running.

3.1.3 Solid Particle Number Emissions

The solid particle number emissions as determined with the two PMP golden PN systems are summarized in Figure 15. The measured solid particle number emissions determined for the different valve positions spanned over a range 5 orders of magnitude (from 5.3×10^{8} to 6.4×10^{13} #/kWh). For comparison, PM results varied over a much narrower range of ~300 (0.09 to 28.5 mg/kWh). At the same time the particle number background was less than 4×10^{8} #/kWh allowing for an accurate determination of the true particle number emissions even downstream of the CRT.

Based on the CVS data, solid particle number emissions over WHTC Cold decreased from 1.86×10^{13} #/kWh at 40% valve opening, to 6.26×10^{12} #/kWh at 10% valve opening, 2.15×10^{12} #/kWh at 2% valve opening and 8.6×10^{10} #/kWh when the bypass pipe was sealed. Results collected at 2%, 10% and 40% valve opening showed similar effects of cycle on the solid particle number emissions. In particular, the hot start repetition of the WHTC cycle resulted in about 20% higher emissions of solid particles. Solid particle number emissions were ~50% higher over ESC mode 12 and ~200% higher over ESC mode 7. The particle emissions downstream the CRT showed different cycle dependence. More specifically, emissions over the cold start WHTC were almost one order of magnitude higher compared to those over the hot start repetition of the test cycle. Additionally, the highest emissions were observed over the ESC mode 12 were the CRT starts regenerating. The real time data showed that solid particle numbers were gradually increasing during the ESC mode 12 test and gradually decreasing over the subsequent ESC mode 7 test. Similar behaviour was observed during the PMP validation exercise activity (Andersson et al. 2010) and can be explained by the reduction of the filter cake during ESC mode 12 where the CRT regenerates due to the high exhaust temperatures and subsequent loading of the CRT during the low temperature ESC mode 7. Release of semivolatile material not removed at 350°C employed in the evapourating tube of the two SPCS units might also contribute to the observed increase of the particle number emissions over ESC mode 12.

The SPCS unit employed on the SPC gave similar results to those determined with the SPCS unit employed in the primary full dilution tunnel. Over the CRT and the 10% valve opening tests the differences were found to be well within the uncertainty of the measurements (±10%). Over the 2% and 40% valve opening tests, the SPCS unit employed in the CVS tunnel yielded ~20% systematically higher particle number emissions. This difference suggests differences in the slopes of the two CPCs whose position was interchanged between these two sets of experiments. Subsequent investigations revealed that one of the CPC units had some linearity problems which were associated with a malfunctioning condenser cooling device. The results obtained with the particular CPC were discarded from the subsequent analysis.

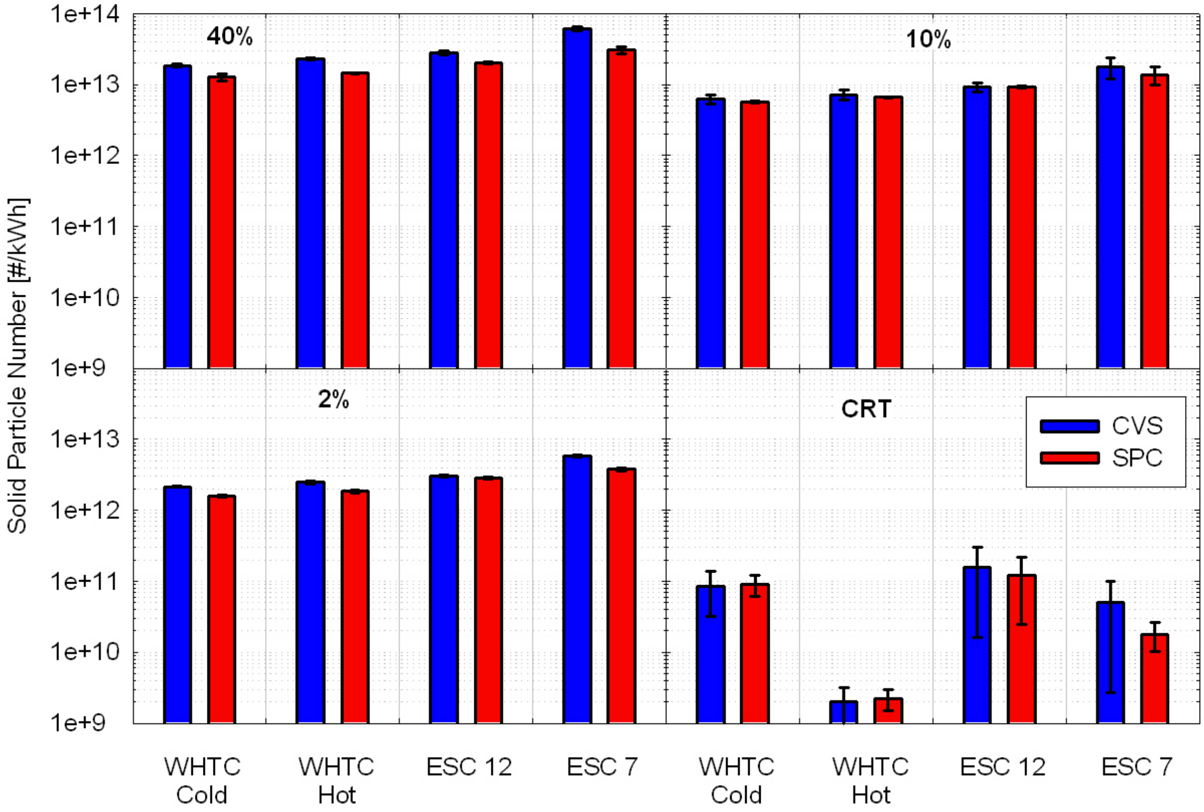

Figure 15: Solid particle number emission rates following the PMP methodology. Error bars correspond to ±1 standard deviation.

3.1.4 Number Weighted Mobility Size Distributions

The number weighted mobility size distributions as measured with the SMPS, sampling directly from the CVS, are summarized in Figure 16. The WHTC cycle average number concentrations at the four mobility diameters investigated are also shown in the figure. The concentrations were determined from equation C3 and were also corrected for the presence of doubly charged particles as described in the annex (section C.2). The accurate representation of the WHTC cycle average size distributions requires that the particle number emissions are repeatable over the four repetitions of the WHTC. This assumption is justified at 40%, 10% and 2% valve opening where the solid particle number emissions exhibited a Coefficient of Variation (CoV) of less than 5% over both WHTC cold and WHTC hot. On the other hand, the CRT out particle number emissions were less repeatable, with a CoV around 60%. Practically, this is prohibitively high for the reconstruction of the size distribution.

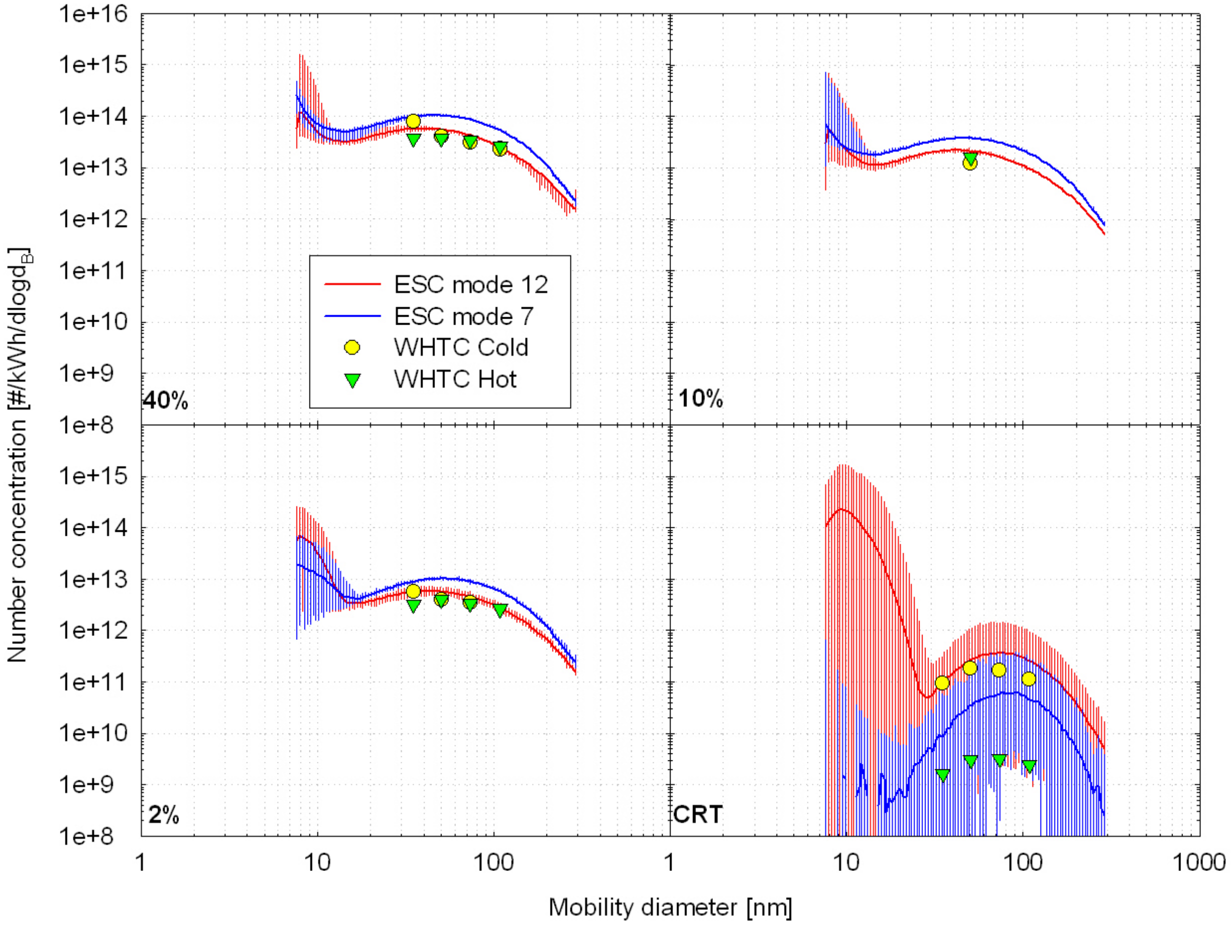

Figure 16: Number weighted size distributions. Error bars indicate the maximum and minimum concentrations from all scans collected at each steady state test. Dots correspond to the cycle average number concentrations of DMA classified particles over the WHTC cycles.

The size distributions obtained at 2%, 10% and 40% valve opening were found to be very similar exhibiting an accumulation mode peaking at 42 nm over ESC mode 12 and 48 nm over ESC mode 7 and a distinct, less stable nucleation mode. The peak of the nucleation mode was generally found to be below 7.64 nm which is the lowest detection limit of the SMPS at the setup employed.

The CRT appears to have a strong effect on the shape of the size distribution. The accumulation mode now peaks at around 75 nm, is narrower (with a geometric standard deviation σ_g of ~1.65 compared to ~1.9) and much more unstable. The number concentration of the accumulation mode particles is gradually increasing over the ESC mode 12 and gradually decreasing during the ESC mode 7 tests. This is a direct consequence of the consumption (over the high exhaust temperature ESC mode 12) and build up (as the exhaust cools down over ESC mode 7) of the filter cake that directly affect the filtration efficiency of the CRT. During the CRT regeneration at ESC mode 12 a significant amount of nucleation mode particles is also emitted and can reach up to three times the number concentration of the accumulation mode particles.

As an additional quality check, the total number concentrations measured with the SMPS were compared to those determined with the SPCS unit (the one employing the properly working CPC). Because of the relatively large cut-off size of the TSI's 3010D CPC employed in the SPCS unit, the SMPS number concentrations were determined as the convolution of the SMPS distribution with the 3010D detection efficiency curve as determined by Liu et al. (2005). The results of these comparisons are shown in Figure 17. Generally, the number concentrations were found to be in good agreement with the SMPS results, the latter giving on average ~20% higher number concentrations. This difference is reasonable given that the aerosol is thermally treated in the SPCS and therefore most of the nucleation mode particles, which are presumably volatile, are completely removed.

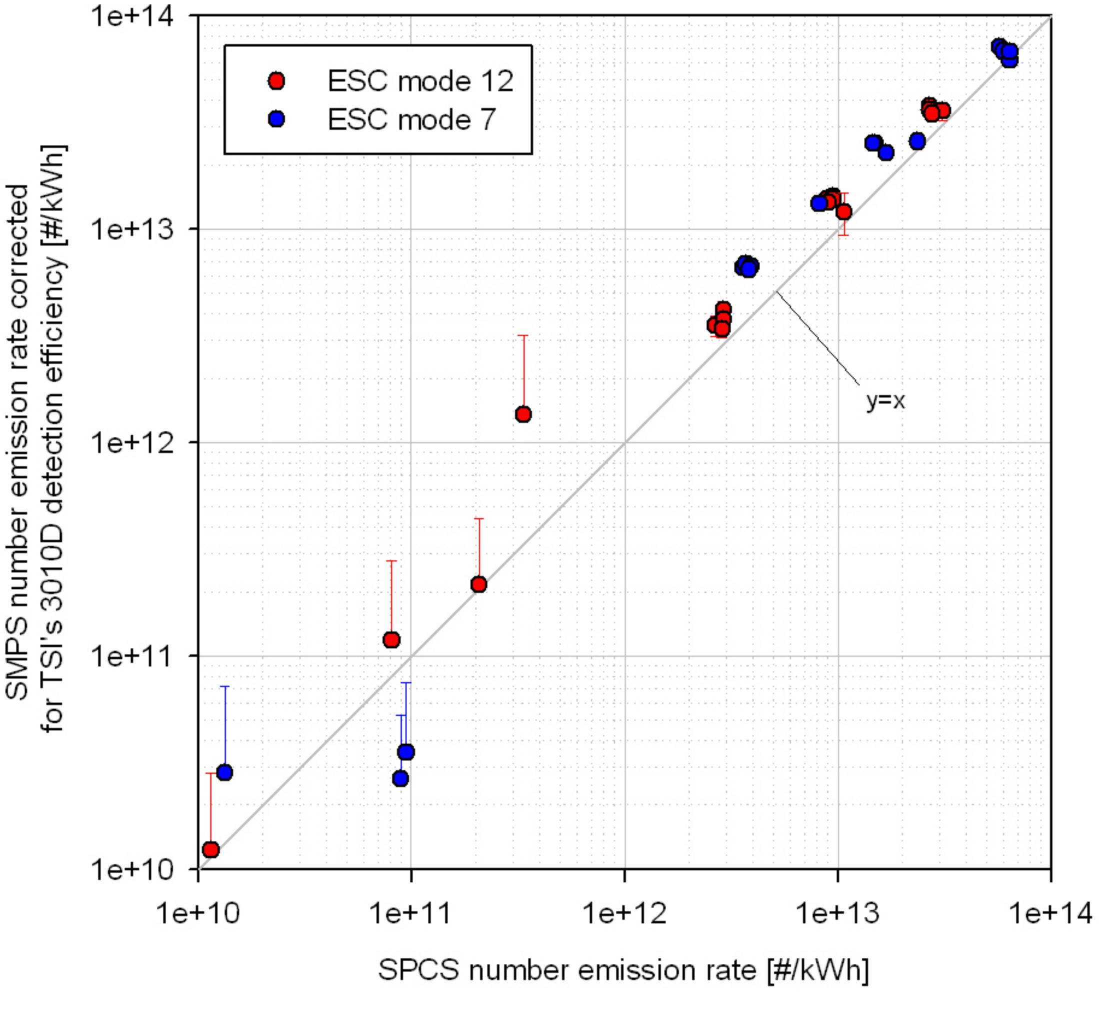

Figure 17: Comparison of SMPS and the SPCS number concentrations over steady states.

3.1.5 Mass Concentration of Airborne Particles

The total mass concentration of the aerosol is related to the number weighted mobility size distribution through the particle effective density (Park et al 2003). Diesel soot particles have a complex fractal like structure which implies a power law dependence of the effective particle density on the mobility diameter. Figure 18 plots effective particle densities measured in independent studies covering a wide range of diesel engines and engine operating conditions. The data suggest a dependence of the effective density to the mobility diameter raised in a power of -0.65±0.08. According to the fractal theory this corresponds to a fractal dimension of 2.35±0.08. This power law dependence tends to break at around 50 nm, that is as the particle size reaches that of the primary soot particle diameter (Mathis et al. 2005). At that size the effective density approaches a constant value around 1 g/cm^3. Most importantly, the experimental data seems to fall within a relatively narrow range, showing little dependence on engine technology and engine operating conditions. Only a simple dataset from the study of Olfert et al. (2007) stands out, suggesting much higher effective densities at larger particle sizes. This was mainly associated with a large production of sulphate particles in the oxidation catalyst at elevated exhaust temperatures as 50 ppm S was employed. Overall, the results suggest that it is possible to calculate the mass concentration from the measured SMPS distributions using the reported effective density profiles. For this purpose, three curves were fitted on the experimental data, corresponding to the average effective density profile and the upper and lower boundaries (also shown in Figure 18).

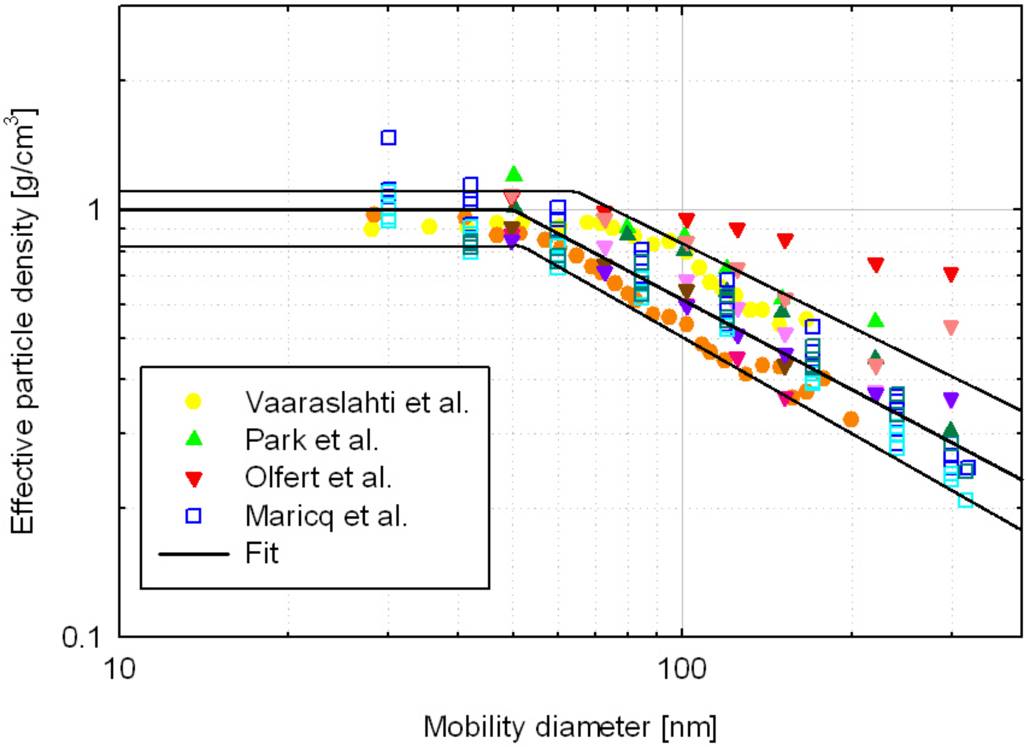

Figure 18: Effective density of diesel exhaust as determined in the studies of Vaaraslahti et al (2006), Park et al. (2003), Olfert et al. (2007) and Maricq et al. (2004). Data obtained at different engine modes are shown with different colors.

The mass emission rates calculated from the SMPS size distributions and the assumed effective density profiles are compared to the gravimetrically and thermo-gravimetrically determined PM from CVS samples, in Figure 19. An exceptional agreement was observed between the SMPS mass and EC at levels above 0.5 mg/kWh which corresponds to the sensitivity limit of the OC-EC technique. The individual differences, when the average effective density profile was employed, were within -7%±8%. This finding suggests that airborne particles only contribute to the EC of the PM samples. The OC mainly originates from adsorption of gaseous compounds.

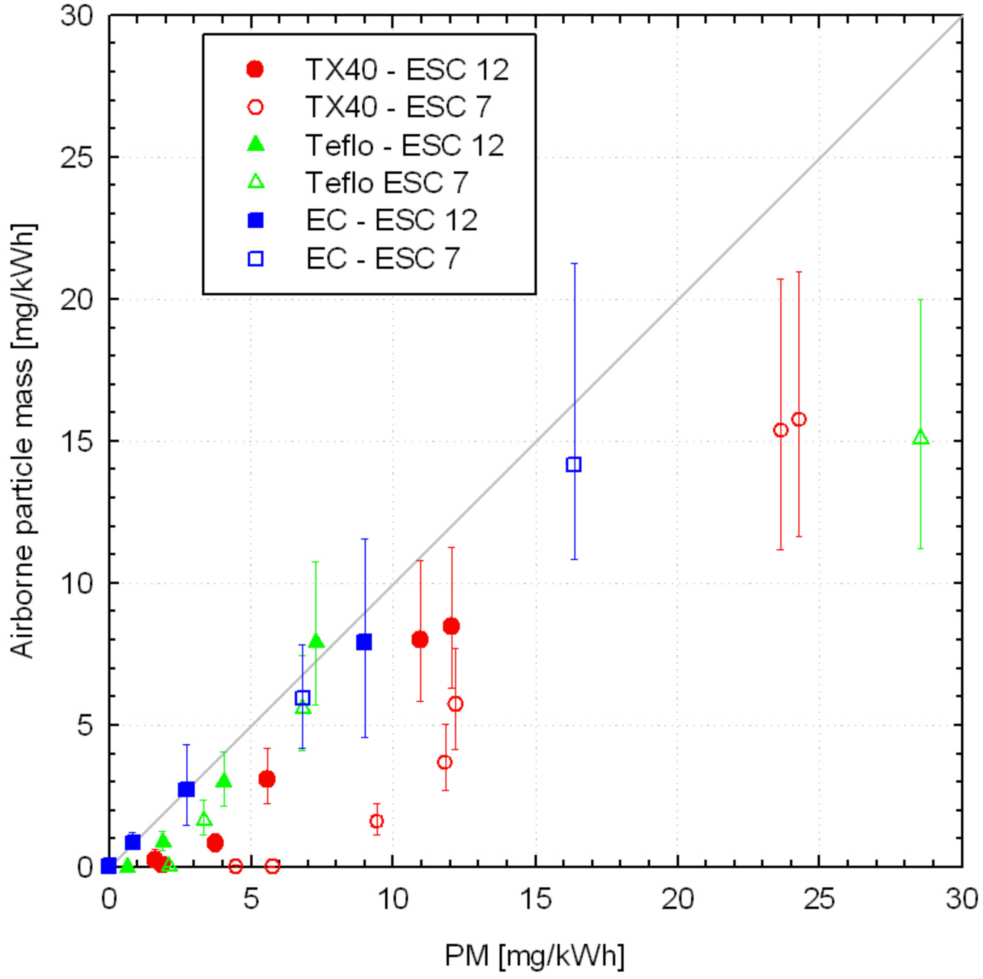

Figure 19: Comparison of the calculated SMPS mass emission rate with PM and EC determined from CVS samples.

The PM emissions determined using TX40 filters were always found to be less than that calculated from the SMPS even when the maximum expected effective density values were employed for the calculations. The individual differences ranged from -1 to -53% at 40% valve opening, from -25 to -77% at 10% valve opening, from -68 to -88% at 2% valve opening and from -61 to -100% at CRT levels, depending on the effective density profile assumed. The observed differences are related to the adsorption artefact on the TX40 filters whose contribution increases as the PM levels decrease, eventually constituting more than 99% of the filter mass loading at CRT emission levels.

Smaller differences were observed when Teflo filters were employed. This is in agreement with the findings of Chase et al (2004), who observed that TX40 filters are associated with a larger adsorption artefact. The individual differences ranged from -61% to +48% at 40% valve opening, from -46% to 10% at 10% valve opening, from -69% to -29% at 2% valve opening and from -97% to -100% at CRT out emission levels.

Figure 20 shows the percentage contribution of the calculated airborne particle mass to the total measured PM emissions. The relative contribution of airborne mass on the total collected PM mass decreases as the PM emission levels decrease (that is with decreasing the bypass valve position). The contribution of airborne particle mass to the total PM mass collected on TX40 filters dropped from approximately 60-70% at 40% valve opening, to 45-55% at 10% valve opening, 16-21% at 2% valve opening and 0-13% at CRT out levels. Teflo filter results suggested a systematically higher contribution of airborne particle mass on the determined PM levels when the CRT was partly bypassed, decreasing from 50-100% at 40% valve opening to 70-78% at 10% valve opening and 43-46% at 2% valve opening. At CRT out levels, the contribution of airborne particle mass to the mass collected on Teflo filter was practically zero.

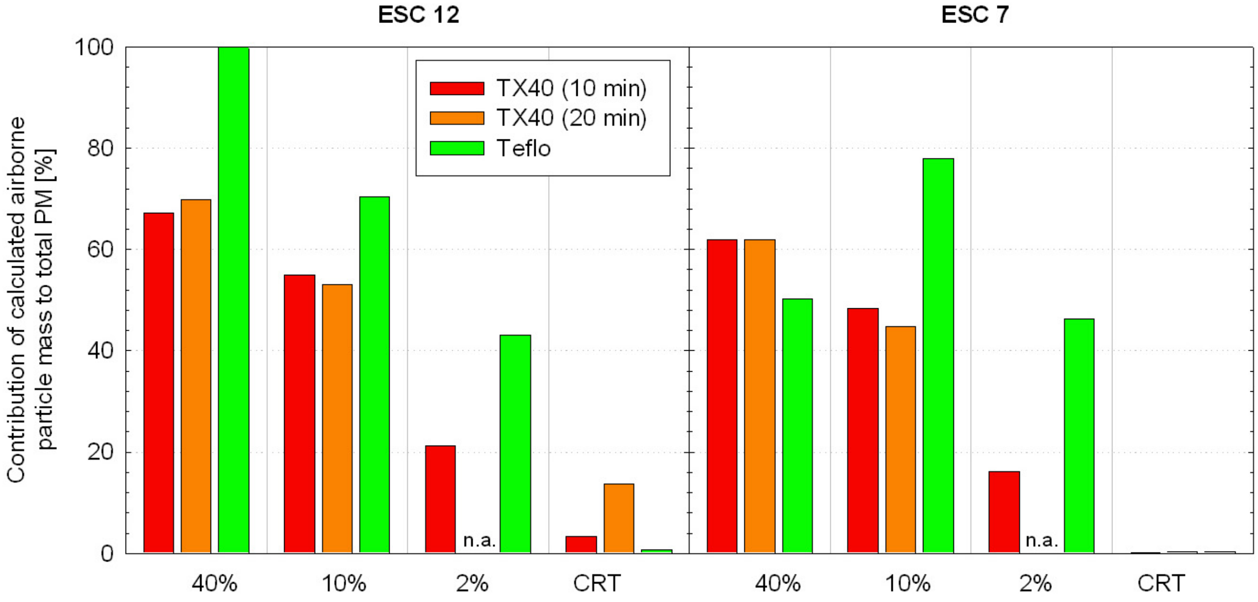

Figure 20: Percentage contribution of calculated airborne particle mass to the total PM.

3.1.6 Real Time Calculation of Airborne Particle Mass

The small dependence of the effective density of diesel particles on engine technology and engine operating conditions allows for a real time calculation of airborne particle mass with a real time particle sizer. This technique as employed successfully by Maricq et al. (2006b) using an electrical Low Pressure Impactor and Symonds et al. (2007) using a Differential Mobility Spectrometer. Both studies revealed a ±20% agreement with gravimetrically determined PM.

Generally the mass concentration of airborne particles can be calculated as the convolution of the volume weighted mobility size distribution with the corresponding effective density profile, i.e.:

$$m = \frac{\pi}{6}\int_0^\infty \rho_{eff}(d_B)\, d_B^3 N(d_B)\, dd_B \qquad 1$$

According to the fractal theory, the effective particle density (ρ_{eff}) is related to the mobility diameter through a power law dependence of the form:

$$\rho_{eff}(d_B) = \rho_0 \left(\frac{d_B}{d_0} \right)^{DF-3} \qquad 2$$

Where DF is the fractal dimension, d_0 is the primary particle diameter and ρ_0 is the primary particle density (Park et al. 2003, Maricq et al. 2004). A fit to experimentally determined effective density data by Maricq et al. 2006b suggested a DF of 2.3 and primary particle size of 20 nm assuming a primary particle density of 2 g/cm^3 (Braun et al. 2004). Diesel exhaust size distributions are also known to be lognormal in shape (Haris S. J. et al. 2001). Under a lognormal assumption, the size distribution is completely specified by three parameters, namely the geometric mean diameter (d_g), the geometric standard deviation (σ_g) and the total number concentration (N_0). Under these assumptions, equation 1 yields:

$$m = N_0 \frac{\pi}{6} \rho_0 d_0^{(3-DF)} d_g^{DF} e^{\frac{DF^2 (\ln \sigma_g)^2}{2}} \qquad 3$$

Where, N_0 is the total number concentration and μ_g the geometric mean diameter of the underlying lognormal distribution. In the above derivation, the presence of nucleation mode particles and the observed break-down of the power law dependence of the effective density on particle size at small sizes were neglected. These two simplifications have a very small effect on the calculated mass concentrations as they both concern sub-50 nm particles whose contribution to PM is minimal (Kittelson 1998) because of their small size.

A closer look at equation 3 reveals that the real time mass concentration scales up with the product of the accumulation mode number concentration (which to a good approximation equals the solid particle number concentration determined with the PMP setup) with the geometric mean mobility diameter raised to the power of DF (around 2.3). The remaining quantities appearing in equation 3 can be considered to a good approximation as constant. The real time traces of the number concentrations at 4 different particle sizes, provide the means to calculate the variation of the geometric mean diameter over the test cycles. This information can then be combined with the SPCS data to calculate the real time mass concentrations. The SPCS number concentrations were also corrected for the CPC detection efficiency curve (since based on the above assumptions the size distribution was also known).

Figure 21 shows the calculated evolution of the geometric mean diameters over the cold start and hot start WHTC cycles at 40% valve opening and CRT out levels. Looking at the 40% valve opening results, it can be seen that the geometric mean diameter is relatively constant over the hot repetition of the WHTC, averaging at around 58 nm. This also holds over the rural and highway part of the cold start WHTC. However over the cold start – urban phase of the WHTC, a lower geometric mean diameter was calculated mainly associated with a relative increase of the concentration at the lower size examined (35 nm). This is an indication of nucleation mode particle formation. The 58 nm average geometric mean diameter is larger from what that determined over the steady state tests (42 and 48 nm). This might be an artefact associated with the day to day variability of the results or even the relatively small number of sizes employed for the calculation of the geometric mean diameter.

Similar trends were observed at the CRT out levels with the geometric standard deviation averaging at a relatively larger size (68 nm) once the engine and the CRT were warmed up, in agreement with what was observed in the SMPS scans over the steady states. Over the cold start phase of the cycle lower geometric mean diameters (down to ~40 nm) were calculated.

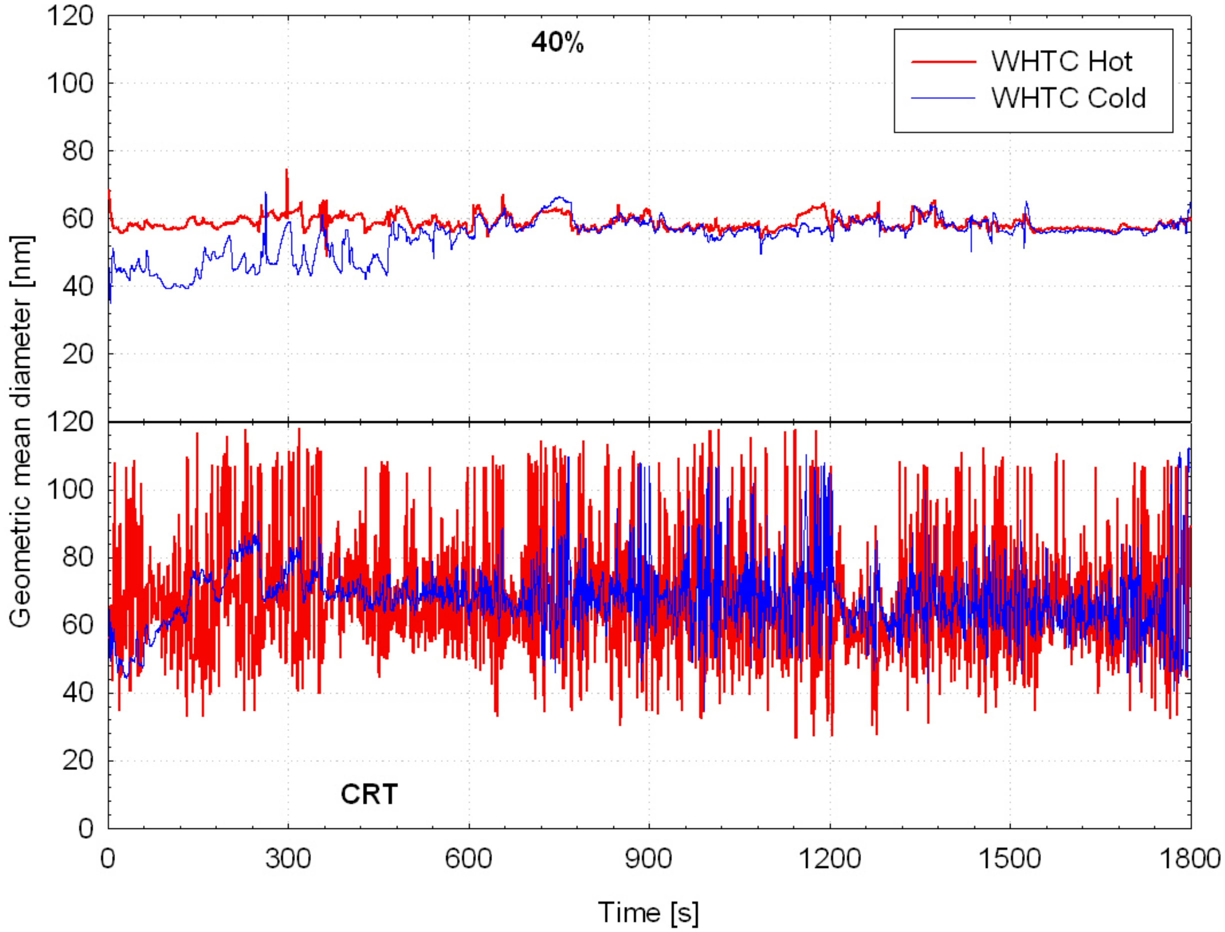

Figure 21: Calculated geometric mean diameters over the cold and hot repetitions of the WHTC at 40% valve opening (upper panel) and CRT out (lower panel) levels.

Figure 22 compares the mass concentrations calculated following this approach with the EC emissions determined from quartz samples over WHTC cold and WHTC hot. It should be noted here that no calculations were performed at 10% valve opening since at this configuration it was not possible to calculate the geometric mean diameter (values are available only for a single size bin Figure 16). The calculations were performed using the power law fits shown on Figure 18 (neglecting the constant density part) for the effective density and a geometric standard deviation of 2.05 which is what the SMPS distributions over steady state suggest for this particular engine (Figure 16). Generally, and given the simplified assumptions employed, a very good agreement was observed. Over WHTC hot the calculated mass concentration was 11% lower at 40% valve opening and 2% lower at 2% valve opening (EC results at CRT levels are below the sensitivity limit of the methodology). Over WHTC cold, a relatively larger difference was observed (~30%). This underestimation is an artefact related to the presence of nucleation mode particles over this test cycle. The cycle average size distributions (Figure 16) indicate that while the number concentrations at 55, 74 and 108 nm are very close to those determined over WHTC hot, there is an increased emission of 35 nm particles over WHTC cold, obviously associated with the formation of nucleation mode particles. Therefore, the calculated geometric mean diameter underestimates the true mean size of the accumulation mode particles, and this results in an underestimation of the mass. This underestimation can only be partly counterbalanced by the associated increase of the particle number emissions, due to the almost (because of the effective density dependence on size) cubic dependence of mass on the particle size. Nevertheless, this increase of the number concentrations is not detected with the SPCS which does not detect these small and most probably volatile particles because the sampled aerosol is thermally treated and the employed CPC has a relatively-large cut-of size (~23 nm).

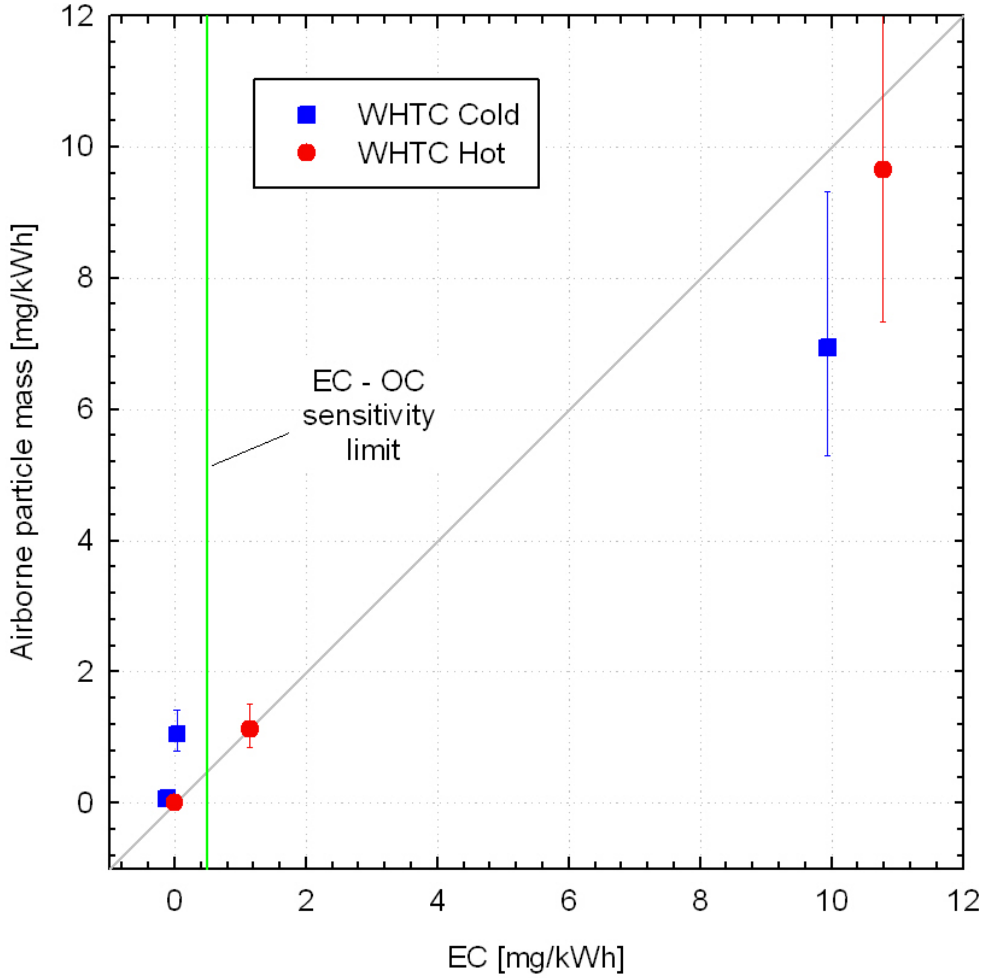

Figure 22: Comparison of the cycle average mass concentrations calculated according to equation 10 with the EC emissions.

3.2 PPMD

3.2.1 Calculations

Figure 23 illustrates a typical mass trace of a QCM crystal during an ESC mode 7 test. The response of the 8th crystal which was used as a reference (in all tests performed) is also shown. The sharp increases and decreases of the crystal response correspond to the onset (corona charger on) and the end (corona charger off) of each sampling period. The mass accumulated during each sampling period should be determined as the difference in the mass just before and just after sampling. The manufacturer's software employs a 55 s average in order to calculate the pre-sample mass and a 230 s average for the calculation of the post-sample mass to allow for a stabilization of the crystal signal. For the same reason, it also disregards the last 5 s recording before the beginning of the sampling and the first 55 s after the sampling period. However, an examination of the real time traces (like the one depicted in Figure 23) indicates that the stabilization time can be even larger. In order to investigate the effect of this assumption to the calculated masses, the calculations were performed employing all possible averaging and delay periods between 30-230 s and >10 s, respectively, using the average value as representative of the mass build up. Before doing this, the raw data were checked for spikes (that were regularly observed) which were manually removed. Any drifts due to pressure, temperature and humidity fluctuations were accounted for by means of directly subtracting the real time mass trace of the reference crystal from that of the measuring crystals. No correction for thermophoretic or diffusion losses was employed.

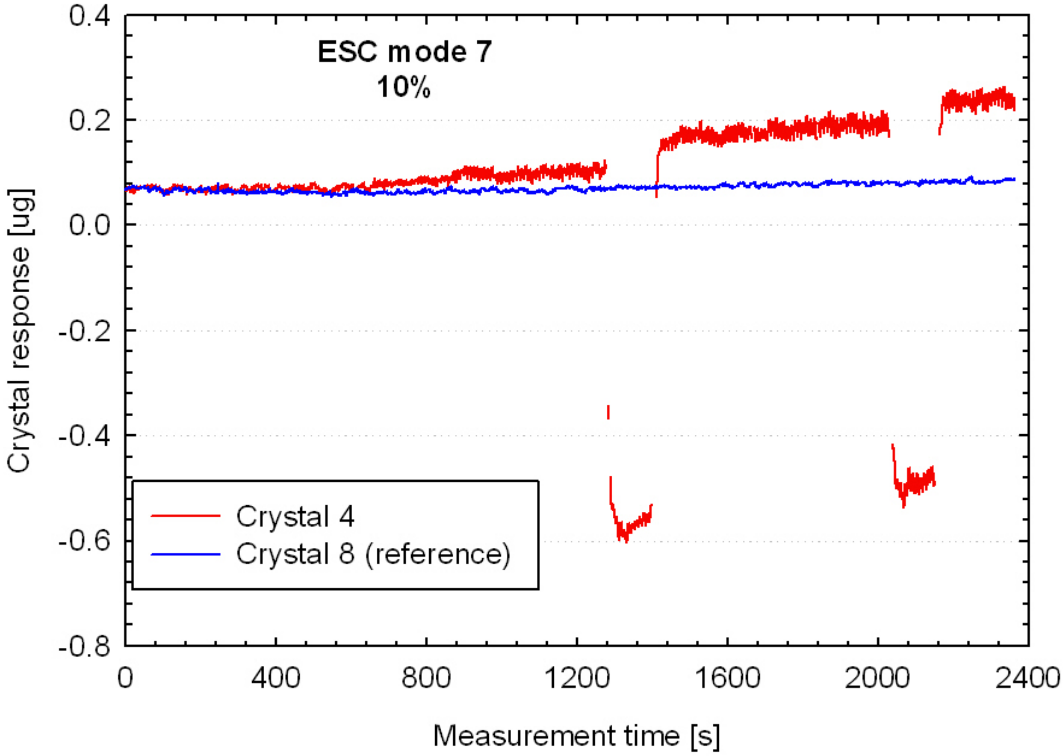

Figure 23: Example response of a QCM crystal.

3.2.2 Correlation of QCM mass to PM and EC

The cycle average mass emissions determined with QCM are compared to PM and EC in Figure 24, for transient and steady states, separately. Steady states allowed for an investigation of the crystal to crystal variability, which is illustrated in the figure as error-bars (±1 standard deviation). In the case of the WHTC results, the error bars correspond to the uncertainty introduced by the ambiguity related to the calculation of the mass loading before and after sampling.

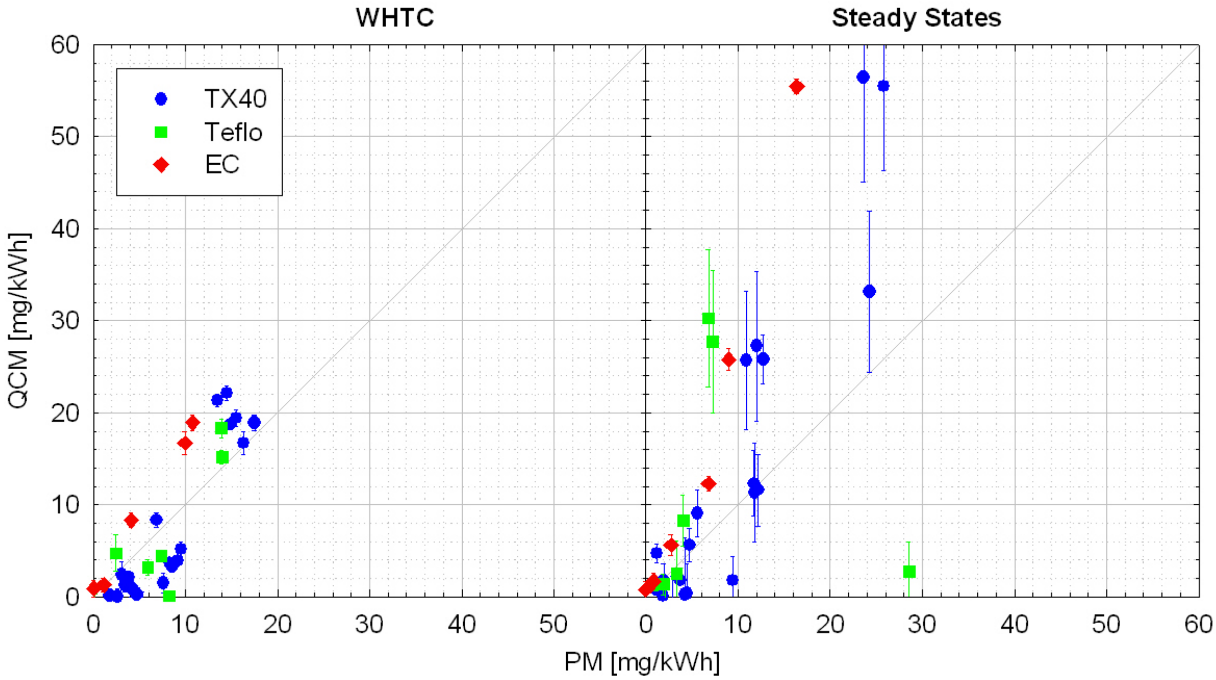

Figure 24: Comparison of the cycle average mass emission rates measured with QCM to those determined gravimetrically and the thermo-gravimetrically determined elemental carbon, over transient (left-hand panel) and steady state (right-hand panel) tests. The error bars illustrate the uncertainty in the QCM results due to the instability of the post-sample and pre-sample mass signal (transient tests) and the crystal-to-crystal differences (steady states).

QCM gave systematically higher mass emissions rates from EC for all valve positions. This is expected since the QCM also collects volatile material and perhaps adsorbed gaseous material. The results suggest a ~50% (±25%) volatile content on the quartz crystals. Figure 25 compares the QCM results to the thermo-gravimetrically determined Total Carbon (TC) emission rates from samples collected on Quartz filters. The relative difference was found to depend on the emission levels, with the QCM results being on average 60% higher at 40% valve opening and 25% higher at 10% valve opening. At lower PM levels the QCM results were lower by 50% one average at 2% valve opening and 80% at CRT out level. This dependence of the correlation on the PM levels could be explained by different adsorption mechanisms on Quartz crystals and Quartz filters.

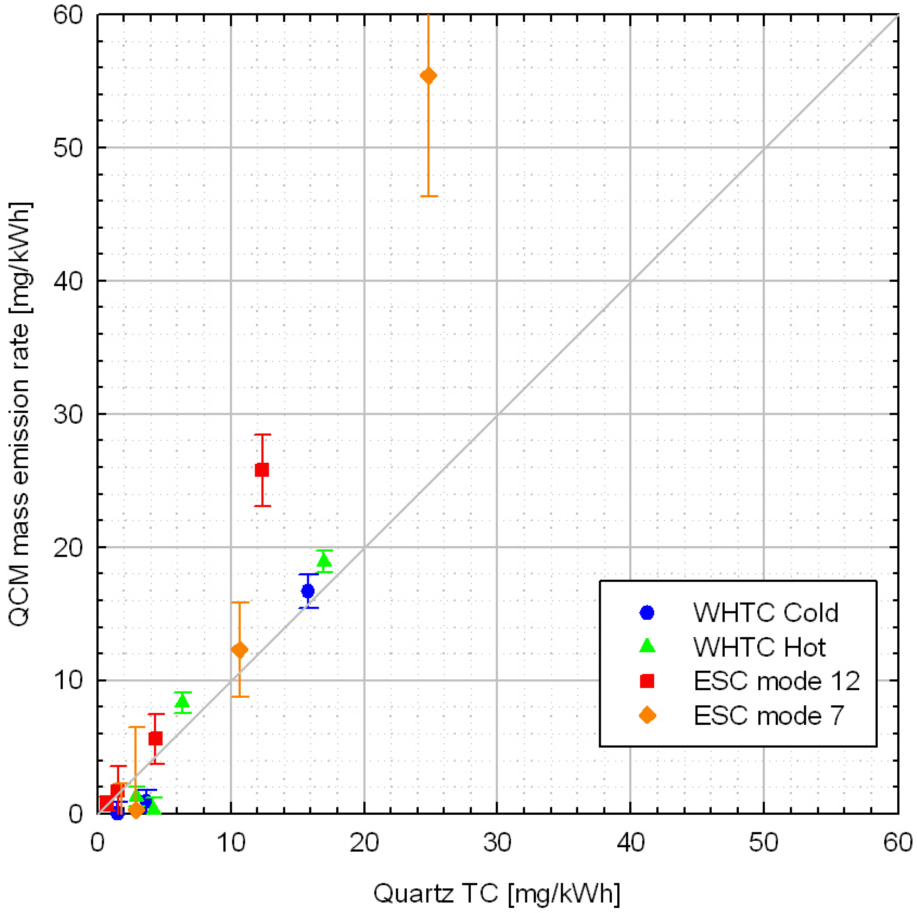

Figure 25: Comparison of the cycle average mass emission rates measured with the QCM to the thermo-gravimetrically determined total carbon from samples collected on Quartz filters.

Similar trends were also observed with TX40 filters, with the QCM measuring on average 75% higher mass at 40% valve opening, 24% lower mass at 10% valve opening, 65% lower mass at 2% valve opening and 73% lower mass at CRT out levels. Results were more consistent when using Teflo filters, with the QCM measuring on average 60% higher mass at 40% valve opening, around 10% higher mass at 10% and 2% valve opening and slightly lower (~10%) at CRT out levels. Again this behaviour is consistent with the general intuition that Teflo filters are less prone to adsorption artefacts (Chase et al. 2004). However the examination of the average differences might be equivocal due to the large scatter in the data. Individual differences ranged between -95% to 140% in the case of TX40 and between -80% and 85% in the case of Teflo. Additionally, two tests at 2% valve opening and five tests at CRT out levels resulted in negative QCM masses.

QCM results were also associated with a relatively large uncertainty. The uncertainty introduced by the ambiguity related to the selection of the averaging window for the calculation of the pre- and post-sample mass (illustrated in the WHTC results), ranged from 4% (±1%) of the measured mass at 40% valve opening to 19% (±9%) at 10% valve opening, 120% (±110%) at 2% valve opening and 540% (±900%) at CRT out levels. A relatively larger uncertainty was introduced from the crystal to crystal differences (illustrated in the steady state results) which was found to be at ~35% (±30%) of the measured values at 40% and 10% valve opening, and ~350% (±750%) at 2% valve opening and CRT out levels.

3.2.3 Correlation of the QCM mass to airborne particle mass

The results presented thus far corresponded to the cycle average emissions. Figure 26 compares the total emitted particulate mass determined with QCM to the calculated airborne particle mass over the QCM sampling periods during WHTC cold and WHTC hot, at the different emission levels examined. At 40% valve opening, the QCM crystals gave measurable quantities of mass which were generally found to follow the pattern suggested by the airborne particle mass traces at a significantly higher level though. QCM gave on average ~120% higher masses over hot WHTC and the rural and highway part of cold WHTC. Over the first 4 sampling intervals of the cold WHTC (480 s), the QCM gave systematically higher emissions averaging at a level ~270% higher than what suggested by the airborne particle mass traces. This is an indication of enhanced adsorption over this cold start part of the test cycle. A similar pattern was observed on the QCM results at 10% valve opening with the measured masses being on average ~4 times lower. Unfortunately, there is no information is available on the airborne particle mass at this emission level.

At 2% valve opening and CRT out levels, the QCM crystals reported negative masses over most part of the cycle. At a first glance this might suggest that QCM is not sensitive enough to detect the particle emissions at these low levels, at least when a 120 s sampling period is employed. However, this could also highlight the difficulties associated with the particulate mass measurements at such low emission levels where most of the PM is adsorbed material, strongly depending on the sampling conditions and the collection material/mechanism.

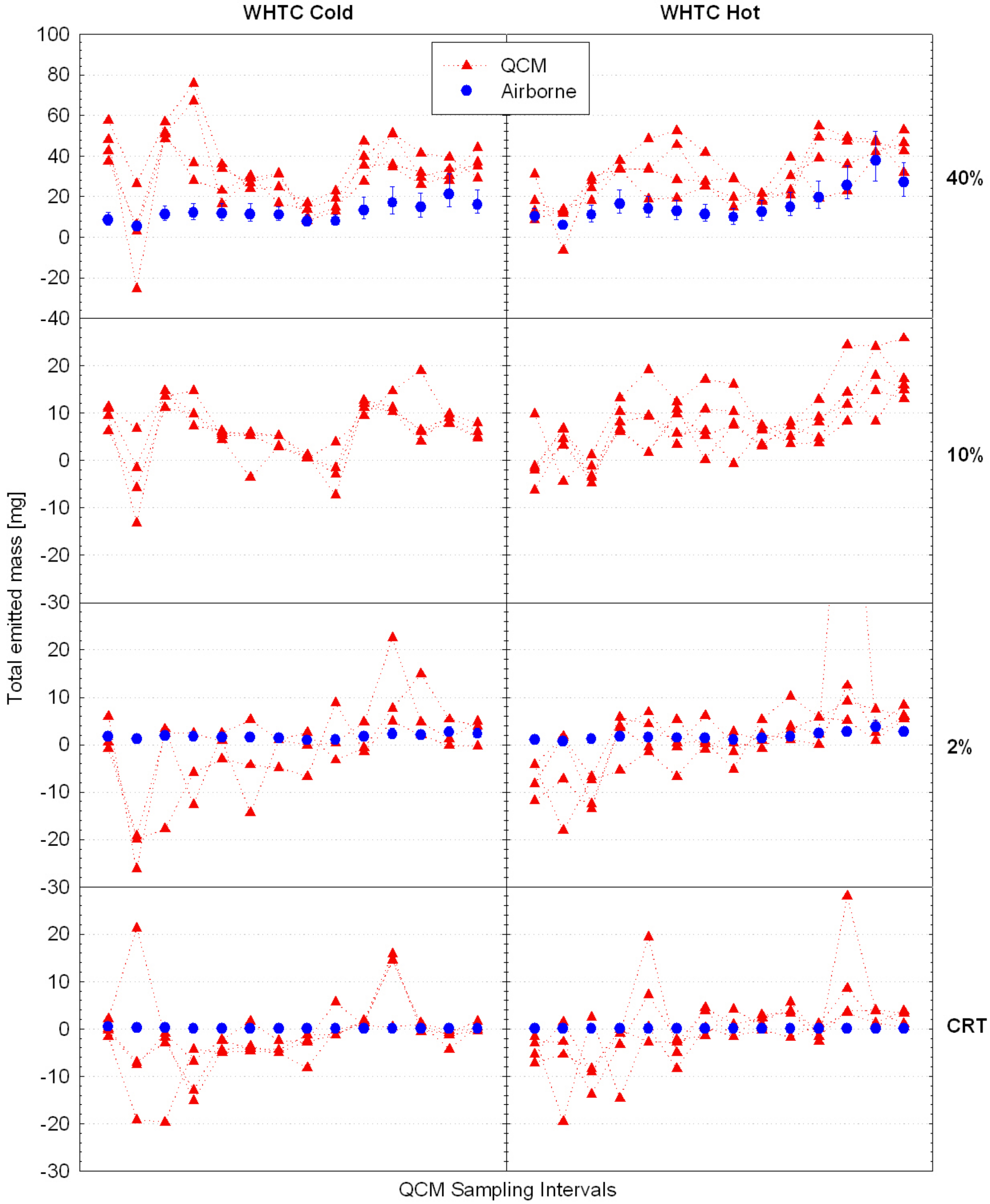

Figure 26: Comparison of the total emitted aerosol mass as determined with the QCM to the calculated airborne particle mass over the QCM sampling periods during WHTC cold and WHTC hot.

3.2.4 Crystal to crystal variability

The steady state tests allow for an investigation of the crystal-to-crystal variability. Figure 27 summarizes the mass emission rates as determined with the different QCM crystals over ESC modes 7 and 12 at the different emission levels examined. Focusing on the results at 40% and 10% valve opening which were found to be above the sensitivity limit of the QCM, it can be seen that a different behaviour is observed over ESC mode 12 and ESC mode 7 tests. However, the ESC mode 12 data might not be suitable for this kind of checks due to the gradual increase of the nucleation mode particles observed in all tests. This increased production of nucleation mode particles can not per se justify an increase in the particle mass emissions due their small size. However this enhanced nucleation suggests increased emission of gaseous precursors that could potentially adsorb on the quartz crystals. The same sequence of crystal changes was employed in all ESC mode 12 tests, with crystal 2 being the first to sample, followed by crystals 3, 4, 5 and so on. All these tests suggested a gradually increasing mass.

On the other hand, the particle emissions were much more stable over ESC mode 7 (as suggested by all real time aerosol instrumentation employed). Looking again at the 40% and 10% valve opening results, some pattern can be revealed on the responses of crystals 3 to 6. This was not the case for crystals 1, 2 and 7.

It is also worth noting that the tests conducted without greasing the crystals yielded similar results to those in which the crystals were greased, at all emission levels examined. This suggests that greasing (and the associated, time-consuming, burning procedure) is not really necessary, at least at the examined emission levels.

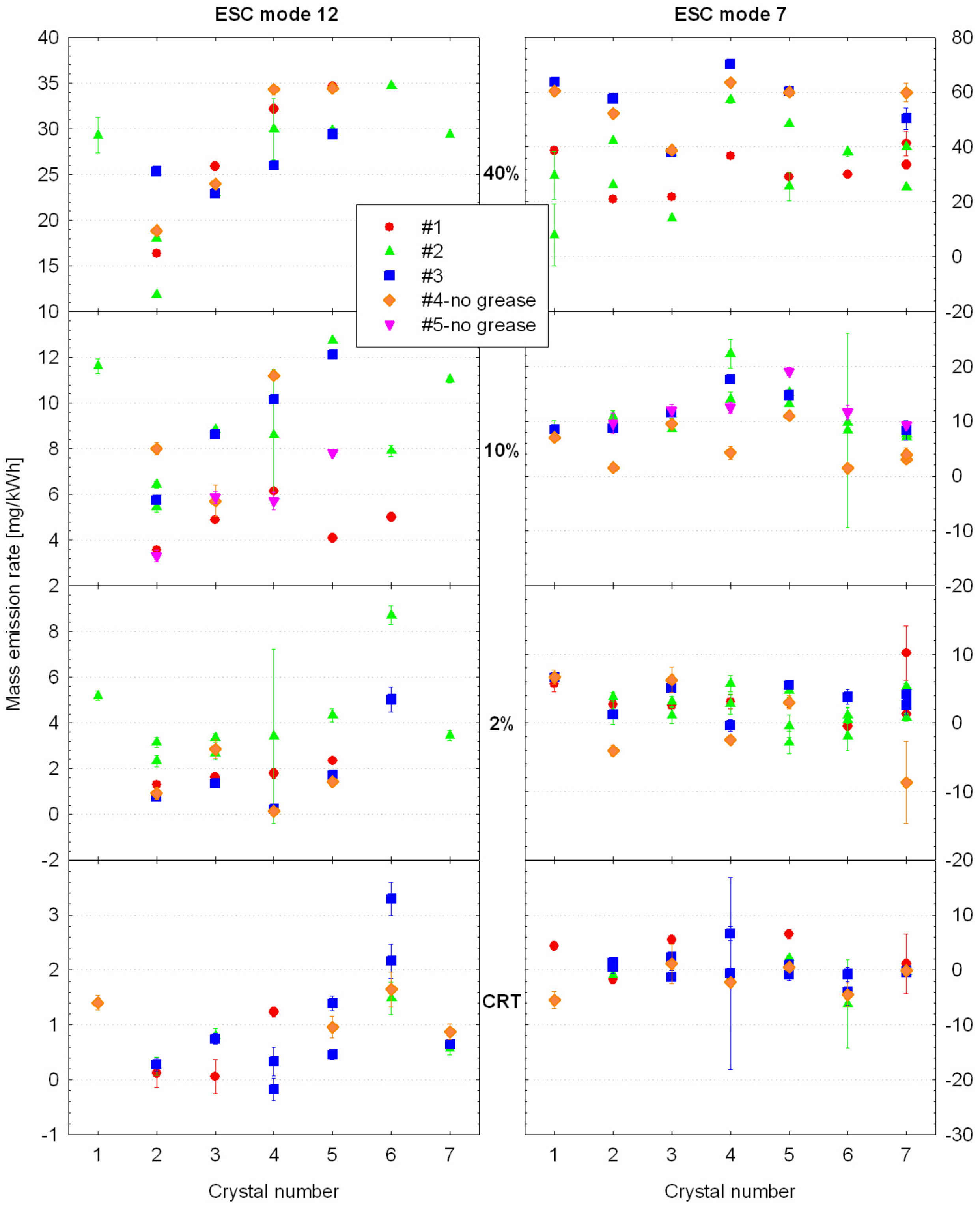

Figure 27: Comparison of the different crystal responses over steady state testing.

3.2.5 Effect of Relative Humidity

An examination of the instrument signal showed that the crystal responses are very sensitive to the fluctuations of the ambient relative humidity. As an example, Figure 28 compares the time evolution of the ambient relative humidity (as measured inside the Sensor's PPMD) and the responses of three crystals that were not sampling during the particular test. It can be seen that the changes in ambient relative humidity have a strong effect on the crystal signal. What is more important, however, is that each crystal behaves differently. This suggests that the QCM results will also depend on which crystal was employed as a reference. It seems that it is absolutely necessary to condition the air sampled through the crystals during their stabilization phase (by-pass air line).

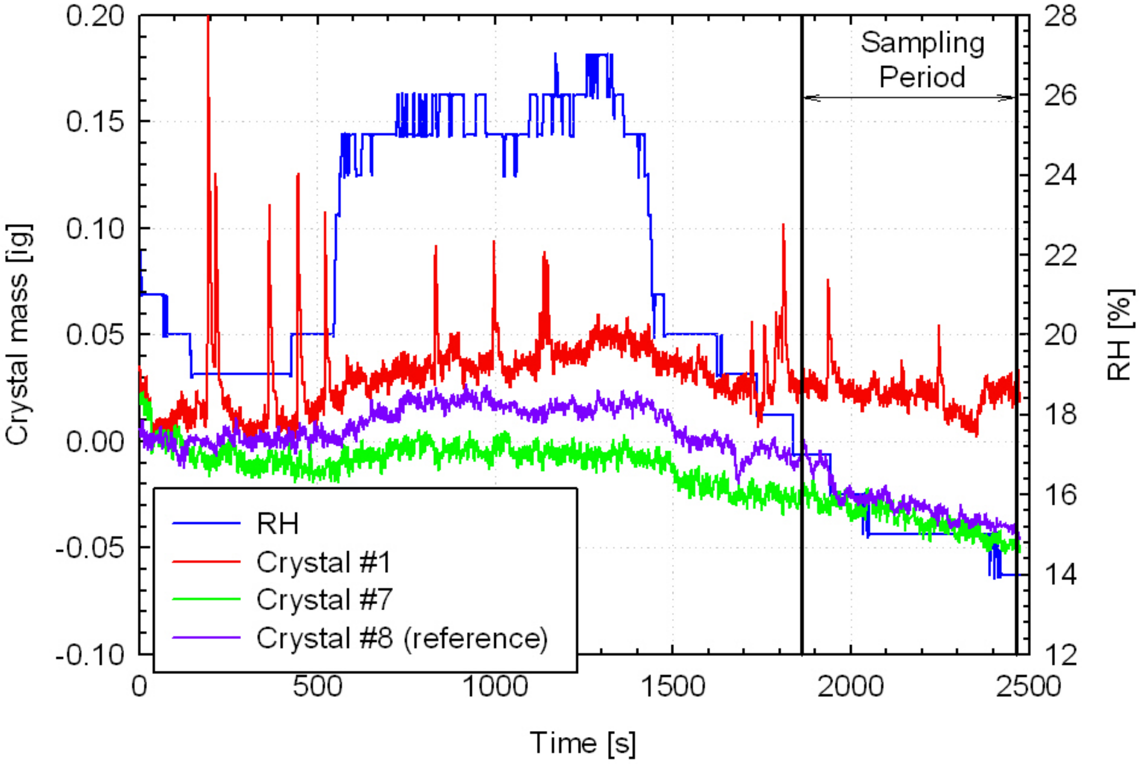

Figure 28: Influence of ambient relative humidity fluctuations to QCM crystal responses.

3.2.6 Checks with PAO droplets

A limited number of tests have been conducted using a polydisperse PAO aerosol. The aerosol generated by the PAO generator was fed in parallel to the TSI's 3936 SMPS and the Carousel QCM. The two instruments were sampling from excess flow at almost ambient pressure. The sample flowrate of the active crystal was measured with a bubble flow meter and found to be 0.49 lpm. Due to the sticky nature of these particles and the relatively low concentrations examined, no greasing of the crystals was employed. Two concentration levels were examined (achieved by means of diluting the produced aerosol in a dilution bridge) and the duration of each test was ~1700 s which was sufficient for all 7 crystals to be employed twice at a sampling period of 120 s.

The PAO particles are spherical in shape having a known density of 0.82 g/cm^3. Therefore, if the number weighted size distribution is known it is possible to calculate the mass weighted size distribution and therefore the total airborne mass. One difficulty however of this approach is that the unavoidable noise in the CPC response can introduce a large uncertainty at the upper part of the size distribution, due to the dependence of mass on the cube of the particle size. A possible way around this is to fit a lognormal distribution on the right side of the measured size distributions. Figure 29 compares the mass weighted size distributions determined with these two approaches. An estimate of the noise level (corresponding to 0.5 #/cm^3 CPC reading) is also included in the figure.

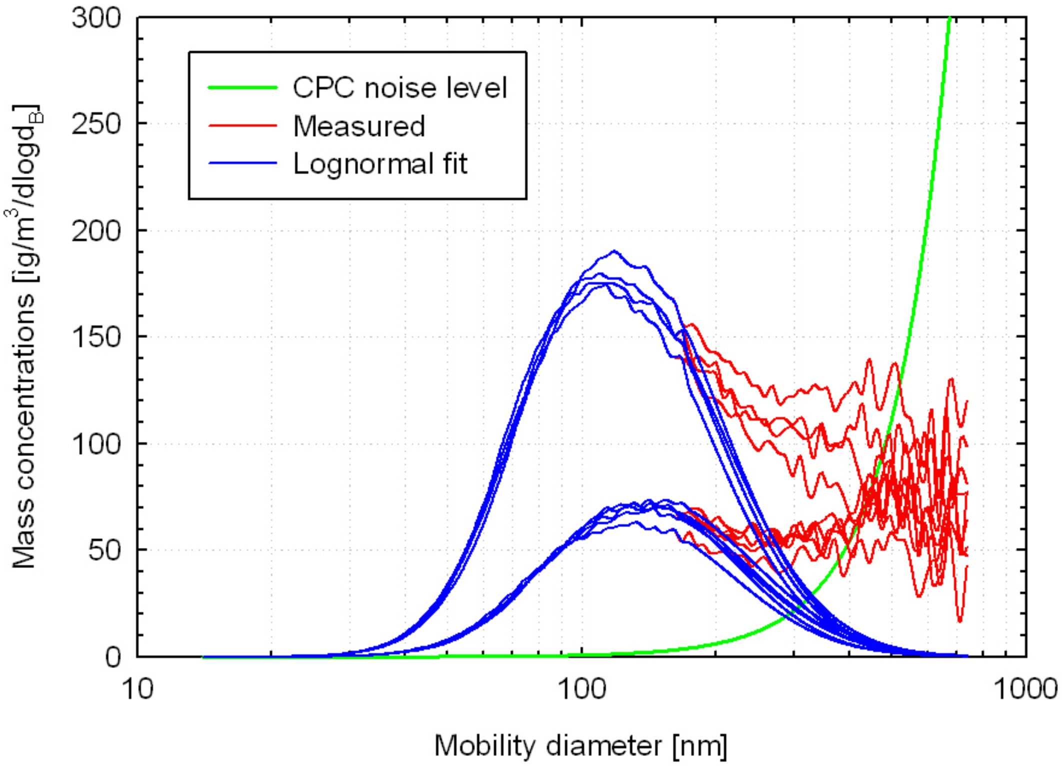

Figure 29: Mass weighted mobility size distributions of the PAO aerosol employed for the QCM checks. Due to the unavoidable noise at the upper size of the size distributions (green curve) a lognormal distribution (blue curves) was fitted to the right side of the measured size distributions (red curves).

Figure 30 compares the PAO mass concentrations measured with the different QCM crystals to those determined from the SMPS distributions following the two approaches described above. At the low concentration levels examined (~40 μg/m^3), almost all QCM tests resulted in negative masses. Four single tests gave mass concentrations very close to what was calculated from the lognormal fit on the SMPS distributions. The vapour pressure of the PAO particles is reported to be ~0.13 kPa (that is close to that of decahexane and much higher than that of diesel nucleation mode particles (~6.7×10^{-6} Pa – Mathis et al. 2004)). It is not clear to what extent this relatively high vapour pressure could have affected the measurements. Some additional investigations are required employing a less volatile material like tetracontane.

At a concentration level of approximately 100 μg/m^3, the average mass concentration determined from all crystals was ~135 μg/m^3. However, a large variation was observed from crystal to crystal and also between repetitions. Additionally, the pattern was different from that seen on the ESC mode 7 tests (Figure 27).

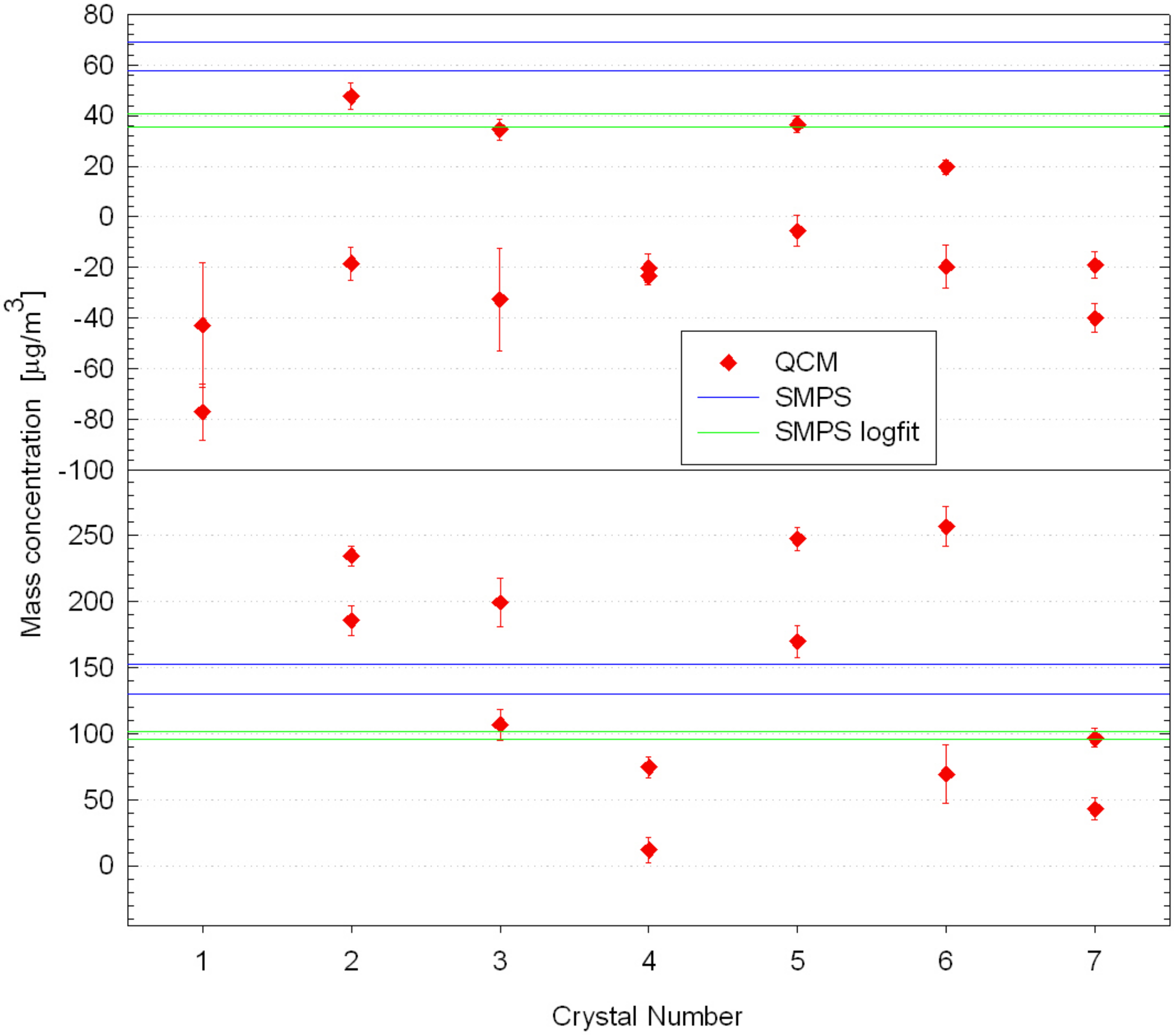

Figure 30: Comparison of the mass concentrations measured with the different QCM crystals to those calculated from the SMPS distributions. In the latter case, the bounds corresponding to the maximum and minimum mass concentration determined over 5 consecutive 300 s scans are shown. Blue lines correspond to the results calculated by means of directly calculating the mass from the measured distributions while green ones to those determined after fitting a lognormal distribution to the upper part of the measured distributions.

3.3 MSS AND GFB

3.3.1 GFB results

The PM emissions determined with the AVL Gravimetric Filter Box are compared to those measured in the CVS tunnel and the reference partial flow system (SPC) in Figure 31. Focusing on the TX40, it can be seen that the filter box gave systematically higher PM emissions, and there appears to be a detection limit of ~10 mg/kWh. The relative differences from SPC increased from 67% (±30%) at 40% valve opening and 46% (±39%) at 10% valve opening to 150% (±113%) at 2% valve opening and 291% (±169%) at CRT out levels. Similar differences were observed from the CVS results, ranging from 27% (±20%) at 40% valve opening to 420% (±258%) at CRT out levels. The most plausible cause of this discrepancy appears to be the very low sample flowrate employed in the filter box (~ 5 lpm). As the emission levels decrease, the contribution of adsorbed material to the collected mass becomes increasingly important. The adsorption mechanism however is quite complicated. In case the filter gets saturated in vapours during the test cycle, the calculated PM will be proportional to the inverse of the total volume sampled. In that case the use of a six times lower flowrate in the Filter box results would result in a 500% higher PM value, which is close to what has been determined at CRT out emission levels.

The use of Teflo filters resulted in a generally better agreement, with the differences from the CVS ranging from 4% (±50%) at 40% valve opening, to 79% (±110%) at 10% valve opening, -47% at 2% valve opening and 46% (±71%) at CRT out levels. This is in agreement with the interpretation given in the previous paragraph, as the Teflo filters are known to be less prone to adsorption artefacts.

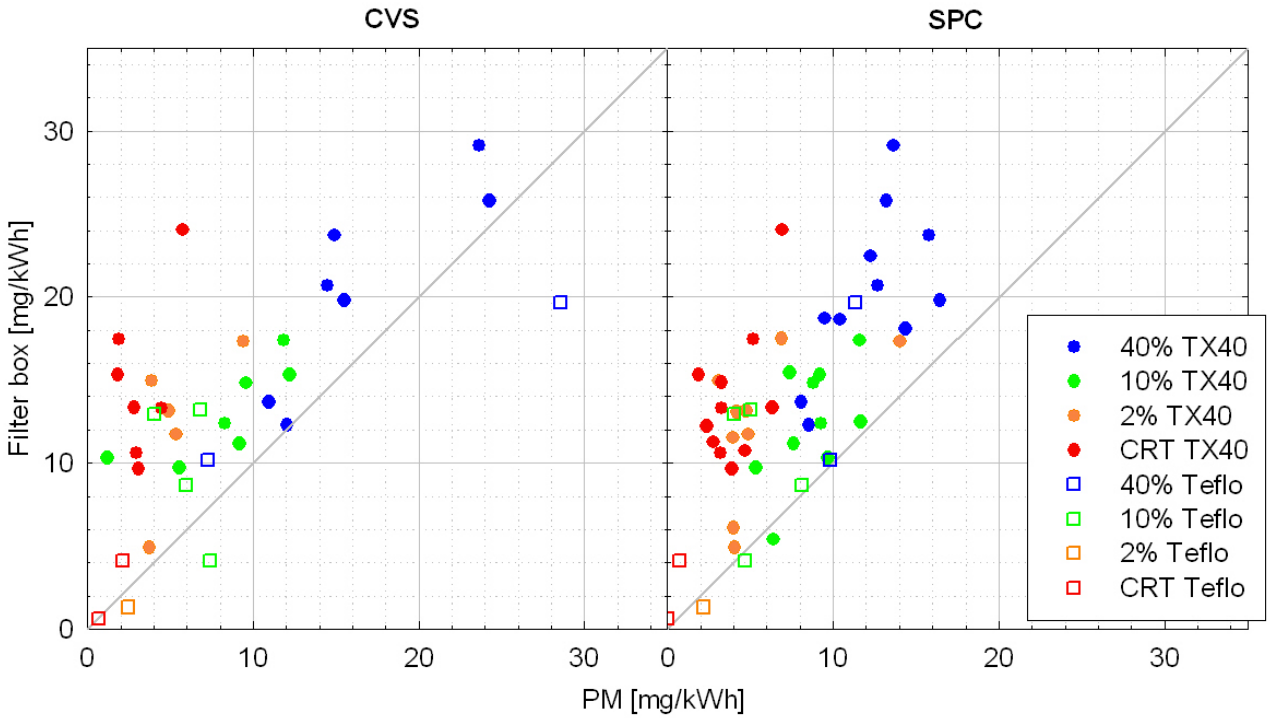

Figure 31: Comparison of the PM emissions measured with the AVL filter box to those measured in the CVS tunnel (left-side panel) and the SPC (right side panel).

3.3.2 MSS results

The cycle average mass emission rates of soot as measured with the MSS of the AVL system are compared to the PM results from CVS and SPC and the thermo-gravimetrically determined elemental carbon emissions in Figure 32. The MSS results were generally found to be in good agreement with EC. The relative difference was -10% (±4%) and 2% (±11%) at 40% and 10% valve opening, respectively. At lower emission levels, the EC collected on the quartz filters was at or bellow the detection limit of the methodology (~0.5 mg/kWh). The two single points above this threshold (1.15 mg/kWh and 0.83 mg/kWh) were found to be in reasonable agreement (differences smaller than ~60%) given the low emission levels.

The gravimetrically determined mass emission rates were systematically higher as the MSS only detects the soot content of PM. In the case of TX40 filters, the relative difference from the SPC system PM (which can also be interpreted as the volatile content of PM) increased from -33% (±7%) at 40% valve opening to -39% (±72%) at 10% valve opening, -70% (±7%) at 2% valve opening and -84% (±7%) at CRT out levels. Similar differences were observed from the PM emissions measured from the CVS tunnel, spanning from -11% (±17%) at 40% valve opening to -87% (±7%) at CRT out levels.

The differences were lower when Teflo filters were employed to collect PM. For example, the differences from the PM measured in the CVS ranged from -26% (±35%) at 40% valve opening, to -30% (±11%) at 10% valve opening, -40% at 2% valve opening and -15% (±123%) at CRT out levels. This again suggests lower adsorption artefact on the Teflo filters.

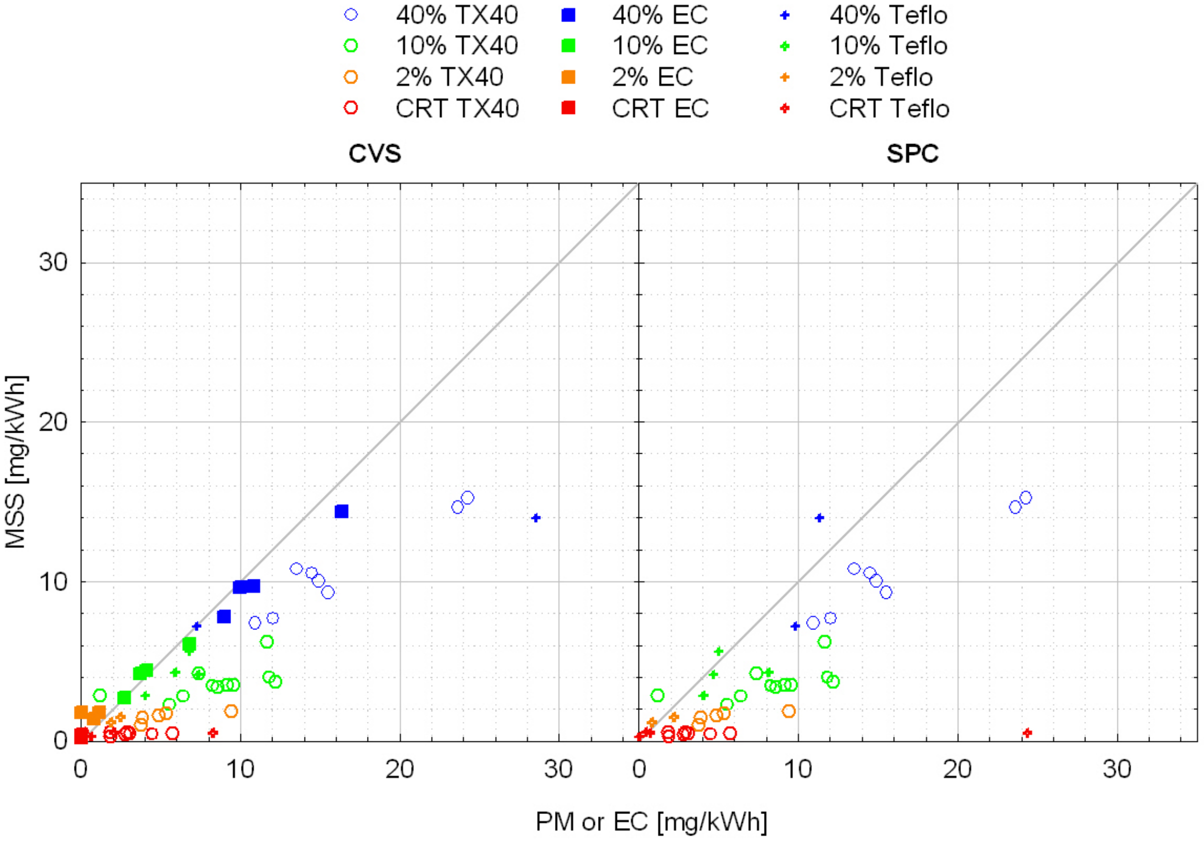

Figure 32: Comparison of the cycle average soot mass emission rates measured with Soot Sensor with PM and the thermo-gravimetrically determined EC.

A second, JRC owned, MSS was measuring in parallel with that of the AVL system in some tests. The cycle average results obtained from the two systems are compared in Figure 33. A very good agreement was observed at emission levels down to 2% valve opening. The relative differences ranged from 5% (±3%) at 40% valve opening to 0% (±3%) at 10% valve opening and -6% (±11%) at 2% valve opening. CRT out levels were close to the detection efficiency of the MSSs and this resulted in a relatively larger difference (-31% ±11%). Even though each MSS utilized a different conditioning unit it is not expected that this had affected the comparisons as the operation of the conditioning unit is not expected to depend on the emission levels. The average exhaust concentrations at CRT out levels measured by the AVL MSS were ~50 µg/m^3 at a dilution ratio of about 6, that corresponds to approximately 10 µg/m^3 at the MSS inlet. The reported detection efficiency of the MSS is 5 µg/m^3.

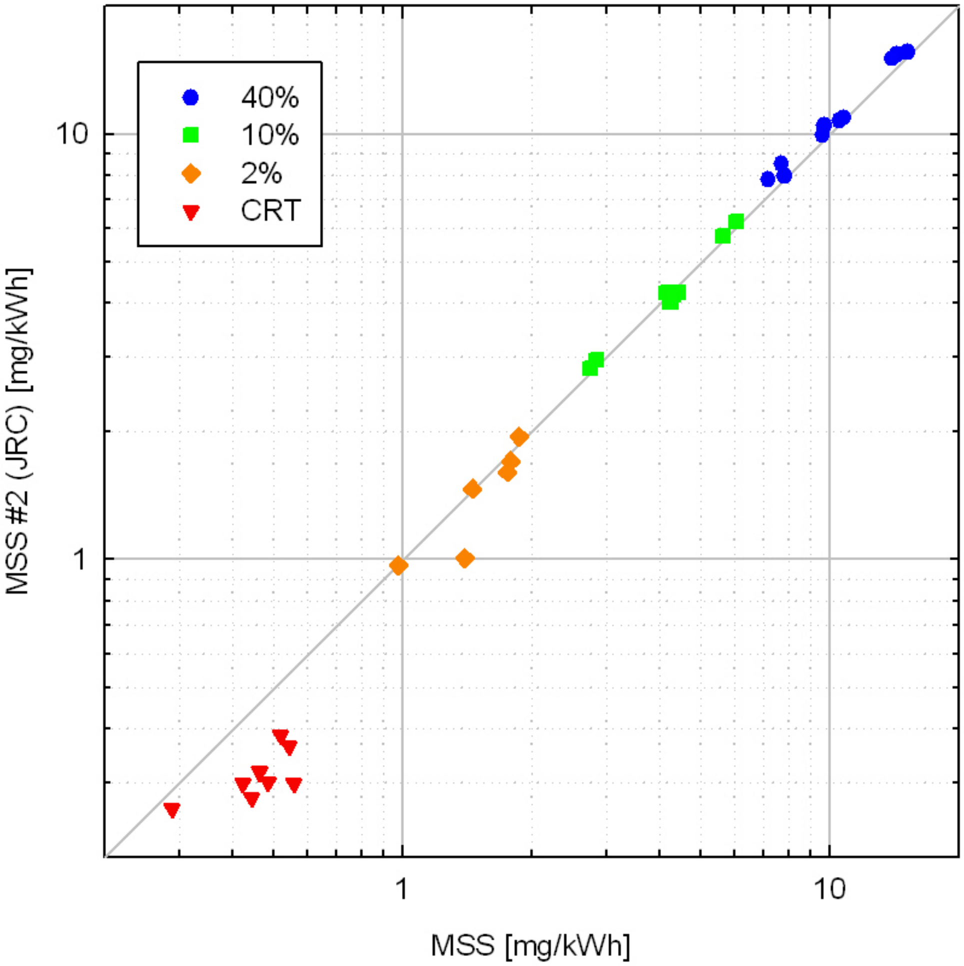

Figure 33: Comparison of the cycle average mass emission rates measured with the two MSSs.

Figure 34 compares the cycle average mass emission rates of soot to the calculated airborne particle mass. A very good agreement was observed down to emission levels corresponding to 2% valve opening. The relative difference was -5% (±10%), -4% (±16%) and 24% (±17%) at 40%, 10% and 2% valve opening, respectively. At CRT out levels however, it seems that the MSS had reached its detection limit which is around 0.3 mg/kWh when a constant dilution ratio of 6 is employed in the conditioning unit.

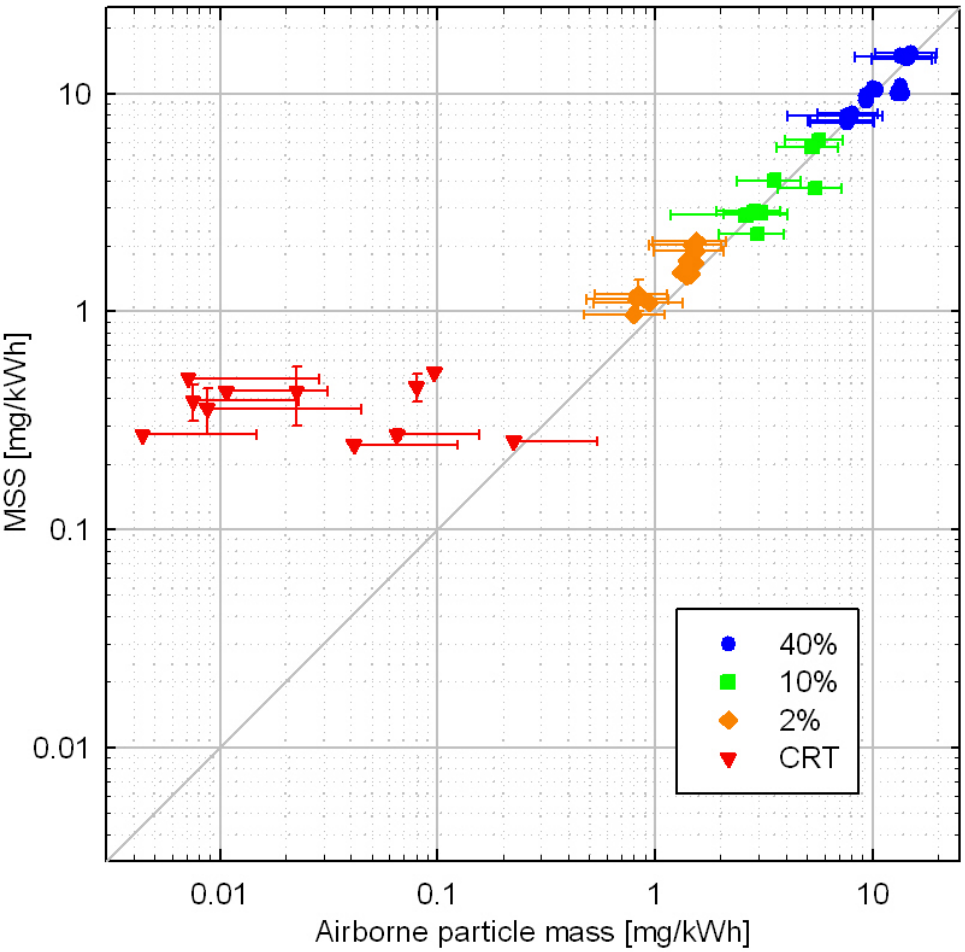

Figure 34: Comparison of the cycle average mass emission rates of soot measured with the MSS to the mass of airborne particles.

Some useful information on the performance of the MSS can be drawn when examining the real time traces of the soot sensor. Figure 34 compares the real time mass emission rates of soot and airborne particle mass. The measured detection efficiency of the MSS, determined by means of filtering the diluted sample entering the JRC owned MSS unit with an HEPA filter, is also shown for comparison. It can be seen that down to emissions corresponding to 2% valve opening, the traces of the MSS are in good agreement with that of the airborne particle mass, and well above the detection efficiency of the instrument. At CRT out levels however and with the exception of the first 400 s of the cold start WHTC, the MSS response is found to be slightly above the detection efficiency of the instrument which is up to 2 orders of magnitude higher the airborne particle mass.

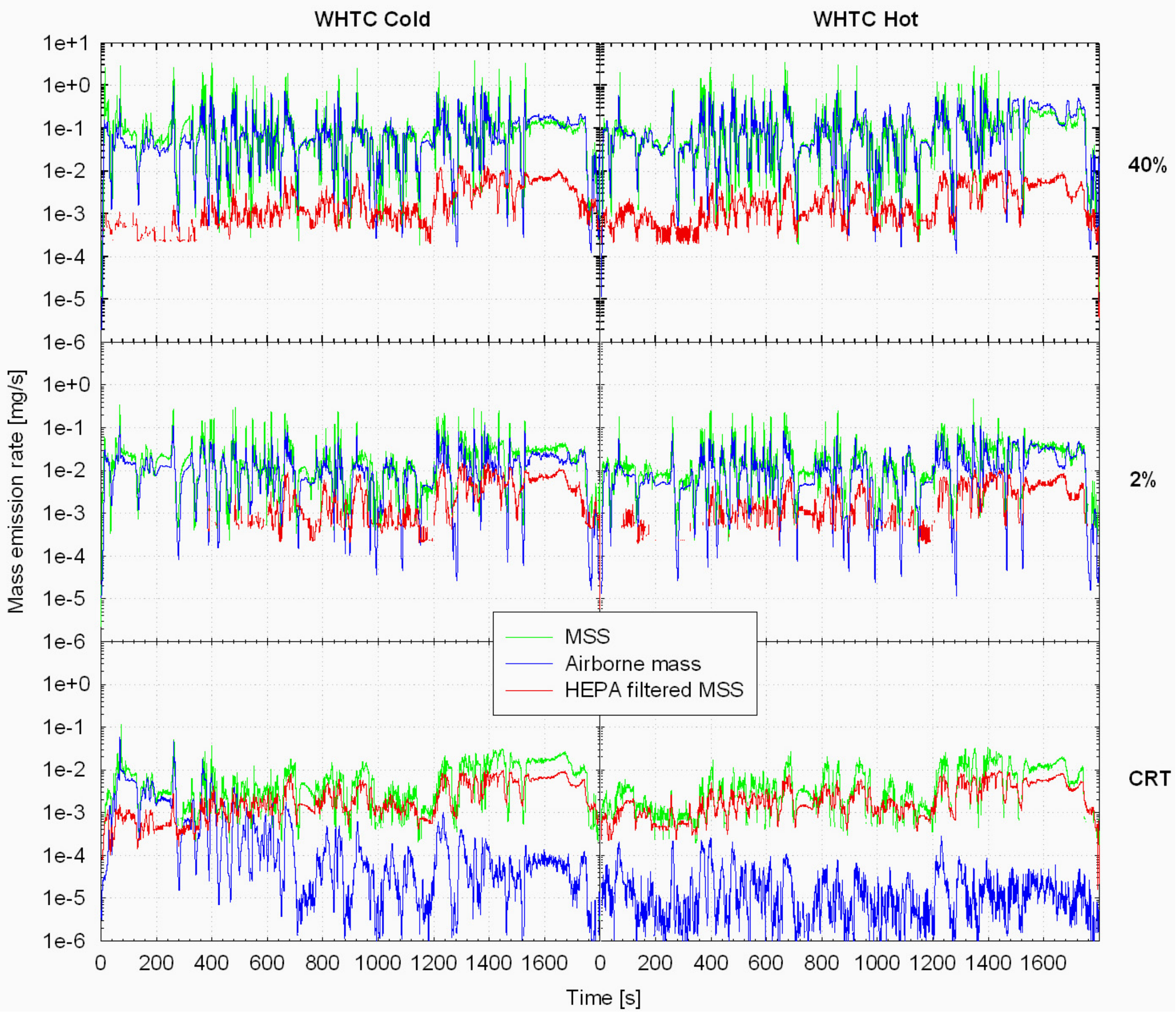

Figure 35: Real time mass emission rates of soot and airborne particles over WHTC cold and WHTC hot at the different emission levels examined.

An examination of the real time responses of the MSS when sampling HEPA filtered samples revealed a pattern that followed the exhaust flowrate which however was generally below the specified detection limit of the instrument (5 ug/m^3). In order to investigate whether this is related to a cross-sensitivity of the MSS to non-soot components of the exhaust, some measurements of HEPA filtered samples employing a lower dilution ratio were performed. Figure 36 compares the MSS responses to HEPA filtered samples over WHTC hot at dilution ratios of 6 and 2. It can be seen that the soot sensor response scales with the inverse of the dilution ratio. This indicates that there exists some interference from some non-soot components in the diesel exhaust. For the particular engine considered, this can lead to an artefact that can reach up to six times the detection limit of the instrument depending on the dilution ratio. This is relatively small but needs to be considered when testing CRT equipped vehicles.

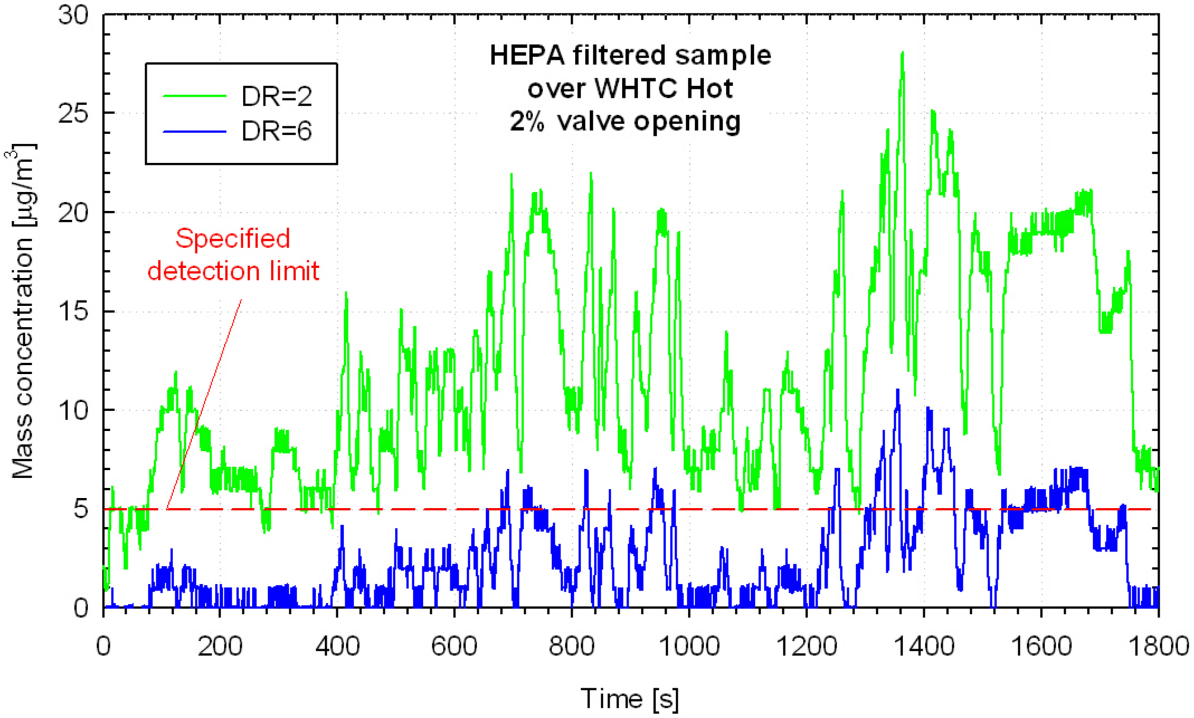

Figure 36: Comparison of the HEPA filtered soot sensor responses over WHTC hot to the specified detection limit of 5 ug/m^3 at dilution ratios of 2 and 6.

3.4 DMM

3.4.1 Correlation with PM

Figure 37 compares the cycle average mass emission rates measured with the DMM to PM and EC as determined from samples collected from the CVS tunnel. The results for the tests in which the DMM was sampling downstream a thermodenuder (left panel of Figure 37) have been corrected assuming an average 73% penetration based on the results of Giechaskiel et al. 2009b.

According to its principle of operation, the DMM is measuring the mass of airborne particles which has found to be very similar to that of EC (Figure 19). The DMM results however were found to be around 90% (±30%) higher than the EC. As it will be shown later, this was partly due to a underestimation of the actual charger efficiency and most importantly due to fouling of the impactors which is estimated to have happen at the very beginning and has thus affected all the measurements.

On the other hand the correlation between the DMM and PM is affected by the quantity of adsorbed material on the filters. In the case of TX40 filters, the relative difference varied from +43% (±8%) at 40% valve opening, to -14% (±15%) at 10% valve opening, 47% (±116%) at 2% valve opening and -96% (±4%) at CRT out levels. The corresponding figures in the case of Teflo filters were 58% (±47%), 43% (±39%), 26% (±14%) and -93% (±13%), respectively, thus suggesting less adsorbed material.

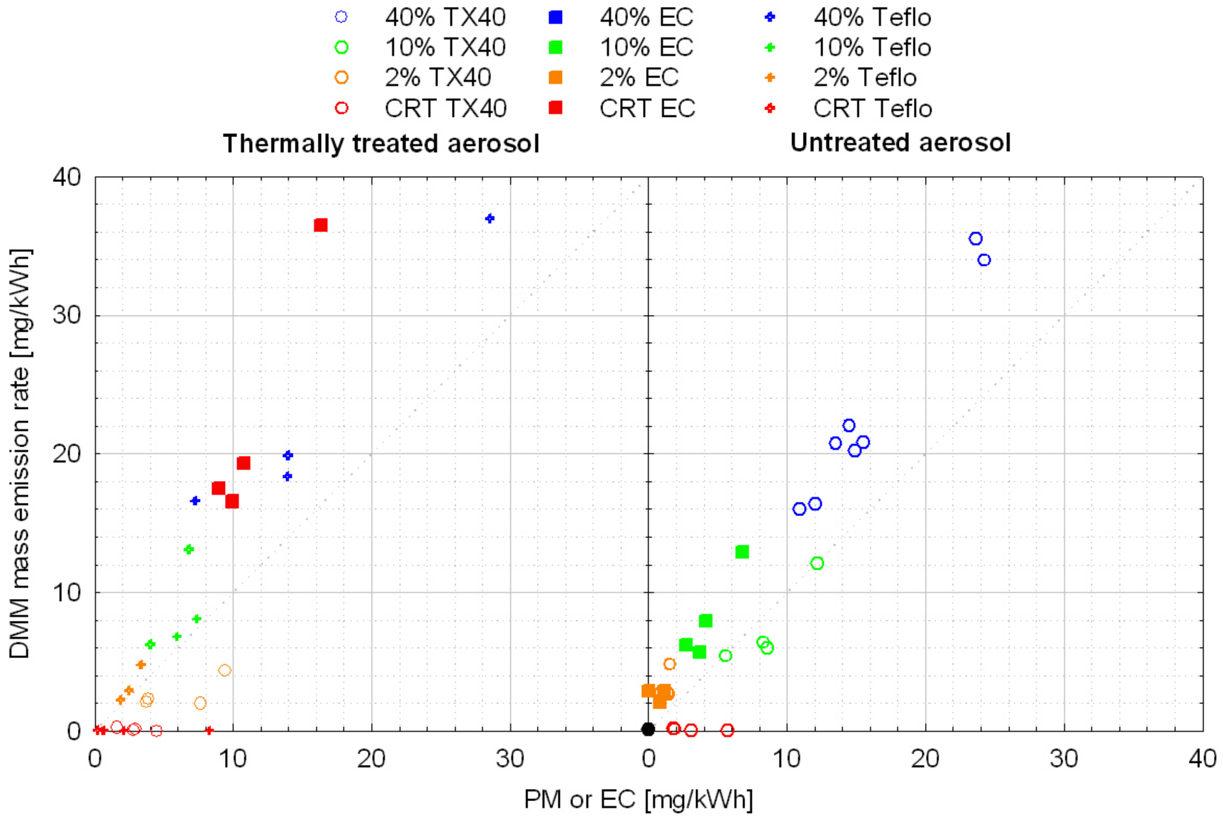

Figure 37: Comparison of the cycle average mass emission rates measured with the DMM to the gravimetrically determined PM and the thermo-gravimetrically determined EC for samples collected from the CVS tunnel. The left panel corresponds to thermally treated DMM samples while the right panel to non-thermally treated DMM samples.

3.4.2 Correlation with airborne particle mass

As already stated, the DMM measures the mass of airborne particles. Therefore the DMM results should be directly comparable to those calculated by means of combining the SMPS and SPCS data. Figure 38 compares the mass emission rates of airborne particles determined using these two approaches. It can be seen that the DMM systematically overestimated the mass of airborne particles. The average difference in the case of thermally treated samples ranged from 103% (±48%) at 40% valve opening, to 118% (±29%) at 10% valve opening, 135% (±61%) at 2% valve opening and 508% (±858%) at CRT out levels.

Similar differences were observed when the DMM sample was not thermally treated. The corresponding figures were 104% (±33%) at 40% valve opening, to 117% (±24%) at 10% valve opening, 143% (±56%) at 2% valve opening and 395% (±460%) at CRT out levels. This agreement between thermally treated and non-thermally treated results suggests that the presence of nucleation mode particles (at least at the levels encountered with this engine/after-treatment) does not affect the DMM mass results.

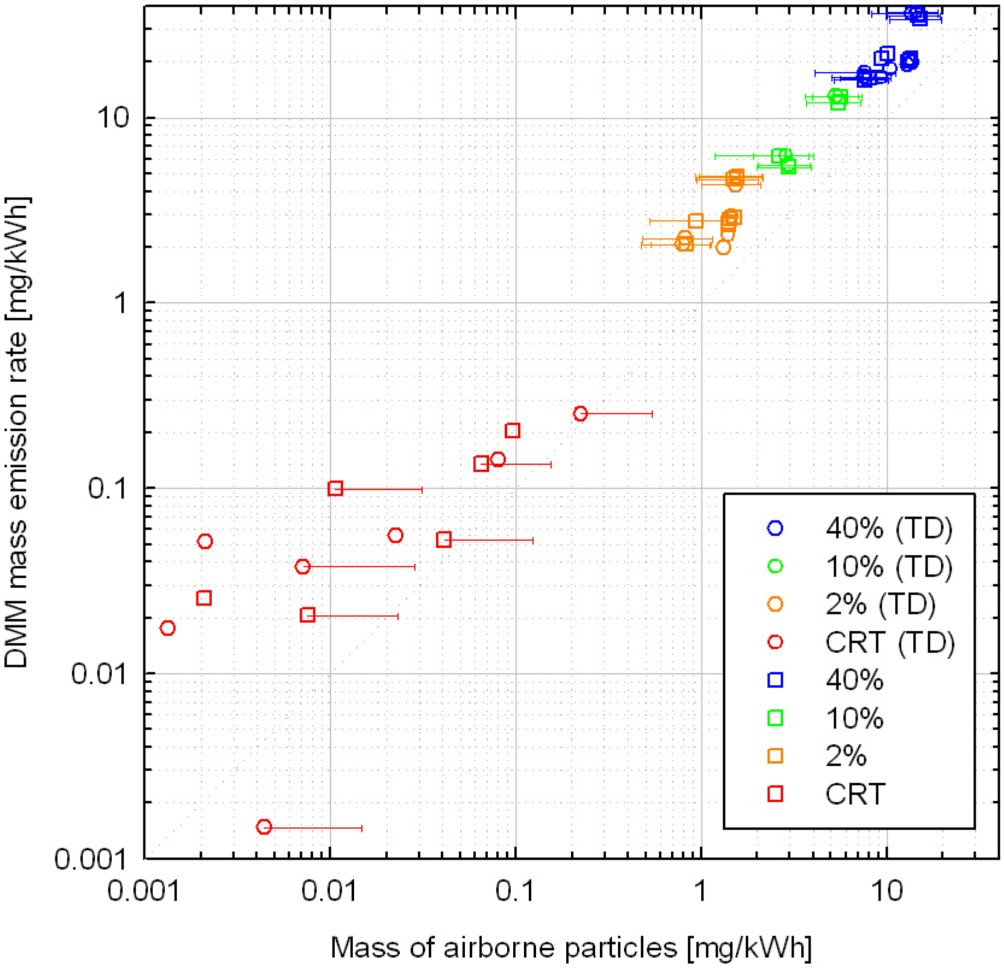

Figure 38: Comparison of the mass emission rates of airborne particle mass measured with the DMM to those calculated using the SMPS/SPCS data.

The real time mass emission rates of airborne particles determined with the two approaches are compared in Figure 39. Similar traces were observed down to emission levels corresponding to 2% valve opening with the DMM giving systematically higher emissions over the entire cycle. The CRT out levels however, with the exception of the first 600 s under cold start, were found to be below the detection limit of the DMM which was quantified to be ~0.6 μg/s at the configuration employed in this campaign (that is sampling from the CVS tunnel).

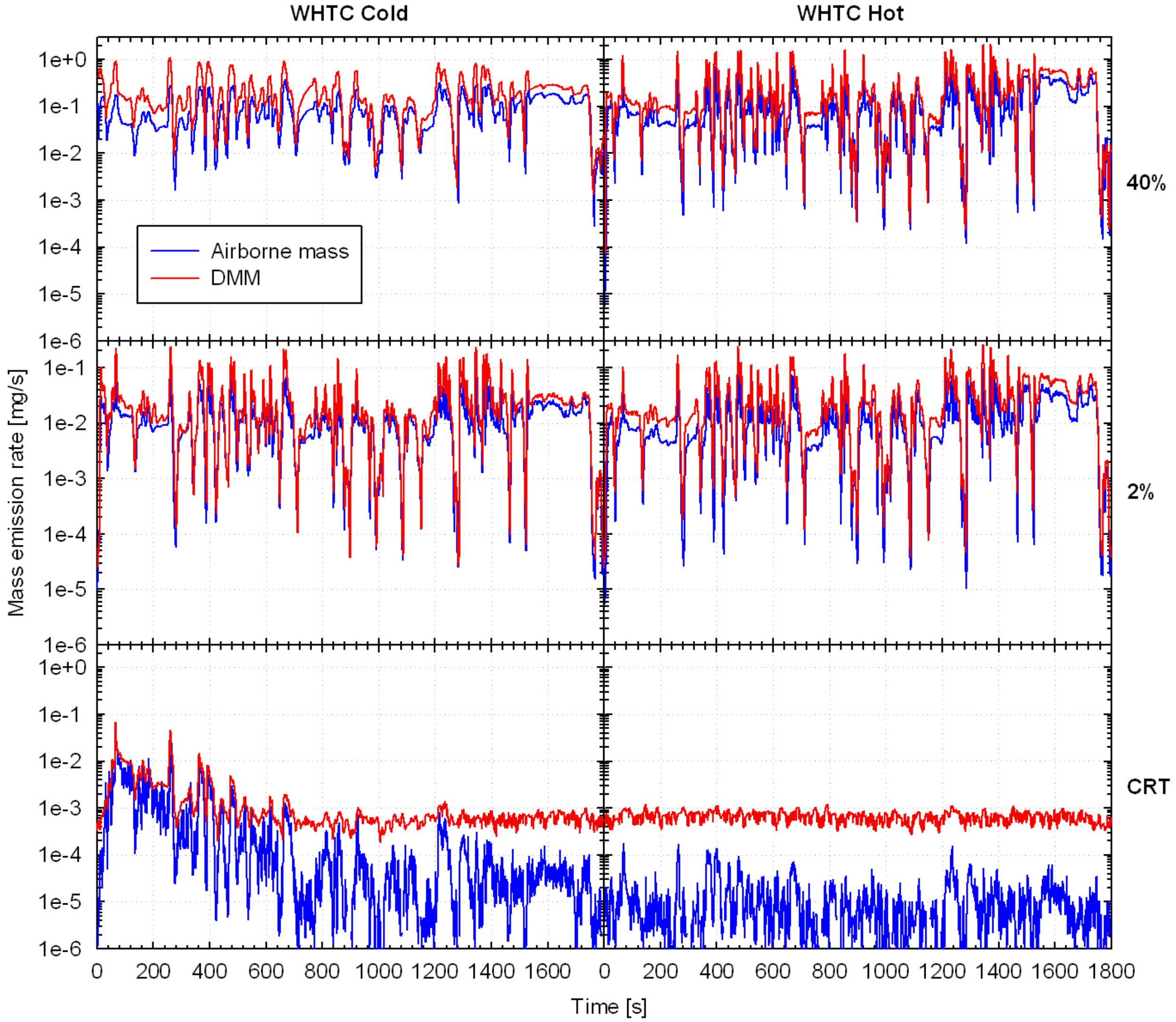

Figure 39: Real time mass emission rates of airborne particles over WHTC cold and WHTC hot as measured with the DMM and calculated by means of combining the SMPS/SPCS data.

3.4.3 DMM number results

An interesting feature of the DMM is that in addition to mass it also provides the number emissions. Figure 40 compares the number emission rates measured with the DMM with those measured with the SPCS connected to the CVS (for thermally treated aerosol) and those measured with the SMPS (for non-treated aerosol).

In the case of thermally treated aerosol, the DMM yielded systematically higher number emission rates with the difference ranging from 197% (±101%) at 40% valve opening, to 300% (±114%) at 10% valve opening and 220% (±104%) at 2% valve opening. At CRT out levels were the DMM reached its sensitivity limit which was around 1×10^{11} #/kWh. These large differences might be related to the severe fouling of the impactors described in the next section which according to Maricq et al. (2006b) will have a disproportionally higher effect on the calculated number concentrations.

A better agreement was observed with the number concentrations measured with the SMPS, with the difference ranging from 10% (±5%) at 40% valve opening, to -26% (±48%) at 10% valve opening and 11% (±29%) at 2% valve opening. This agreement however, mostly results from the different size ranges covered by the two instruments. The last impactor stage of the DMM has a nominal aerodynamic cutoff size of 30 nm which is close to that of the SPCS (23 nm mobility size) but much higher than that of the SMPS (7.6 nm mobility at the configuration employed). The size distributions (Figure 16) suggest that a significant amount of particles (30% to 100% depending on the magnitude of the nucleation mode) are found below 30 nm.

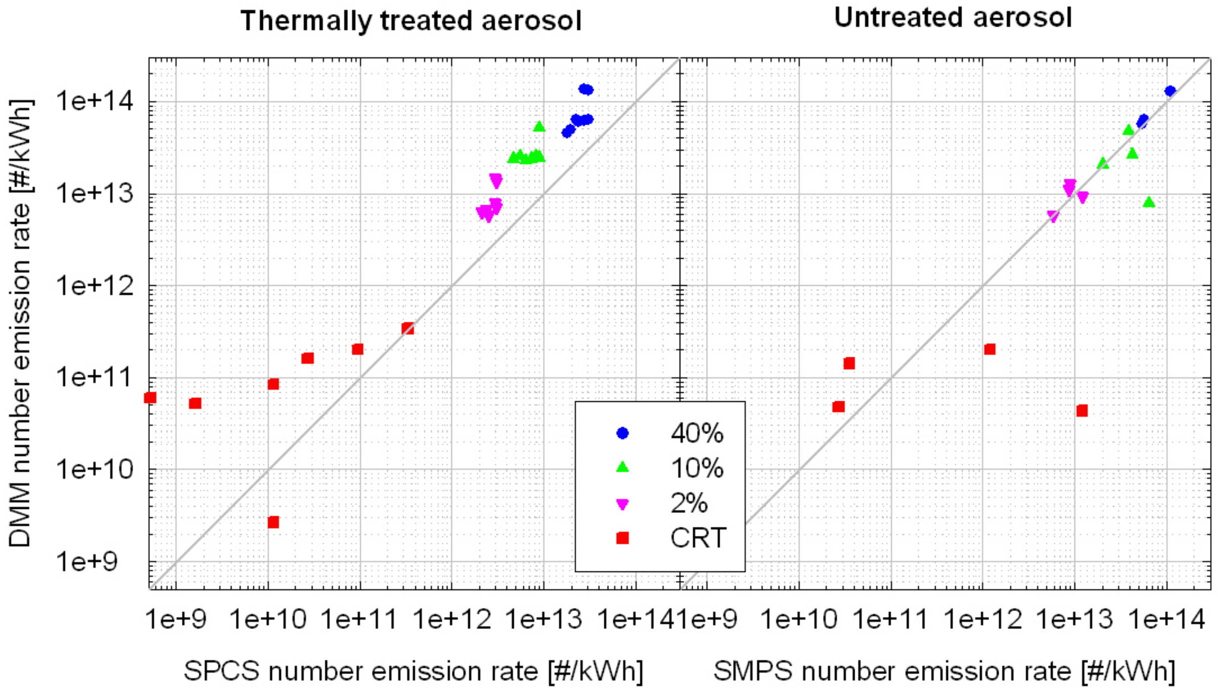

Figure 40: Comparison of the number emission rates measured with the DMM for thermally treated (left panel) and untreated (right panel) aerosol with the SPCS (left panel) and SMPS (right panel) number concentrations.

3.4.4 Impactor overloading problem

The DMM charger and impactors were not cleaned between testing. At the end of the campaign, a visual inspection revealed that the impactors were very dirty. This severe fouling of the impactors is expected to have shifted the impactor collection efficiencies. This is clear when comparing the measured impactor currents over consecutive tests. For example Figure 41 compares the DMM impactor currents (normalized with respect to the total impactor current) over ESC mode 12 at 10% valve opening, measured in three consecutive measurement days. Even, though the DMM was sampling downstream a thermodenuder in the first measurement day, it is clear that the current weighted distribution is shifted towards larger sizes from day to day. The total mass of particles passing through the DMM at 10% valve opening was around ~70 μg/day. During the tests at 40% valve opening (which followed that at 10% valve opening) the daily particle mass sampled from the DMM was ~230 μg. Unfortunately, and since the measurement campaign started with testing at high emission levels exhaust configuration, the overloading of the impactors have affected all DMM tests.

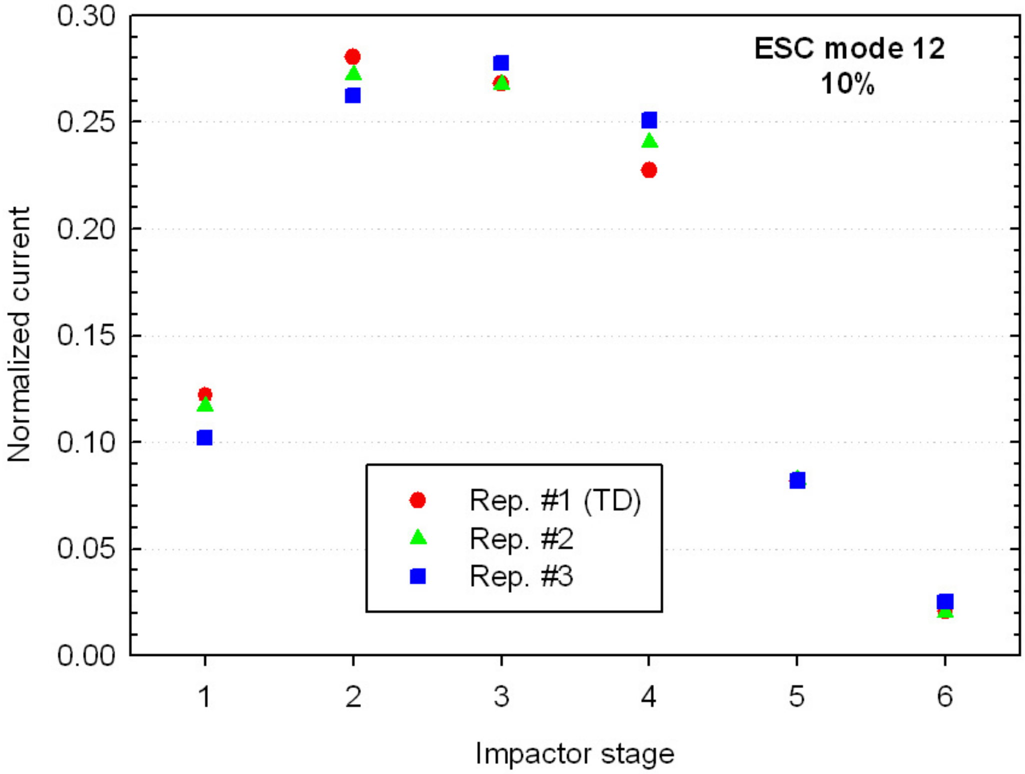

Figure 41: Evolution of the normalized DMM impactor currents over ESC mode 12 in three consecutive measurement days.

3.4.5 Calibration experiments

At the end of the measurement campaign a number of tests were performed aiming at the characterization of the DMM charger efficiency and the DMM mobility and impactor stages collection efficiencies. The DMM was thoroughly cleaned before these experiments. The calibration was performed using spherical PAO particles produced with the setup shown in Figure 12. The results have been corrected for the presence of doubly charged particles by means of appropriate selection of the DMA classified sizes, as described in Maricq et al. (2004). As an additional safety measure, the classified particles were selected from the upper wing of the size distribution.

Figure 42 summarizes the impactor collection efficiency results. Since the DMM does not incorporate a back-up filter, it was not possible to determine the collection efficiency of stage 1. Additionally, it was also not possible to measure the collection efficiency of the last stage due to its relatively large cutoff size (~520 nm aerodynamic diameter). The measured cut-off sizes were generally found to be larger than those suggested by the manufacturer. The cut-off sizes of stages 2, 3, 4 and 5 were determined to be 58, 99.3, 131.5 and 245 nm, respectively, that is 13%, 15%, 15% and 3% higher from the nominal ones.

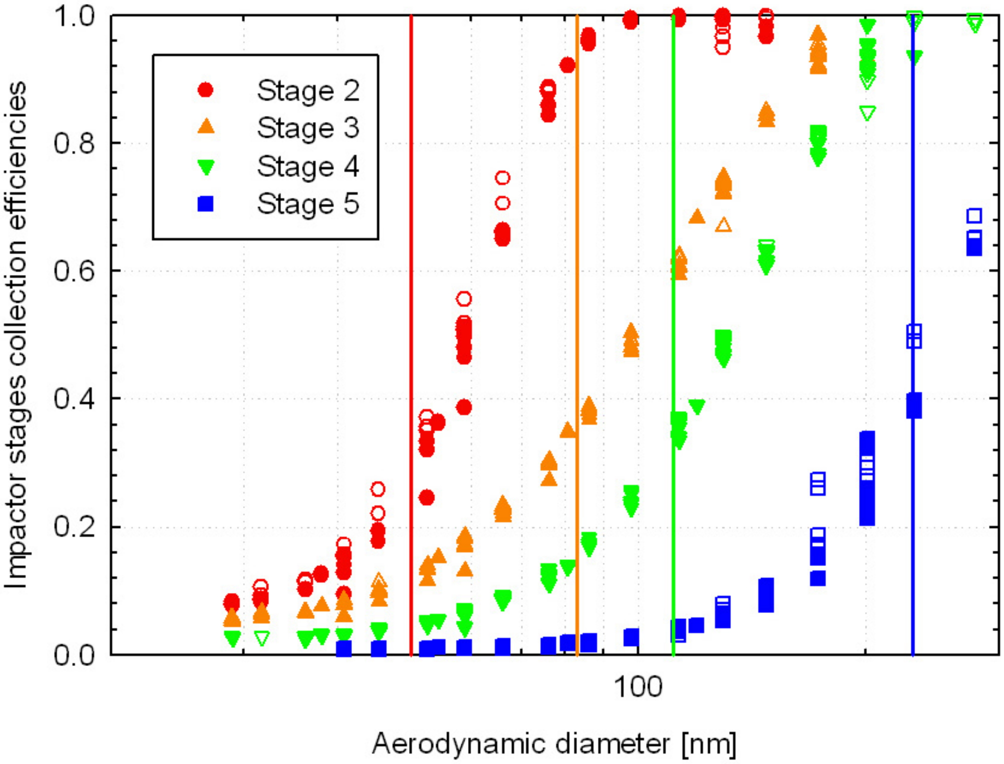

Figure 42: Measured DMM impactor collection efficiency curves. Open symbols correspond to tests in which the DMA classified particles were neutralized. Vertical lines show the nominal 50% cutpoint diameters of the impactors.

The same data set allowed for an calculation of the mobility collection efficiency defined as the ratio of the mobility stage current to the total measured current (impactors plus mobility), after correcting the data for the presence of doubly charged particles. The results of these calculations are shown in Figure 43. At sizes bellow ~50 nm (data shown in red dots) the calculated values strongly depend on the collection efficiency curve of the first impactor as some of these small particles escape collection. An exact determination of the mobility stage collection efficiency is very important for an accurate calculation of the DMM mass emissions. Unfortunately, the collection efficiency curve employed in the DMM software was not available so it was not possible to examine its accuracy.

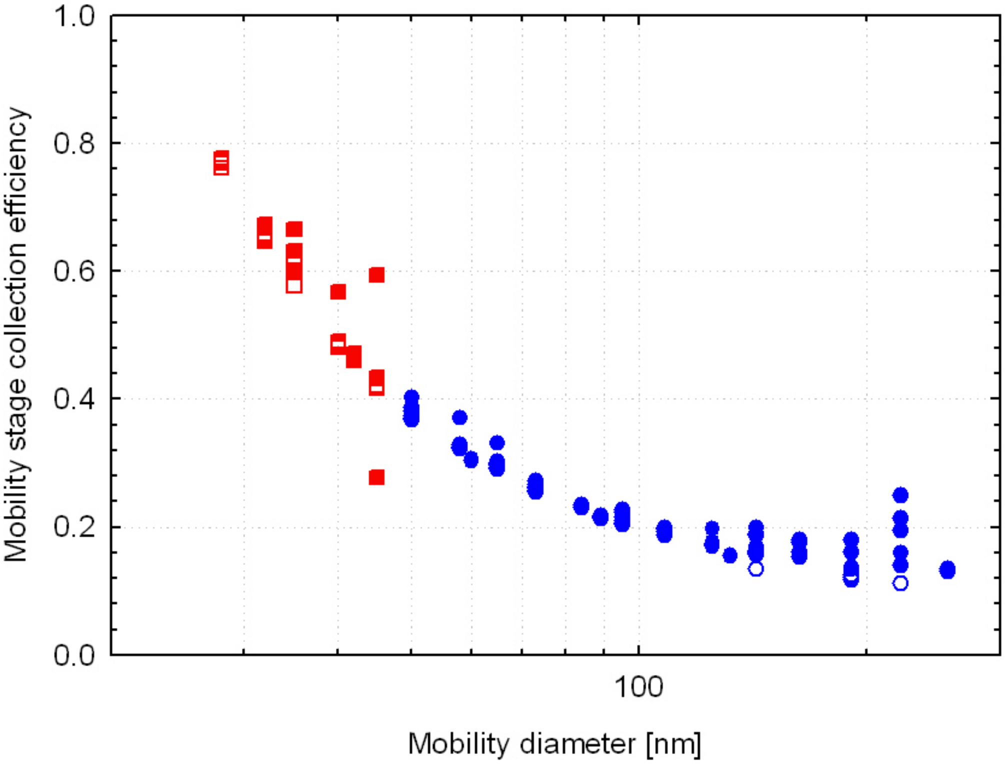

Figure 43: Measured collection efficiencies of the DMM mobility stage.

The particle number concentration is related to the measured currents through the DMM charger efficiency. Therefore, an accurate calculation of the number and thus mass concentrations also requires an accurate characterization of the charger efficiency. The measured charger efficiencies are plotted against the mobility diameter in Figure 44. It can be seen that the measured charger efficiencies were systematically higher (by ~17%) from what suggested by Dekati. This underestimation is translated to a 17 overestimation of the number and mass concentrations. Again, there are some uncertainties for the measured charger efficiency at sizes below 50 nm as the collection efficiency of impactor stage 1 was unknown.

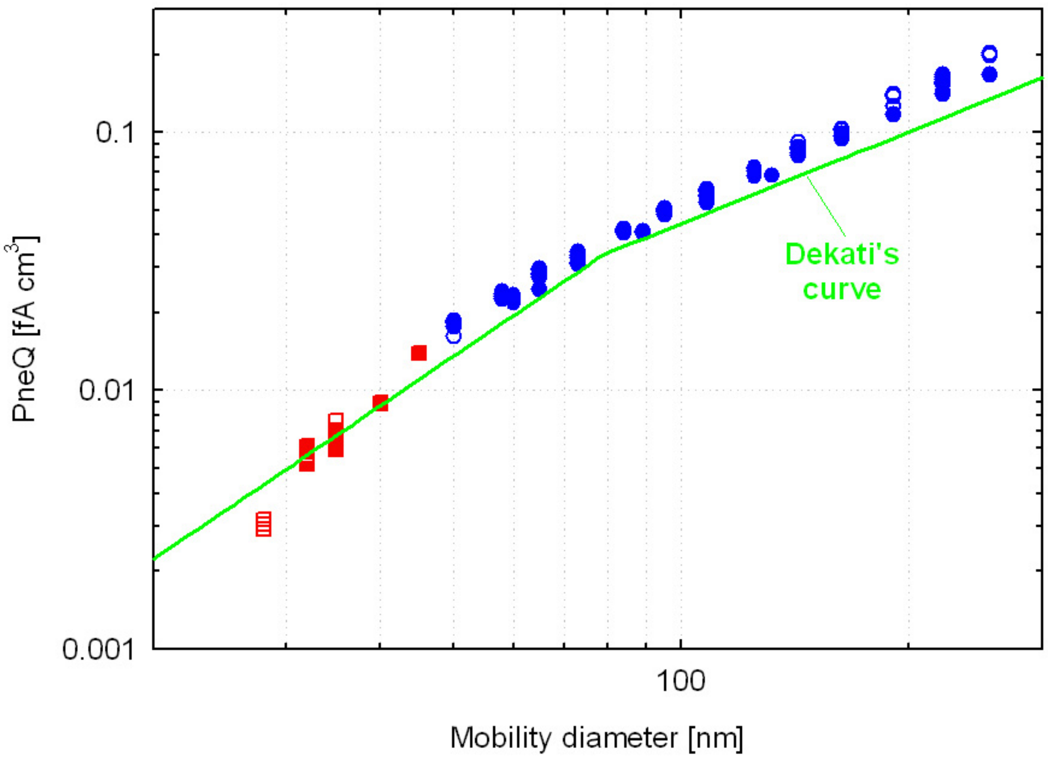

Figure 44: Measured DMM charger efficiencies.

3.5 OBS

3.5.1 PM results

The PM emissions as determined with the OBS system are compared to those determined from the CVS tunnel and the reference partial flow system (SPC) in Figure 45. Generally a very good agreement was observed over the whole range of emission levels examined. When TX40 filters were employed, the average difference from the CVS tunnel results ranged from 3% (±28%) at 40% valve opening, to -10% (±3%) at 10% valve opening, -36% (±19%) at 2% valve opening and -6% (±7%) at CRT out levels. The corresponding figures when Teflo filters were employed were -17% (±16%) at 40% valve opening and 11% (±15%) at 10% valve opening. At lower emission levels, the mass collected on the Teflo filters was very low while some times negative masses were determined leading in relatively larger differences. The single positive data pair at 2% valve opening suggested a 71% difference.

A generally good agreement was also observed between the PM emissions determined with the OBS and the SPC systems. The difference, when TX40 filters were employed, ranged from 45% (±16%) at 40% valve opening, to 18% (±30%) at 10% valve opening, -17% (±24%) at 2% valve opening and -20% (±30%) at CRT out levels. When Teflo filters were employed, the difference was 35% (±34%) ate 40% valve opening and 18% (±30%) at 10% valve opening.

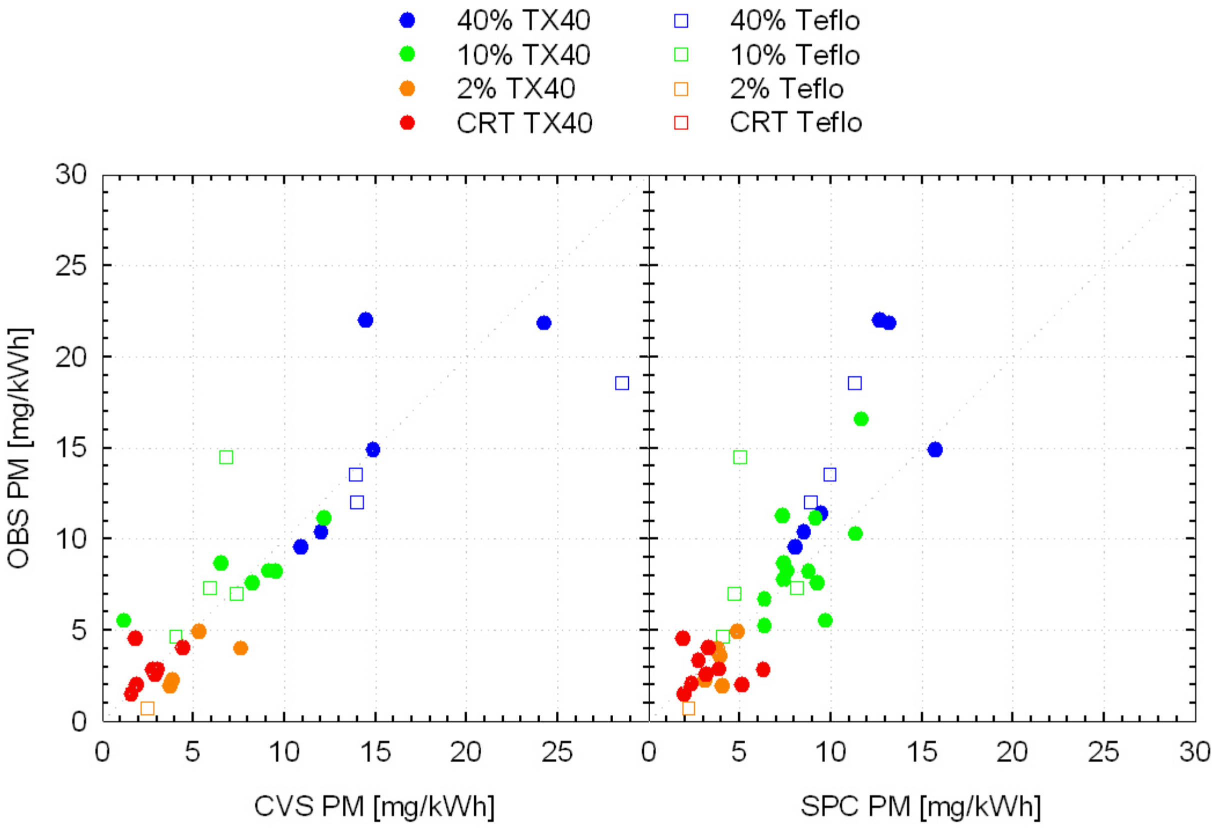

Figure 45: Comparison of the PM emissions measured with the OBS system to those determined from the CVS tunnel (left-side panel) and the SPC (right side panel).

3.5.2 Comparison of the DCS length to the length calculated from the SMPS distributions

The DCS employed in the OBS system has a nominal charging efficiency that is proportional to the mobility diameter (Jung et al. 2005). Therefore the measured current is proportional to the total length of the sampled aerosol. The OBS software directly outputs the calculated length of the sample aerosol. The use of the SMPS over steady states allowed for an accurate calculation of the total aerosol length. Figure 46 compares the lengths determined with these two instruments over all steady states.

It can be seen that the DCS yielded systematically lower particle length emissions over all exhaust aftertreatment configurations examined. On average the OBS gave 50% (±8%) lower total aerosol lengths per kWh at 40%, 10% and 2% valve opening. As it will be shown in the next section, this systematic difference is associated with a malfunction of the corona charger which was found to produce significantly lower ion concentrations.

At CRT out levels the correlation was not so good with the individual differences ranging from 3% to -99%. At these low emission levels a large and unstable nucleation mode was observed (Figure 16). These nucleation mode particles are known to have a strong and nonlinear dependence on the sampling parameters, mainly dilution ratio, dilution temperature, residence time and relative humidity of the dilution air (Mathis U. 2004). Therefore, small differences at the realization of the dilution conditions on the OBS and the CVS tunnel can have a pronounced effect on the length of the nucleation mode particles. This could explain the increased variability at those particular emission levels.

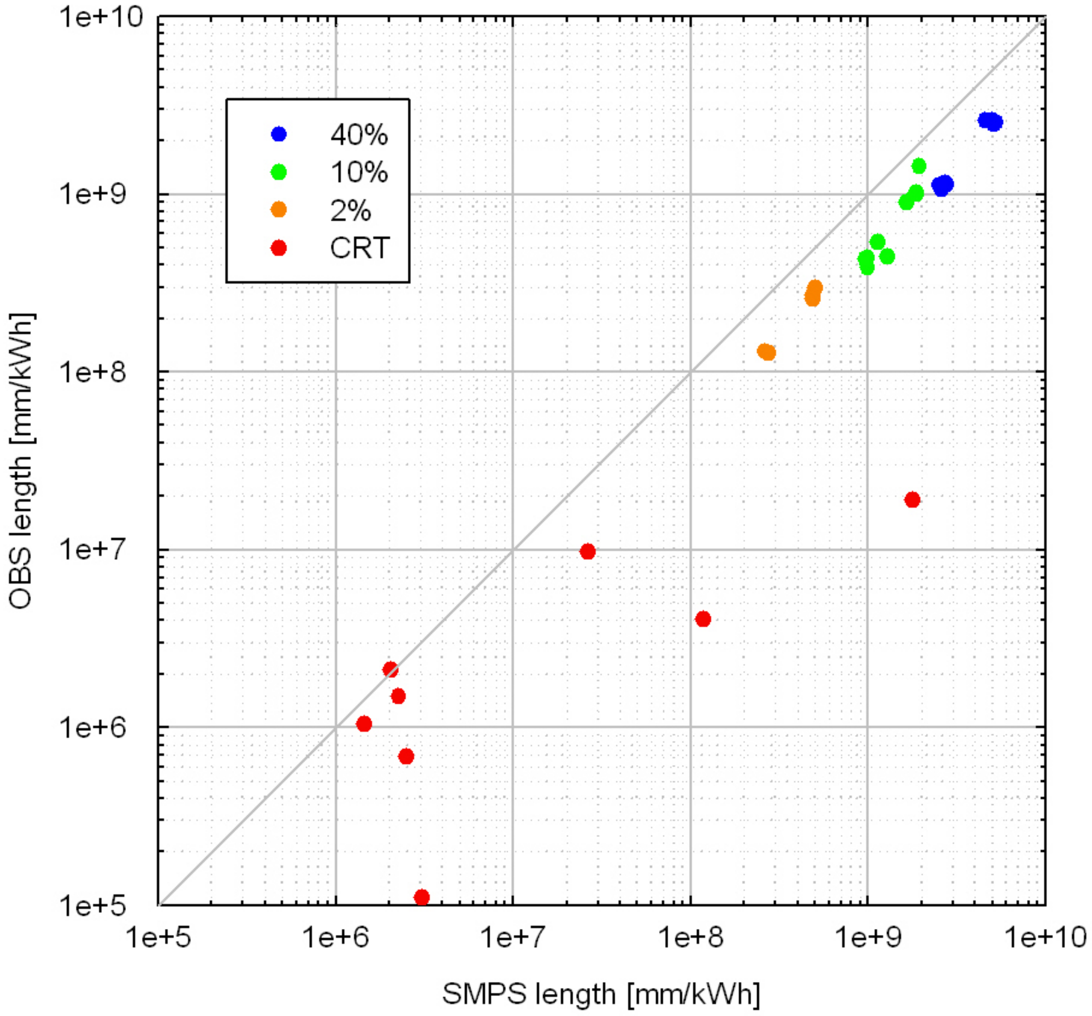

Figure 46: Comparison of the total aerosol length measured with the OBS to that calculated from the SMPS distributions over all steady state tests.

3.6 DCS CALIBRATION WITH PAO DROPLETS

In order to investigate the reason for the systematic differences observed between the DCS and the SMPS results a number of tests were performed aiming at the characterization of the corona charger efficiency. Mono-disperse PAO particles were produced for this purpose using the setup illustrated in Figure 12. All particles classified in the DMA are positively charged. Diesel exhaust soot particles however are known to follow a Boltzman charge distribution while nucleation mode particles carry even less charges (Maricq M 2006). In order to investigate the effect of particle charging state, some tests were performed employing a neutralizer downstream the DMA (that would bring the classified aerosol to a charging state similar to that of diesel aerosol), which in some tests was replaced by a neutralizer stage replica carrying no radioactive source. The presence of multiply charged particles was accounted for by means of appropriate selection of the classified particle sizes following the procedure described in Annex C (section C.3).

The results of these charging efficiency experiments are summarized in Figure 47. The calculated charging efficiencies were found to be well bellow (~75% lower) the instrument specifications. The most possible explanation for this difference is fouling of the needle that affected the ion production. This was verified in some checks suggested by the manufacturer in which the ion trap was switched off and the current measured was found to be ~20 pA. A properly working charger should produce a current around 40 and 60 pA. The deterioration of the charger efficiency is inline with the differences observed between the total particle lengths measured with the DCS and the SMPS.

The relatively large variability in the calculated charger efficiencies does not allow for an accurate determination of the slope of the curve. Focusing on the neutralizer monodisperse aerosol tests, it seems that the lower production of ions have not affected the slope of the charger efficiency. It is therefore expected that the DCS signal was still proportional to the total length but with a lower proportionality constant.

The tests conducted without neutralizing the classified particles resulted in higher charger efficiencies for mobility diameters below 100 nm. At these sizes, the charging efficiency of the corona charger was less than 1, i.e. less than the charge already carried by the particles. Since the charger employed is a unipolar charger producing positive ions it was not possible to effectively reduce the charging state of these small particles.

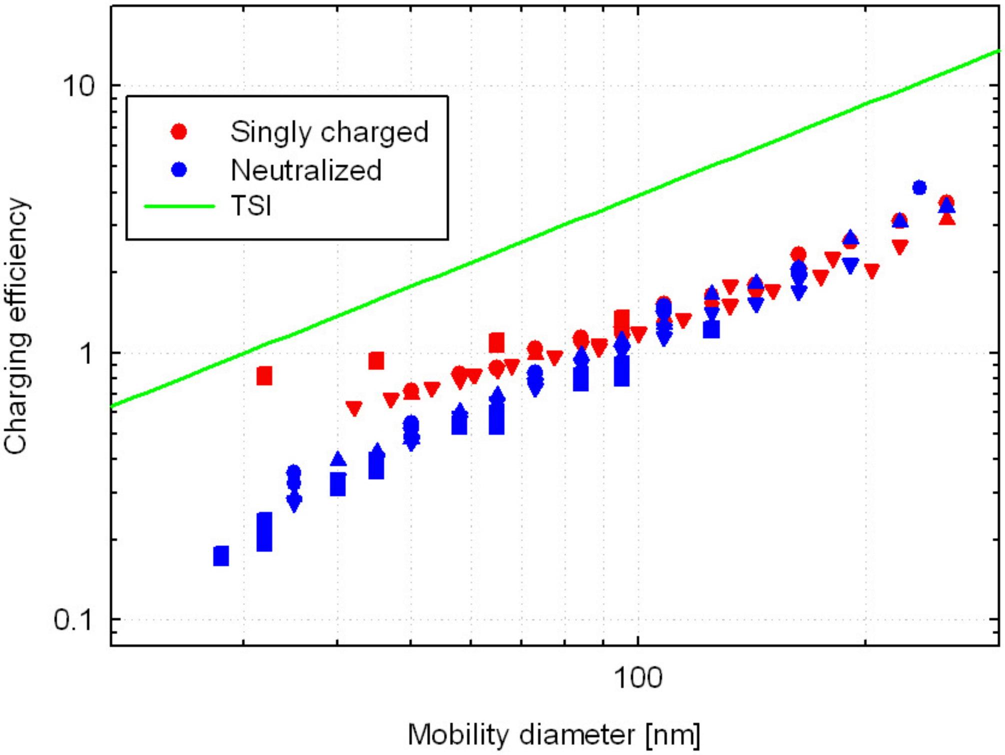

Figure 47: Measured charging efficiencies of the DCS-100 unit. Results obtained with or without neutralizing the DMA classified aerosol are shown with blue and red dots, respectively. The charging efficiency determined by the manufacturer is also shown as a green line.

3.7 THEORETICAL INVESTIGATIONS

The nominal charger efficiency of the DCS is proportional to the mobility diameter raised to the power of 1.13 (Jung et al. 2005). This was verified by the calibration experiments described in the previous section. Since the DCS is intended to monitor the evolution of particle mass over the PM sampling period it is important to investigate how the DCS signal correlates to the mass of airborne particles which can be calculated according to equation 3.

The current measured by the DCS is related to the underlying size distribution through equation:

$$I = \int_0^{\infty} Pn(d_B) eQN(d_B) dd_B \tag{4}$$

Where, Pn is the charger efficiency, e is the elementary charge, Q is the sample flowrate and N is the number weighted mobility size distribution.

Again under the assumption that the exhaust aerosol is lognormally distributed, equation 4 has an explicit solution:

$$I = eQAN_0 d_g^C e^{\frac{C^2(\ln \sigma_g)^2}{2}} \tag{5}$$

Where A and C are the fitted parameters to the charger efficiency curve:

$$Pn = Ad_B^C \tag{6}$$

Dividing equations 3 and 5 yields:

$$\frac{m}{I} = \frac{\pi \rho_0 d_0^{(3-DF)}}{6eQA} d_g^{DF-C} e^{\frac{\ln(\sigma_g)^2}{2}(DF^2 - C^2)} \tag{7}$$

An examination of Equation 7 indicates that in general the DCS response is not proportional to mass. Any fluctuations of the effective particle density can not be detected by the DCS. However this is not really expected to have a significant effect on the results as there exist several studies suggesting that the effective particle density is little affected by the engine operating conditions (e.g. Figure 18).

However, and since C is 1.13 while DF is around 2.3 (for soot particles), the DCS shows a different dependence on the geometric mean diameter and the geometric standard deviation of the size distribution. In that respect, any changes in the size distribution during the measurement period will have a different effect on the mass and the DCS response traces. As an example, Figure 48 shows the real time variation of the geometric mean diameter over WHTC cold at 40% valve opening as determined from the 4 DMA-CPC traces at different DMA voltages (section 3.1.6). Combining this info with the solid particle number emission rates measured with the SPCS, provided the means of calculating the cumulative number, mass and DCS charger traces over the cycle, which are also shown in Figure 48. For the calculation of mass emission rates, a geometric standard deviation of 2.05 and a fractal like structure completely specified by a fractal dimension of 2.3 and an effective particle density of 1 g/cm^3 at 50 nm (which corresponds to the best fit of the experimental data presented in Figure 18) were employed. The cumulative current trace is found to lack behind the cumulative mass trace. This is associated to the gradual increase of the geometric mean diameter (as the engine heats up) during the cycle resulting in a relatively larger increase of mass over the last part of the cycle. The difference between the cumulative current and mass traces was on average 10% reaching a maximum value of 33%.

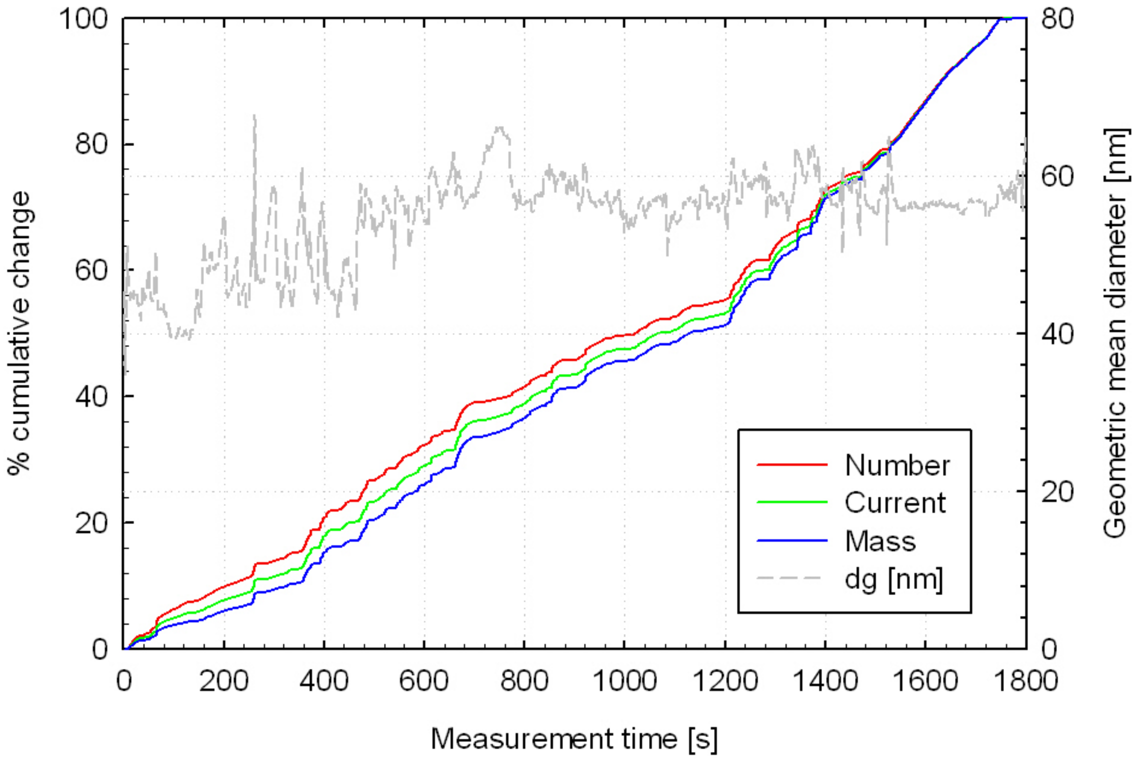

Figure 48: Calculated differences in the cumulative number, mass and DCS current traces over WHTC cold due to the real time variation of the geometric mean diameter.

The different dependence of the DCS current and airborne particle mass on the particle size also raises questions regarding the sensitivity of the DCS signal to the presence of nucleation mode particles which due to their small size have a negligible contribution to mass. For example, Figure 49 (top panel) compares the DCS and the SPCS responses over an ESC mode 12 test at 10% valve opening where an unstable nucleation mode was observed. At the start of the test a large nucleation mode was detected peaking at a size below 7.6 nm (which is the lowest size range at the SMPS configuration employed), which was then gradually decreasing (bottom panel of Figure 49). On the other hand the accumulation mode was found to be very stable during the test. The contribution of this nucleation mode to the airborne particle mass is calculated to be less than 1%, assuming that these are volatile particles of density 1.2 g/cm^3. Even though the presence of these particles does not really affect the mass emissions it had a strong effect on the DCS signal which almost doubled during this nucleation event.

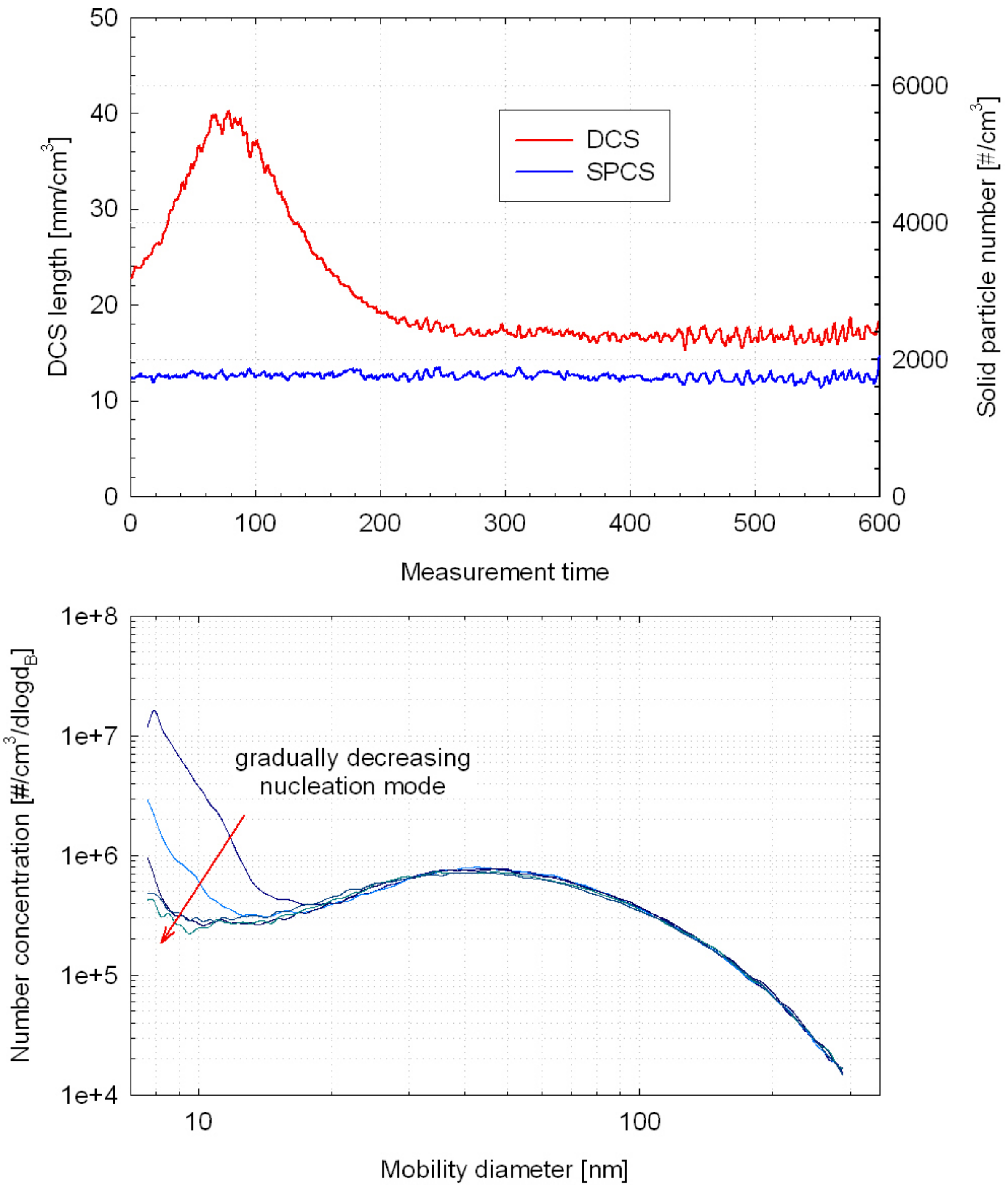

Figure 49: Dependence of the DCS signal in the presence of unstable nucleation mode particles over ESC mode 12 at 10% valve opening.

In the general case of a bimodal size distribution, the DCS response and the airborne particle mass are related to the underlying size distributions through the following equations:

$$I = I_{acc} + I_{nuc} = N_{0,acc} eQAd_{g,acc}^{C} e^{\frac{C^2 \left(\ln \sigma_{g,acc}\right)^2}{2}} + N_{0,nuc} eQAd_{g,nuc}^{C} e^{\frac{C^2 \left(\ln \sigma_{g,nuc}\right)^2}{2}} \qquad 8$$

$$m = m_{acc} + m_{nuc} = N_{0,acc} \frac{\pi}{6} \rho_{0,acc} d_{0,acc}^{(3-DF,acc)} d_{g,acc}^{DF,acc} e^{\frac{DF_{acc}^2 (\ln \sigma_{g,acc})^2}{2}} + N_{0,nuc} \frac{\pi}{6} \rho_{nuc} d_{g,nuc}^3 e^{\frac{9(\ln \sigma_{g,nuc})^2}{2}} \qquad 9$$

Where, $d_{g,acc}$, $\sigma_{g,acc}$, $N_{0,acc}$ and $d_{g,nuc}$, $\sigma_{g,nuc}$, $N_{0,nuc}$ are the geometric mean diameters, the geometric standard deviations and the total number concentrations of the accumulation and nucleation mode, respectively. ρ_{nuc} is the density of the nucleation mode particles which are considered to be spherical while DF_{acc} is the fractal dimension of the accumulation mode particles which further have an effective particle density of $\rho_{0,acc}$ at $d_{0,acc}$. It can be shown that:\

$$\frac{\frac{I_{nuc}}{I_{acc}}}{\frac{m_{nuc}}{m_{acc}}} = \frac{\rho_{0,acc}}{\rho_{nuc}} d_{0,acc}^{(3-DF_{acc})} \frac{d_{g,acc}^{(DF_{acc}-C)}}{d_{g,nuc}^{(3-C)}} \frac{e^{\left(\frac{DF_{acc}^2}{2} \ln(\sigma_{g,acc})^2 - \frac{9}{2} \ln(\sigma_{g,nuc})^2\right)}}{e^{\left[\frac{C^2}{2}\left(\ln(\sigma_{g,acc})^2 - \ln(\sigma_{g,nuc})^2\right)\right]}} \qquad 10$$

The above ratio can be considered as indicative of the relative effect that the nucleation mode will have on the DCS current compared to the airborne mass. This ratio was calculated for a range of bimodal distributions and density profiles and was found to mostly depend on the geometric mean diameter of the nucleation mode and (to a lesser extend) of the accumulation mode. The results of those calculations are summarized in Figure 50. It can be seen that the relative difference in the contribution of nucleation mode particles on the mass and DCS current increases as the mean size of nucleation mode particles decreases and as the mean size of the accumulation mode particles decreases. The results of these calculations are also in quantitative agreement with the results presented in Figure 49 suggesting a ratio of ~90 to 360 at a nucleation mode peaking at 5 nm while experimental data suggested a value of ~100.

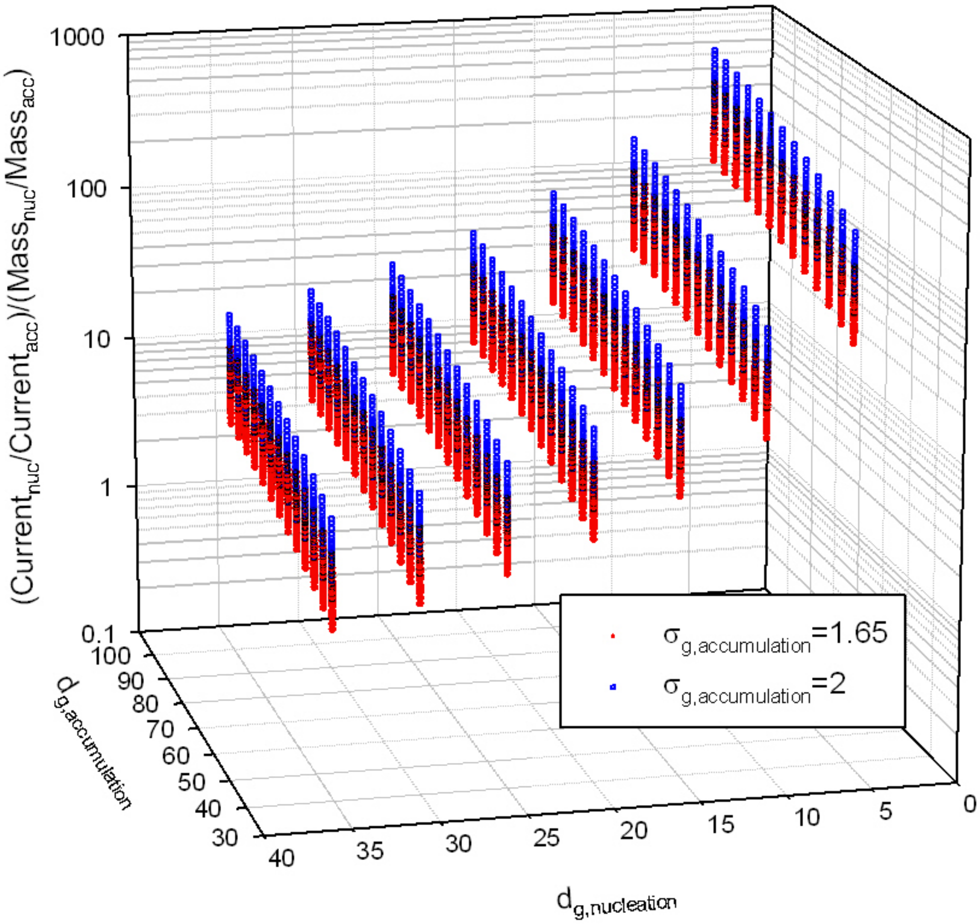

Figure 50: Estimated relative influence of the nucleation mode particle formation on the DCS current and the airborne particle mass.

3.8 M-PSS

3.8.1 PM results

The PM emissions as determined with the m-PSS system are compared to those determined from the CVS tunnel and the reference partial flow system (SPC) in Figure 51. When TX40 filters were employed, the correlation appears to depend on the emission levels. At 40% valve position the mPSS gave systematically lower PM by -32% (±11%) and -9% (±20%) compared to the CVS and SPC samples, respectively. At lower emission levels, the mPSS gave systematically higher PM with the difference from SPC results ranging from 17% (±18%) at 10% valve opening, to 26% (±39%) at 2% valve opening and 44% (±44%) at CRT out levels. The corresponding differences from the CVS results were 16% (±13%), 9% (±35%) and 82% (±40%) at 10% valve opening, 2% valve opening and CRT out levels, respectively.

During the first two tests in which Teflo filters were employed (10% and 40% valve opening) the masses collected on m-PSS were systematically lower than those collected in the SPC (~40% ±20%) and the CVS tunnel (~50% ±15%). An examination of the filters revealed a pattern resembling that of the relatively coarse support grid suggesting non uniform deposition on the filter (Figure 52). In the remaining tests, a finer support grid was employed which resulted in much more uniform deposition patterns. However, it is difficult to evaluate the performance of the m-PSS during those tests due the relatively large uncertainty in the Teflo mass results at such very low emission levels (2% valve opening and CRT out levels).

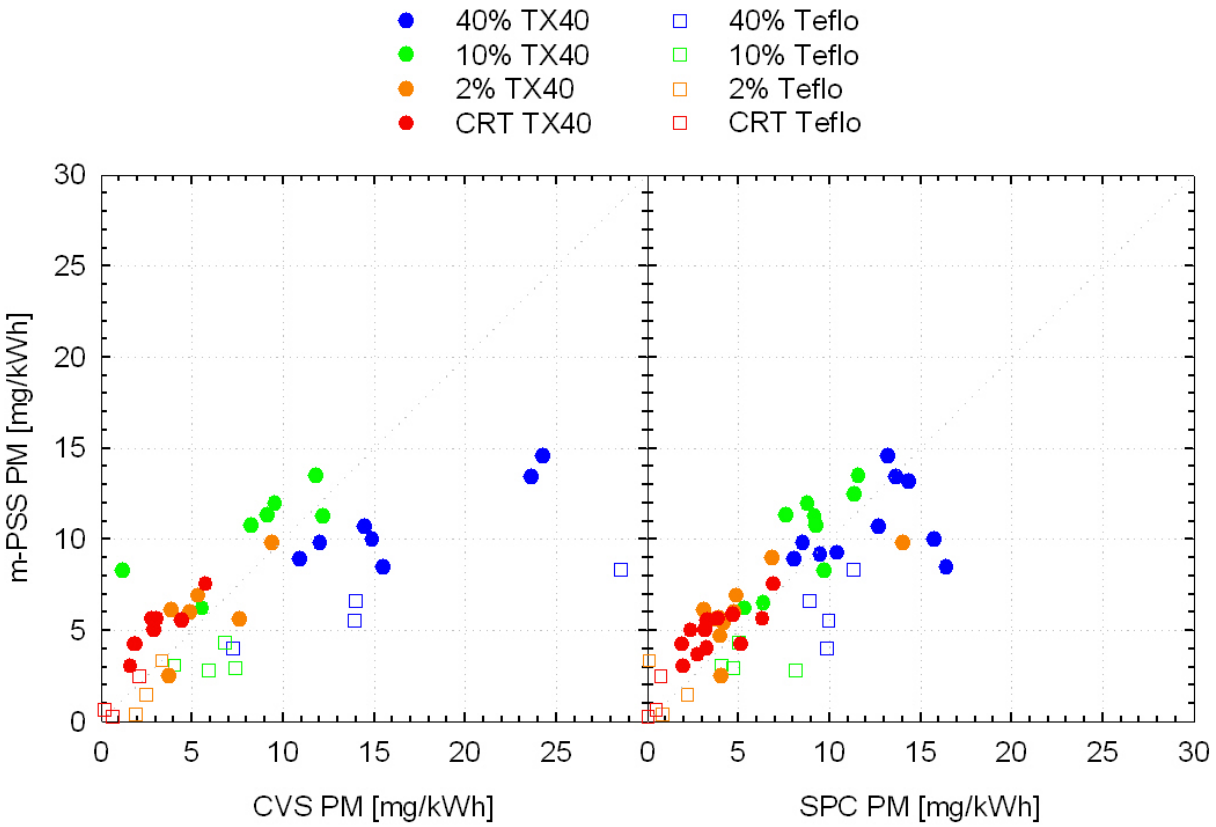

Figure 51: Comparison of the PM emissions measured with the m-PSS system to those determined from the CVS tunnel (left-side panel) and the SPC (right side panel).

Figure 52: Loaded Teflo filter collected from the m-PSS from an ESC 12 test at 10% valve opening.

The m-PSS was the only partial dilution system that was not supplied with conditioned compressed dilution air. The necessary dilution air was taken from ambient and is internally conditioned. The background tests conducted allowed for an evaluation of the conditioning efficiency. Figure 53 compares the filter loadings of m-PSS and SPC during the background tests. Since the same total flowrate and sampling time was employed, the masses are directly comparable. The TX40 results suggest that the mPSS has 150% (±150%) higher PM background. The single background test with Teflo filter when a fine support grid was employed gave similar background levels (~15% higher) suggesting that this background originates from adsorption of gaseous phase material, even though it is difficult to draw a definite conclusion from a single test (given the large uncertainty in the Teflo tests at such low emission levels).

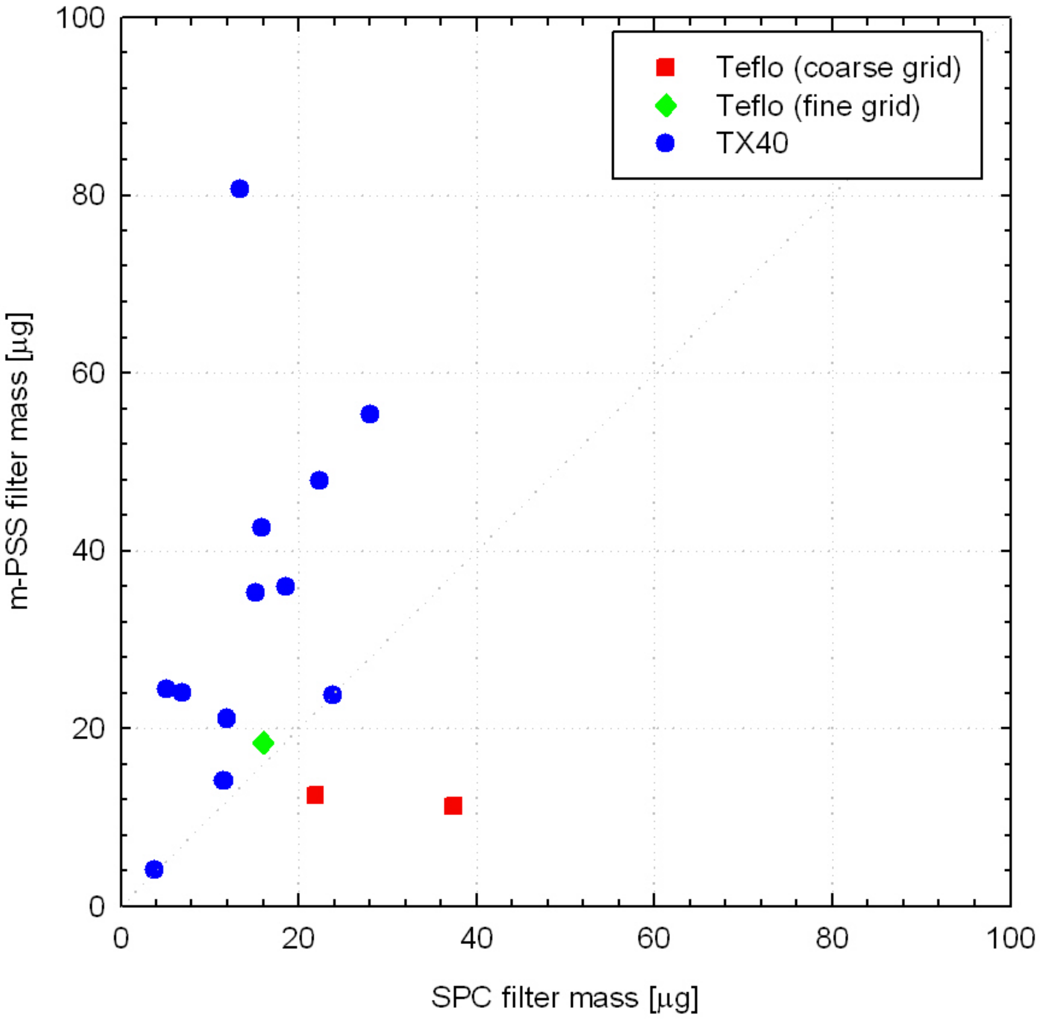

Figure 53: Comparison of the background filter masses collected on the m-PSS and the SPC.

3.8.2 Real time sensor

The m-PSS employed in this campaign incorporated a prototype particle sensor developed by Pegasor for the real time measurement of particle mass. However, the signal provided from the particular sensor was found to significantly drift over time. Figure 54 shows two such example cases. Electrometers are known to be sensitive to temperature fluctuations, but this could not be the case in the particular experiments since special care was taken to heat-up the m-PSS before the start of each test. A dummy filter was installed and the m-PSS was left running in flush mode, until the temperature stabilized to ~47 °C. At that point the pre-weighted test filters were installed and the testing started. Eventually, and after consulting Control Sistem and Pegasor, it was revealed that this was a problem related to the grounding of the sensor. Due to the nature and magnitude of the problem, the particle sensor data were disregarded.

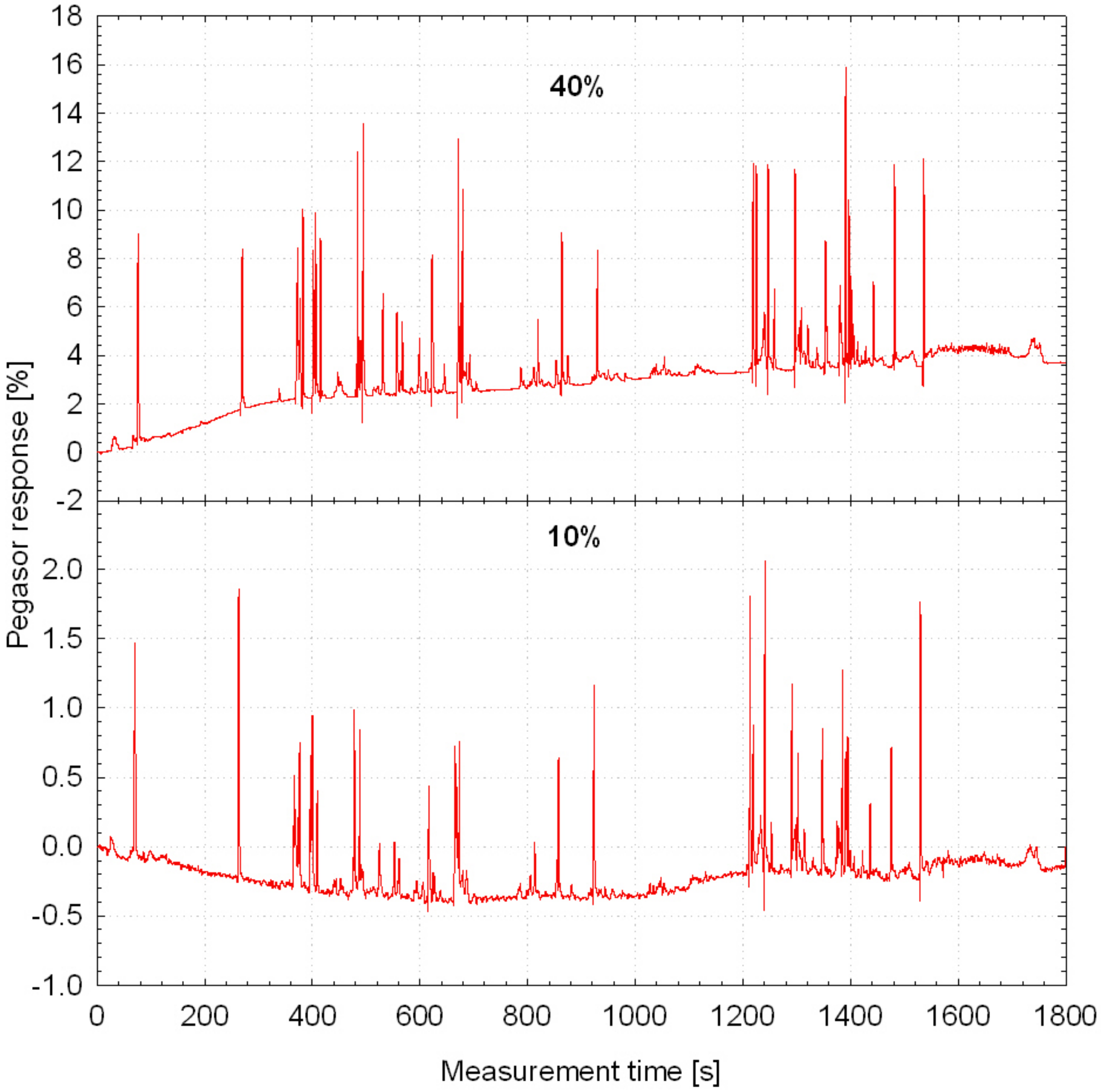

Figure 54: Typical Pegasor responses illustrating the drift of the sensor signal during the test cycle.

4 CONCLUSIONS

This study investigated the performance of five in total candidate PEMS-PM systems at diesel exhaust PM levels spanning from 20 mg/kWh (Euro V) to post CRT. The different emission levels were simulated by means of a CRT/bypass configuration. The PEMS-PM systems evaluated included Horiba's On Board System with Transient PM measurement (OBS-TRPM), AVL's Micro Soot Sensor (MSS) and Gravimetric Filter Box (GFB), Control Sistem's micro Particulate Sampling System (m-PSS), Sensors Portable Particulate Measurement Device (PPMD) and Dekati's Mass Monitor (DMM). This section summarizes the major conclusions of the study.

4.1 NATURE OF PARTICULATE MATTER

The measured PM mass was found to depend on the filter medium employed at these low emission levels with Teflo filters yielding generally lower PM. The differences become more pronounced with decreasing emission levels. Thermo-gravimetric analysis of Quartz fiber filter samples suggested that at CRT-out levels PM consistent entirely of volatile OC. This was also the case at a 2% bypass valve opening where the solid particle number emissions where 2 orders of magnitude higher. This indicates that PM emissions do not scale up with the concentration of soot particles at such low emission levels. Since CRT and DPF systems only control the solid part of the particulate emissions, it is questionable whether the gravimetric procedure will be sensitive enough to identify a malfunction in such aftertreatment devices. This further highlights the importance of incorporating a more sensitive real time sensor in the PEMS-PM system.

All real time sensors responded to a physical property of airborne suspended particles (soot mass concentration, length, or mass). The mass of the airborne solid particles, as calculated by means of combining measured number concentrations and particle size with information on effective particle density from the literature, was found to correlate very well with EC down to CRT out levels. This suggests that PM filter mass contains a significant amount of adsorbed material at these low emission levels.

The PM background was also found to yield filter masses equivalent to those expected from Euro VI technology engines. Almost all of the background was volatile OC but it was not clear whether it originated from the dilution air of desorption of deposited volatile material. The relatively higher background levels measured with only the PEMS system that did not operate on laboratory conditioned dilution air suggests that the conditioning of the dilution air can contribute to this. Further research is needed in order to better understand the origin of background PM.

4.2 PPMD

Based on its operation principle, the QCM is capable of quantifying the mass of both airborne particles and the adsorbed gaseous components of PM. However, relatively large differences were observed between the QCM and the gravimetrically determined masses. To a certain extent this might be associated with different adsorption mechanisms in the Quarts crystals and the different filter media examined (Teflo, Quartz fiber and TX40), which is expected to have significantly contributed to the PM mass at the low emission levels examined.

The most important finding however was relatively large crystal to crystal variability. This had a significant impact on the accuracy of the measurements even at concentration levels of circa 100 μg/m^3 and when PAO droplets were employed. At engine exhaust emission levels below 2% valve opening, the QCM results exhibited a very large scatter yielding some times negative masses (especially over the first half part of the WHTC cycle). It is not clear whether this is attributed to desorption of gaseous material or the sensitivity limits of the QCM. Whatever the case, it seems necessary to use higher sampling times at such low emission levels.

Furthermore, the crystal responses were found to depend strongly on the relative humidity of the by-pass air line with each crystal showing a different dependence. Due to this inherent crystal-to-crystal variability it seems necessary to condition the bypass air line in order to reduce the fluctuations of the relative humidity during the stabilization period of the crystals.

4.3 MSS AND GFB

PM results determined with the GFB were found to be systematically higher from those determined in CVS and SPC, with the actual difference increasing as the emission levels decreased. This is most probably associated with the use of very low sample flowrate (5 lpm) and the significant contribution of adsorbed material at the low emission levels examined. Adsorption of gaseous compounds is not expected to scale up with measurement time and correspondingly the total volume sampled. The much better agreement observed when Teflo filters were employed, verifies that this is mostly related to an adsorption artefact. A plausible way around this inconsistency might be the use of a spacer to effectively reduce the stain area of the filter.

The MSS correlated well with the thermo-gravimetrically determined EC, as expected. The two MSS employed exhibited a very good agreement in all tests with the exception of those at CRT out emission levels, where the two instruments differed by circa 30%. A comparison of the MMS real time traces to estimations of the airborne particle mass (from the particle number measurements) indicated that the MSS has reached its sensitivity limit at CRT out emissions. This was found to be ~0.2 mg/kWh based on measurements of HEPA filtered samples, which translates to around 10^{12} #/kWh. The measured concentrations were found to scale with the inverse of the dilution ratio suggesting a cross sensitivity of the MSS response to some gaseous compounds at these very low levels. Some more work is needed in order to better understand the origin of this kind of interference and if possible improve the sensitivity of the instrument.

4.4 DMM

Unfortunately, it was found that the DMM inlet aerosol concentrations were high enough to result in overloading of the impactors. This affected the collection efficiency curves from the very first measurement day, to an extent that might have affected the results of the DMM. Calibration experiments at the end of the measurement campaign also revealed that the charger efficiency of the DMM charger was underestimated but also errors in the cut-off sizes of the impactors of the order of ~15%. All these are expected to contributed significantly to the observed ~100% overestimation of the mass concentrations and the even larger overestimation of particle number concentrations (~200%). As with all real time sensors examined, particle emissions downstream a CRT were well below the sensitivity of the DMM with the exception of the cold start phase of the WHTC. The detection limit is mainly controlled by the noise levels of the electrometers (~2 fA) which correspond to a mass concentration of ~0.3 ug/m3 and a number concentration of ~300 #/cm^3. When sampling from the CVS this translates to ~0.03 mg/kWh and ~5×10^{10} #/kWh.

4.5 OBS

The OBS system was found to accurately reproduce the PM emissions measured from the CVS and the partial flow tunnel systems at all emission levels examined which spanned from ~15 mg/kWh to CRT out levels.

The DCS however was found to systematically underestimate the actual total aerosol length over all tests. This was found to be related to fouling of the needle that resulted in a reduced production of ions. Calibration tests with PAO droplets showed that this had mainly affected the absolute levels but did not the slope of the charging efficiency. Therefore the instrument responses were still proportional to the total length of the aerosol as also verified by the very good correlation observed between SMPS and DCS results.

The relevance of the DCS signal to the airborne particle mass was also investigated. It was shown that the measured signal is proportional to the geometric mean diameter of the size distribution raised to the power of ~1 while the particle mass is proportional to the geometric mean diameter raised to the power of the fractal dimension which is around 2.3. As size distribution is changing during the cycle, the correlation between the DCS signal and mass also changes.

The most important implication however of this difference in the particle size dependence of the DCS signal and the airborne particle mass, is the increased sensitivity of the DCS response to nucleation mode particles. This was experimentally verified in some ESC 12 tests where an unstable nucleation mode resulted in a twofold increase of the DCS response but had an estimated maximum contribution of less than 1% in the airborne particle mass. It appears to be necessary to thermally treat (e.g. using a thermodenuder or a catalytic stripper) the sample entering the DCS in order to ensure that nucleation mode particles are not present. According to the manufacturer, the use of increased ion trap might also effectively reduce the sensitivity of the instrument to these nucleation mode particles, but this needs to be confirmed experimentally.

The DCS exhibited a very good sensitivity. Again the limit factor is the zero level of the electrometer (~2 fA) which for the size distributions measured with the particular engine is in the order of 0.01 mg/kWh or 10^{10} #/kWh.

4.6 M-PSS

A reasonable agreement was observed between the PM emissions determined with the mPSS and those measured in the CVS tunnel and the SPC, when TX40 filters were employed. The relatively coarse support grid employed however, appeared to have resulted in a non-uniform deposition of particles on Teflo filters resulting in significantly lower PM results. The background PM levels were also found to be systematically higher from those on the CVS and SPC suggesting that a more efficient conditioning of the dilution air is required.

The response of particle sensor employed showed significant drifts during the measurements which were attributed to grounding problems. Due to this unstable behaviour it was not possible to evaluate the sensor.

5 LIST OF SPECIAL TERMS AND ABBREVIATIONS

ACEA	European Automobile Manufacturers Association
CD	Cold Diluter
CO_2	Carbon Dioxide
CPC	Condensation Particle Counter
CRT	Continuously Regenerating Trap
CVS	Constant Volume Sampler
DCS	Diffusion Charge Sensor
DMA	Differential Mobility Analyzer
DMM	Dekati Mass Monitor
DPF	Diesel Particulate Filter
EC	Elemental Carbon
ESC	European Stationary Cycle
ET	Evapouration Tube
GFB	Gravimetric Filter Box
HD	Hot Diluter
HEPA	High Efficiency Particulate Air
JRC	Joint Research Centre
LAM	Laser Aerosol Monitor
MAW	Moving Average Window
m-PSS	Micro Particulate Sampling System
MFC	Mass Flow Controller
MPS	Micro Proportional Sampling system
MSS	Micro Soot Sensor
NTE	Not To Exceed
OBS	On Board System
PAO	Poly(alpha)-olephin

PCRF	Particle Concentration Reduction Factor
PEMS	Portable Emissions Measurement System
PM	Particulate Matter
PMP	Particle Measurement Programme
PN	Particle Number
PPFS	Proportional Partial Flow Sampling
PPMD	Portable Particulate Measurement Device
PSS	Pegasor Particle Sensor
SCR	Selective Catalytic Reduction
SMPS	Scanning Mobility Particle Sizer
SPC	AVL’s Smart Sampler
SPCS	Solid Particle Counting System
TC	Total Carbon
TD	ThermoDenuder
TRPM	TRansient PM measurement

6 REFERENCES

Andersson J., Mamakos A., Giechaskiel B., Carriero M. and Martini G. “Particle Measurement Programme (PMP) Heavy duty Inter-laboratory Correlation Exercise (ILCE_HD) Final Report.”. JRC Report, 2010, EUR 24561 EN – 2010.

Birch M. E. and Cary R. A. "Elemental Carbon-Based Method for Monitoring Occupational Exposures to Particulate Diesel Exhaust." Aerosol Science and Technology, 1996, 25, 221-241.

Bonnel P., Carriero M., Forni F., Alessandrini S., Montigny F., Demircioglu H. and Giechaskiel B. “EU-PEMS PM Evaluation Program – First Report.” JRC Report, 2010, EUR 24543 EN – 2010.

Braun A., Huggins F. E., Seifert S., Ilavsky J., Shah N., Kelly K. E., Sarofim A. and Huffman G. P. “Size-Range Analysis of Diesel Soot with Ultra-Small Angle X-ray Scattering.” Combustion and Flame, 2004, 137, 63-72.

Chase R. E., Duszkiewicz G. J., Richert J. F., Lewis D., Maricq M. M. and Xu N. “PM Measurement Artefact: Organic Vapour Deposition on Different Filter Media.“ SAE technical papers, 2004, 2004-01-0967.

Frank B. P., Saltiel S., Hogrefe O., Grygas J. and Lala G. G. “Determination of mean particle size using the electrical aerosol detector and the condensation particle counter: Comparison with the scanning mobility particle sizer.” Journal of Aerosol Science, 2008, 39, 19-29.

Giechaskiel B., Carriero M., Martini G., Bergmann A., Pongratz H. and Jörgl H. “Comparison of Particle Number Measurements from the Full Dilution Tunnel, the Tailpipe and Two Partial Flow Systems”. SAE technical papers, 2010, 10 PFL-0114.

Giechaskiel B., Alessandrini S., Forni F., Martinez-Lozano P., Leseur D., Carriero M. And Martini G. “Particle Measurement Programme (PMP) Heavy-Duty (HD) Interlaboratory Exercise. Exploratory work at JRC (Oct’07 – Feb’08)”. JRC Report, 2008, EUR 23426 EN – 2008.

Giechaskiel B., Wang X., Horn H. G., Spielvogel J., Gerhart C., Southgate J., Jing L., Kasper M., Drossinos Y. and Krasenbrink A. “ Calibration of Condensation Particle Counters for Legislated Vehicle Number Emission Measurements.” Aerosol Science and Technology, 2009, 43, 1164-1173.

Giechaskiel B., Carriero M., Martini G., Krasenbrink A. and Scheder D. “Calibration and Validation of Various Commercial Particle Number Measurement Systems.” SAE technical papers, 2009b, 2009-01-1115.

Giechaskiel B., Carriero M., Bonnel P., Schindler W., Scheder D., Bassoli C. and Niemela V. “Feasibility of Particulate Mass and Number Measurement with Portable Emission Measurement Systems (PEMS) for In-Use Testing. SAE Technical Paper, 2011-01-11ICE-0211

Harris S. J. and Maricq M. M. “Signature Size Distributions for Diesel and Gasoline Engine Exhaust Particulate Matter.” Journal of Aerosol Science, 2001, 32, 749-764.

Hinds W. C. “Aerosol Technology: Properties, Behaviour and Measurement of Airborne Particles.” New York. John Willey & Sons.

Horiuchi M. K., Saito S. and Ichihara S. “The effects of Flow-Through Type Oxidation Catalysts on the Particulate Reduction of 1990’s Diesel Engines.” SAE technical papers, 1990, 900600.

Jung H and Kittelson D. “Characterization of Aerosol Surface Instruments in Transition Regime”. Aerosol Science and Technology, 2005, 39, 902-911.

Kittelson D. E. “Engines and Nanoparticles: A Review”. Journal of Aerosol Science, 1998, 29, 575-588.

Knutson E. O. and Whitby K. T. “Aerosol Classification By Electric Mobility: Apparatus, Theory and Applications.” Journal of Aerosol Science, 1975, 6, 443-451.

Liu W., Osmondson B. L., Bischof O. F. and Sem G. J. “Calibration of Condensation Particle Counters.” SAE technical papers, 2005, 2005-01-0189.

Mader B. T. and Pankow J. F. “Gas/Solid Partitioning of Semivolatile Organic Compounds (SOCs) to Air Filters. 3. An Analysis of Gas Adsorption Artefacts in Measurements of Atmospheric SOCs and Organic Carbon (OC) When Using Teflon Membrane Filters and Quartz Fiber Filters” Environmental Science and Technology, 2001, 35, 3422-3432.

Maricq M. M. and Xu N. “The Effective Density and Fractal Dimension of Soot Particles from Premixed Flames and Motor Vehicle Exhaust.” Journal of Aerosol Science, 2004, 35, 1251-1274.

Maricq M. M. “On the Electrical Charge of Motor Vehicle Exhaust Particles.” Journal of Aerosol Science, 2006, 37, 858-874.

Maricq M. M., Xu N. And Chase R. “Measuring Particulate Mass Emissions with the Electrical Low Pressure Impactor.” Aerosol Science and Technology, 2006b, 40, 68-79.

Mathis U., Kaegi R., Mohr M. and Zenobi R. “TEM analysis of volatile nanoparticles from particle trap equipped diesel and direct-injection spark-ignition vehicles.” Atmospheric Environment 38, 4347-4355.

Mathis U., Ristimäki J., Mohr M., Keskinen J., Ntziachristos L., Samaras Z. and Mikkanen P. “Sampling Conditions for the Measurement of Nucleation Mode Particles in the Exhaust of a Diesel Vehicle.” Aerosol Science and Technology, 2004, 38, 1149 – 1160.

Mathis U., Mohr M., Kaegi R., Bertola A. and Boulouchos K. “Influence of Diesel Engine Combustion Parameters on Primary Soot Particle Diameter.” Environmental Science and Technology, 2005, 39, 1887-1892.

Olfert J.S., Symonds J.P.R. and Collings N. “The effective Density and Fractal Dimension of Particles Emitted from a Light-Duty Diesel Vehicle with a Diesel Oxidation Catalyst.” Journal of Aerosol Science, 2007, 38, 69-82.

Park K., Cao F., Kittelson D. and McMurry P. “Relationship between Particle Mass and Mobility for Diesel Exhaust Particles”. Environmental Science and Technology, 2003, 37, 577-583.

Rubino L., Bonnel P., Carriero M. and Krasenbrink A. “Portable Emission Measurement System (PEMS) For Heavy Duty Diesel Vehicle PM Measurement: The European PM PEMS Program.” SAE Technical Paper, 2009, 2009-24-0149.

Sem J. G. “Design and performance characteristics of three continuous-flow condensation particle counters: a summary.” Atmospheric Research, 2002, 62, 267-294.

Schindler W., Haisch C., Beck H. A., Niessner R., Jacob E., and Rothe D. “A photoacoustic sensor system for time resolved quantification of diesel soot emissions.” SAE technical papers, 2004, 2004-01-0968.

Silvis W., Marek G., Kreft, N. and Schindler W. “Diesel Particulate Measurement with Partial Flow Sampling Systems: A New Probe and Tunnel Design that Correlates with Full Flow Tunnels.” SAE technical papers, 2002, 2002-01-0054.

Symonds J. P.R., Kingsley R. St. J., Olfert J. S., Campbell B. W. and Swift S. J. “Diesel Soot Mass Calculation in Real-Time with a Differential Mobility Spectrometer.” Journal of Aerosol Science 2007, 38, 52-68.

Vaaraslahti K., Ristimäki J., Virtanen A., Keskinen J., Giechaskiel B. and Solla A. ”Effect if Oxidation Catalysts on Diesel Soot Particles.” Environmental Science and Technology, 2006, 40, 4776-4781.

Wang S. C. and Flagan R. C. “Scanning Electrical Mobility Spectrometer.” Journal of Aerosol Science, 1989, 20, 1485-1488.

Wei Q, Akard M., Porter S. and Nakamura H. ”The Effect of Drive Cycles on PM emission Characteristics from Gasoline Vehicle.” SAE technical papers, 2009, 2009-01-1119.

Wiedensohler A. “An Approximation of the Bipolar Charge Distribution for Particles in the Submicron Size Range.” Journal of Aerosol Science, 1987 19, 387-389

ANNEX A: TEST FUEL SPECIFICATIONS

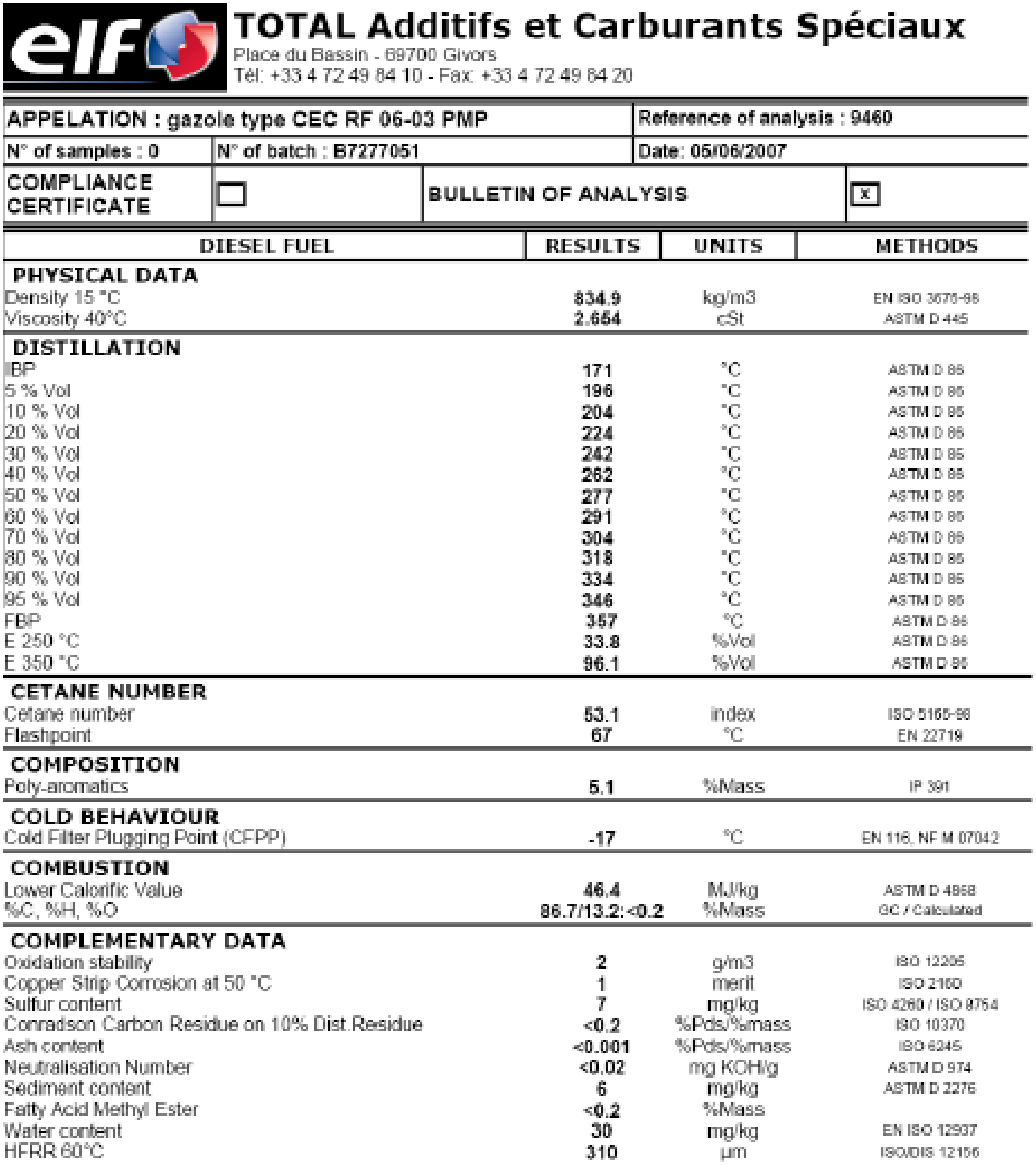

TOTAL Additifs et Carburants Spéciaux
Place du Bassin - 69700 Givors
Tél: +33 4 72 49 84 10 - Fax: +33 4 72 49 84 20

APPELATION : gazole type CEC RF 06-03 PMP		**Reference of analysis : 9460**	
N° of samples : 0	**N° of batch : B7277051**	**Date: 05/06/2007**	
COMPLIANCE CERTIFICATE	☐	**BULLETIN OF ANALYSIS**	☒

DIESEL FUEL	RESULTS	UNITS	METHODS
PHYSICAL DATA			
Density 15 °C	**834.9**	kg/m3	EN ISO 3675-98
Viscosity 40°C	**2.654**	cSt	ASTM D 445
DISTILLATION			
IBP	**171**	°C	ASTM D 86
5 % Vol	**196**	°C	ASTM D 86
10 % Vol	**204**	°C	ASTM D 86
20 % Vol	**224**	°C	ASTM D 86
30 % Vol	**242**	°C	ASTM D 86
40 % Vol	**262**	°C	ASTM D 86
50 % Vol	**277**	°C	ASTM D 86
60 % Vol	**291**	°C	ASTM D 86
70 % Vol	**304**	°C	ASTM D 86
80 % Vol	**318**	°C	ASTM D 86
90 % Vol	**334**	°C	ASTM D 86
95 % Vol	**346**	°C	ASTM D 86
FBP	**357**	°C	ASTM D 86
E 250 °C	**33.8**	%Vol	ASTM D 86
E 350 °C	**96.1**	%Vol	ASTM D 86
CETANE NUMBER			
Cetane number	**53.1**	index	ISO 5165-98
Flashpoint	**67**	°C	EN 22719
COMPOSITION			
Poly-aromatics	**5.1**	%Mass	IP 391
COLD BEHAVIOUR			
Cold Filter Plugging Point (CFPP)	**-17**	°C	EN 116, NF M 07042
COMBUSTION			
Lower Calorific Value	**46.4**	MJ/kg	ASTM D 4868
%C, %H, %O	**86.7/13.2:<0.2**	%Mass	GC / Calculated
COMPLEMENTARY DATA			
Oxidation stability	**2**	g/m3	ISO 12205
Copper Strip Corrosion at 50 °C	**1**	merit	ISO 2160
Sulfur content	**7**	mg/kg	ISO 4260 / ISO 8754
Conradson Carbon Residue on 10% Dist.Residue	**<0.2**	%Pds/%mass	ISO 10370
Ash content	**<0.001**	%Pds/%mass	ISO 6245
Neutralisation Number	**<0.02**	mg KOH/g	ASTM D 974
Sediment content	**6**	mg/kg	ASTM D 2276
Fatty Acid Methyl Ester	**<0.2**	%Mass	
Water content	**30**	mg/kg	EN ISO 12937
HFRR 60°C	**310**	µm	ISO/DIS 12156

ANNEX B: Cyclone cut-points (URG-2000-30EP, 91 lpm 2.5 μm)

Flow Rate [lpm]	*Cut-Point [μm]*
1.0	99.76
3.5	35.84
6.0	23.07
8.5	17.36
11.0	14.06
13.5	11.89
16.0	10.35
18.5	9.19
21.0	8.29
23.5	7.56
26.0	6.96
28.5	6.46
31.0	6.03
33.5	5.66
36.0	5.34
38.5	5.05
41.0	4.80
43.5	4.57
46.0	4.37
48.5	4.18
51.0	4.01

Flow Rate [lpm]	*Cut-Point [μm]*
51.0	4.01
53.5	3.86
56.0	3.72
58.5	3.59
61.0	3.47
63.5	3.36
66.0	3.25
68.5	3.15
71.0	3.06
73.5	2.98
76.0	2.90
78.5	2.82
81.0	2.75
83.5	2.68
86.0	2.62
88.5	2.56
91.0	2.50
93.5	2.45
96.0	2.39
98.5	2.34
101.0	2.30

ANNEX C: CALIBRATION OF THE SMPS

The SMPS unit was employed for the calibration of the PEMS real time instrumentation and the calculation of the mass concentration of airborne particles emitted by the engine. In that respect it is important to verify that it operated according to its specifications. For this purpose, a number of checks have been performed aiming at the investigation of the efficiency of the neutralizer, the accuracy of the size classification and the slope of the 3010 CPC employed for particle detection. These are described in the following paragraphs.

C.1 Charging Efficiency of the Neutralizer

In all engine tests the SMPS was equipped with a 10 years old TSI's 3077 neutralizer utilizing ^{85}Kr as a radioactive source. The activity of the particular neutralizer has dropped to almost half (~1 mCi) its initial level (2 mCi). In order to investigate whether this decrease of the activity has affected the measurements, some comparability tests have been performed with a 10 mCi ^{85}Kr neutralizer manufactured by Eckert and Ziegler GmbH, which was received just after the completion of the engine measurement campaign. The test aerosol was PAO droplets produced with the JRC's homemade PAO generator. The size distribution of the produced aerosol was measured with the SMPS, changing the neutralizer between scans. An initial scan performed without neutralizer showed that the PAO droplets were not charged (CPC indications were at the noise levels (~0.05 #/cm^3) during the scan). The SMPS operated on a sheath flowrate of 3 lpm, a sample flowrate of 0.3 lpm and a scan time of 300 s. The necessary make-up air for the 3010 CPC was provided from the lab's compressed air line through a mass flow controller.

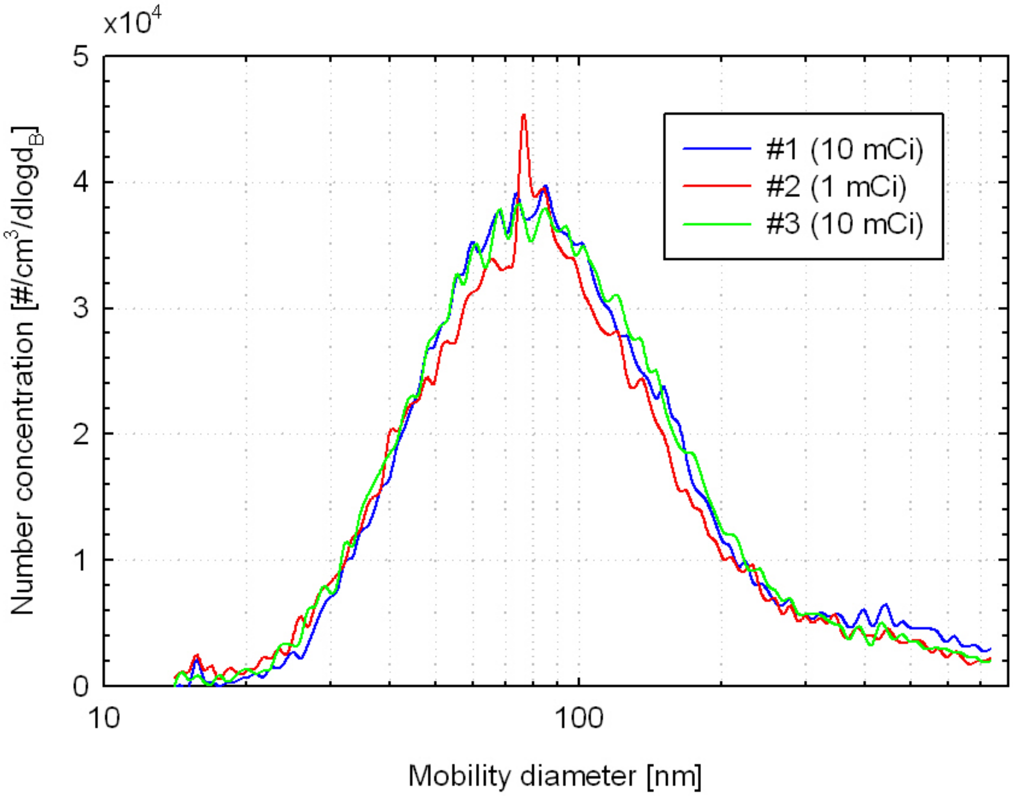

Figure C1: PAO size distributions employing neutralizers having different activity levels. SMPS operated at a sheath over sample flows of 3/0.3 lpm and a scan time of 300 s.

Figure C1 summarizes the results of these tests. No clear differences could be observed. It needs to be stressed here that the particular experiments correspond to a severe condition were the neutralizer is facing a completely uncharged aerosol. Diesel soot particles are known to have a charge distribution close to that achieved in the neutralizer (Maricq M. 2006). It is therefore expected that the 1 mCi activity of the neutralizer employed in the engine tests was sufficient.

C.2 Size Classification in the DMA

Size classification in the SMPS is performed in the DMA column. When the sheath air flow is recirculated (as in the TSI unit used here), the size of the transmitted aerosol depends only on the applied voltage, the employed sheath flowrate and the geometry of the column through the following equation (Knutson et al. 1975):

$$\frac{d_B}{C_C(d_B)} = \frac{2neVL}{3\mu Q_{sh} \ln\left(\frac{r_2}{r_1}\right)} \qquad \text{C1}$$

Where, d_B is the mobility diameter, n is the number of elementary charges carried by the particle, e is the elementary charge (1.6×10^{-19} Coulomb), V is the applied voltage on the DMA column, Q_{sh} is the sheath flowrate, μ is the gas dynamic viscosity, l is the effective length of the DMA while r_1 and r_2 are inner and outer radii of the DMA, respectively. C_C is the slip correction factor (Hinds 1999) which is a function of particle mobility diameter and the gas mean free path (λ):

$$C_C(d_B) = 1 + 2.34\frac{\lambda}{d_B} + 1.05\frac{\lambda}{d_B}\exp\left(-0.39\frac{d_B}{\lambda}\right) \qquad \text{C2}$$

Therefore uncertainties in the geometric characteristics of the DMA, the employed sheath air flowrate and the applied voltage are directly translated to uncertainties in the measured particle size. The accuracy of the DMA unit in terms of classifying aerosol particles was checked with PolyStyrene Latex spherical particles (Thermo Scientific 3500A) having a NIST traceable size of 498±5 nm. An aqueous solution of these PSL particles was prepared by means of adding 10 drops of concentrated suspensions (1% by mass) on 250 ml of purified deionized water (Milli-Q). The diluted PSL suspension was then fed to the CETAC U5000AT+ Ultrasonic Nebulizer. The size distribution of the produced aerosol (which was a mixture of PSL spheres and residual particles from impurities in the water and the surfactant used in the concentrated PSL suspensions to prevent coagulation) was then measured employing the setup shown in Figure C2.

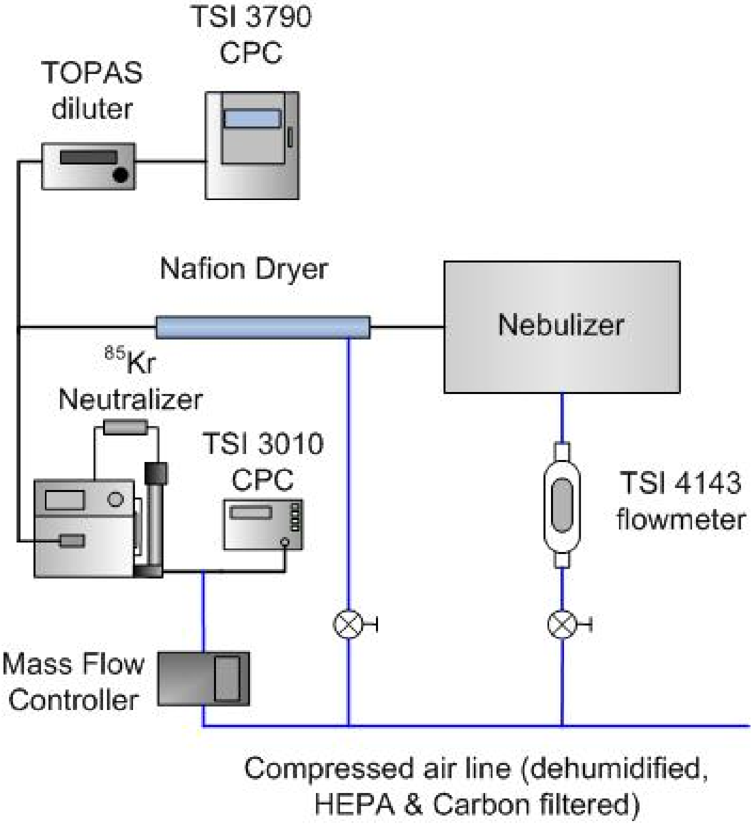

Figure C2: Setup employed for the calibration of the SMPS with PSL particles.

The PSL aerosol produced by the nebulizer first passed through a nafion dryer to further dehumidify the sample. Comparison checks with and without the nafion dryer showed no differences in the recorded size distributions, which suggests that the aerosol was effectively dried in the nebulizer. The number concentration of the produced aerosol was measured with a TSI's 3790 CPC sampling downstream of a TOPAS diluter. At the same time the number weighted mobility size distribution was measured with the TSI's 3936L10 SMPS. The latter operated either in 300 s scanning mode or in voltage step mode by manually controlling the DMA voltage. The sheath and sample flowrates employed in these experiments were 3 and 0.3 lpm. The necessary conditioned make-up air was supplied from the compressed air line through a mass flow controller. The flowrates (SMPS sheath & sample, 3010 CPC and 3790 CPC) were measured before and after the tests with a bubble flowmeter (Gillian Gilibrator-2).

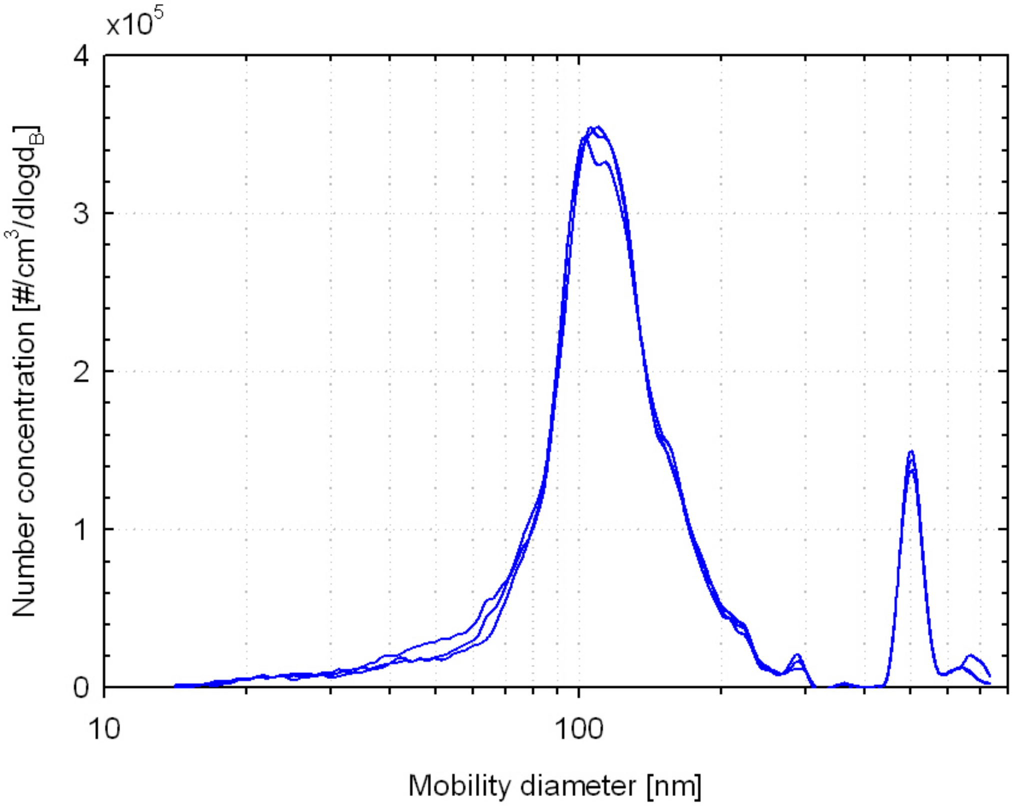

Figure C3: SMPS size distributions of resuspended 498 nm PSL particles.

Figure C3 shows the measured size distributions over three consecutive scans. The narrow peak at 500 nm corresponds to the resuspended PSL particles while the broader distribution peaking at 105 nm corresponds to the residue particles. In order to better quantify the location of the PSL peak, a number of fixed voltages covering the size range 475 to 520 nm were applied in the DMA and the corresponding CPC indications recorded for 120 s. The corresponding upstream concentrations were then calculated employing the formula:

$$N(d_B)\left[\frac{\#}{cm^3 d\log d_B}\right]=\frac{C_{CPC}\left[\frac{\#}{cm^3}\right]}{f^{+1}(d_B)\Omega\eta_{CPC}\eta_{DMA}q_s} \qquad \text{C3}$$

Where C_{CPC} is the last 60 s average of the measured CPC concentration (no coincidence correction was applied as the maximum recorded concentrations was only 330 #/cm^3), $f^{+1}(d_B)$ is the probability that a particle of mobility diameter d_B carries 1 positive charge (Wiedensohler 1987), Ω is the area under the DMA transfer function (Knutson et al. 1975), q_s the flowrate of the extracted aerosol from the DMA while η_{CPC} and η_{DMA} the detection efficiency of the CPC and the particle penetration through the DMA (both assumed to be 1 at these large sizes). The results of these tests are summarized in Figure C4. It can be seen that the midpoint of the PSL distribution lies well within the uncertainty range provided by the PSL manufacturer. It was therefore concluded that the 3081 DMA employed in this campaign is accurately calibrated and no correction was applied in the recovered size distributions.

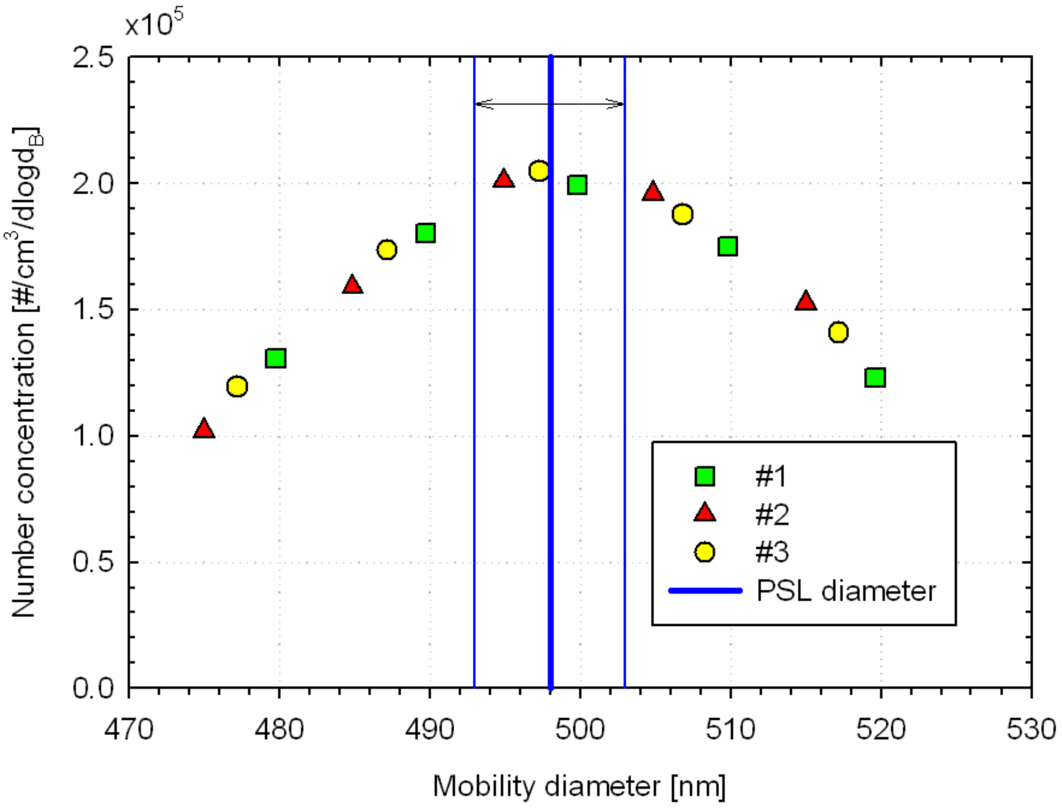

Figure C4: Size distribution of resuspended 498 nm PSL particles over three consecutive DMA voltage steps.

C.3 Slope of the TSI's 3010 CPC employed in the SMPS unit

For an accurate calculation of the SMPS number concentrations it is important to quantify the slope of the employed CPC. This requires comparison of the CPC response to DMA classified monodisperse aerosol to that of a reference CPC or an electrometer (Giechaskiel et al. 2009). The DMM, operating with its charger and mobility stage voltage turned-off, served as a reference electrometer (at the sizes examined, particle losses in the charger – mobility section was found to be minimal). Test were conducted employing the setup shown in Figure 12. In this configuration, the sum of the 6 DMM stage currents corresponds to charge carried by the DMA classified aerosol. This is related to the number concentration through:

$$I_{DMM}[fA] = N[cm^{-3}]e[Cb]Q_{DMM}[lpm]10^{15}\frac{fA}{A}10^{3}\frac{cm^{3}}{dm^{3}}\frac{1\min}{60s} \qquad \text{C4}$$

Where, Q_{DMM} the sample flowrate of the DMM (8.75 lpm). The above equation is strictly valid only when all of the classified particles carry a single positive charge. In practice some multiply charged particles are also transmitted through the DMA most of them being doubly charged. By appropriately selecting the size of the classified aerosol, it is possible to approximately correct for this (Maricq et al. 2004). This approach is based on the assumption that the interference from triply and higher charged particles is negligible compared to that of doubly charged particles. Starting from a given mobility diameter (d_{B0}), the electrical mobility corresponding to particles of that size carrying one charge is calculated.

$$Z = \frac{neC_C}{3\pi\eta d_B} \qquad \text{C5}$$

The mobility diameter (d_{B1}) of a larger doubly charged particle having the same electrical mobility is then calculated. If the concentrations (or current) measured with the particle detector downstream the DMA set at these two sizes is N_0 and N_1, respectively, then the contribution of doubly charged particles on the concentration (or current) of d_{B0} is:

$$N_{doubly,0} = N_1 \frac{f^{+2}(d_{B1})}{f^{+1}(d_{B1})} \qquad \text{C6}$$

Where $f^{+2}(d_{B1})$ and $f^{+1}(d_{B1})$ are the probabilities that particles of size d_{B1} carry 2 and 1 positive charges, respectively. At sufficiently large sizes (d_N), at the right wing of the distribution, this contribution diminishes due to the steep decrease of particle number concentration with increasing size, that is:

$$N_{N-1} >> N_N \frac{f^{+2}(d_{BN})}{f^{+1}(d_{BN})} \qquad \text{C7}$$

At this point it can be assumed that the concentration measured at size $d_{B,N-1}$ corresponds to the desired concentration of singly charged particles. Starting from this point, the concentrations of singly charged particles for all previous sizes can then be calculated using equation C6.

The sizes employed in the particular tests were 45, 58, 84, 125 and 193 nm. The CPC counts were converted to concentrations using the measured sample flowrate (0.96 lpm as determined with the bubble flowmeter) and the empirical coincidence correction formula prvided by the manufacturer, even though the concentrations were below the threshold value of 10000 cm^{-3}. The results of these tests are summarized in Figure C5. Open symbols correspond to the CPC concentrations while solid symbols correspond to the concentrations determined with the electrometers of the DMM impactors. No data is shown at 193 nm as the total DMM impactor current was very close to the noise level. Two tests repetitions were performed, the results of which are shown with different colors/symbols. The results from the large sizes examined suggest an average difference of 0.85±0.03 which is close to the value of 0.88 which has been determined 4 months ago, in some intercalibration tests with the golden CPC units employed in the Heavy Duty PMP validation exercise. The smaller difference (~4%) observed at 45 nm is because the collection efficiency of the last DMM impactor is less than 100% at that size (the cut-off size is ~ 40 nm in aerodynamic scale, i.e. 45 nm in mobility scale given the 0.82 g/cm^3 density of PAO). The 3010 CPC detection efficiency is expected to have reached the peak concentration at this size (Sem 2002).

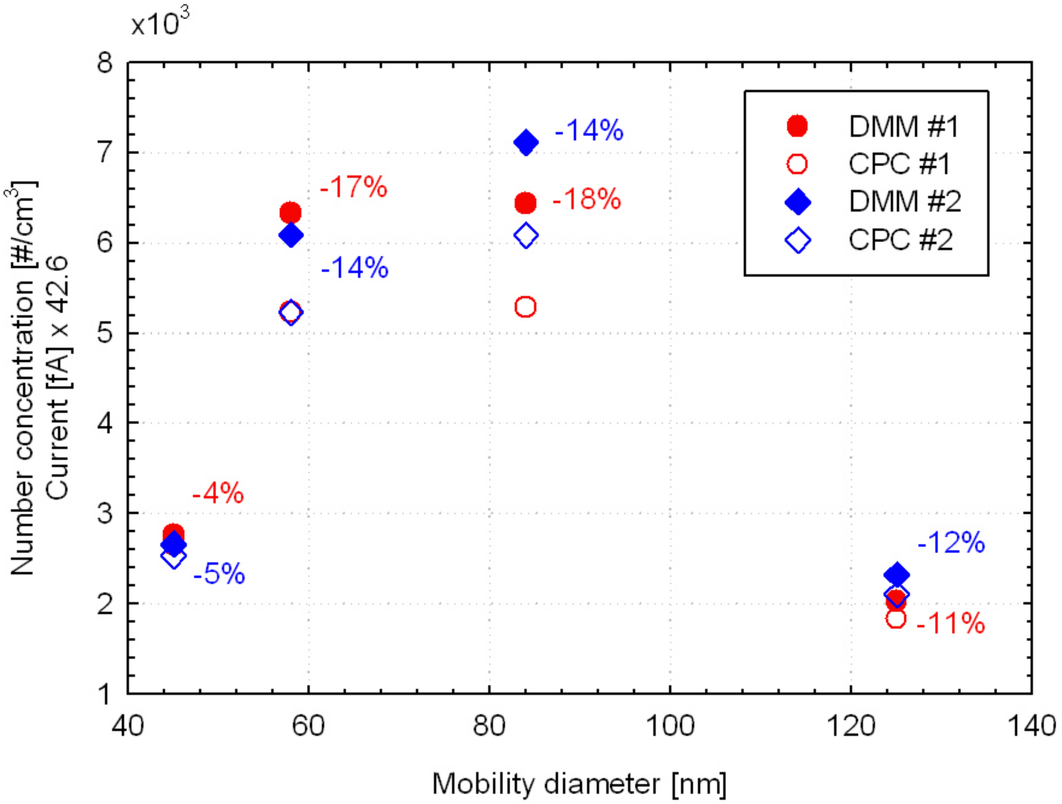

Figure C5: Calibration of the 3010 CPC against the electrometers of the DMM. Open dots illustrate the measured CPC number concentrations while filled dots correspond the number concentrations calculated from the total electrometer current of the DMM. The relative differences are also shown.

European Commission

EUR 24793 EN – Joint Research Centre – Institute for Energy
Title: EU-PEMS PM EVALUATION PROGRAM - Second Report - Study on Post DPF PM/PN Emissions
Author(s): A. Mamakos, M. Carriero, P. Bonnel, H. Demircioglu, K. Douglas, S. Alessandrini, F. Forni, F. Montigny, D. Lesueur
Luxembourg: Publications Office of the European Union
2011 – 96 pp. – 21 x 29.7 cm
EUR – Scientific and Technical Research series - ISSN 1018-5593 (print), ISSN 1831-9424 (online)

ISBN 978-92-79-19931-8 (print)
ISBN 978-92-79-19932-5 (online)

doi:10.2788/95192

Abstract

This study evaluated the performance of five in total candidate PEMS-PM systems at diesel exhaust PM levels spanning from 20 mg/kWh (Euro V) to post CRT. The different emission levels were simulated by means of a CRT/bypass configuration. The PEMS-PM systems evaluated included Horiba's On Board System with Transient PM measurement (OBS-TRPM), AVL's Micro Soot Sensor (MSS) and Gravimetric Filter Box (GFB), Control Sistem's micro Particulate Sampling System (m-PSS), Sensors Portable Particulate Measurement Device (PPMD) and Dekati's Mass Monitor (DMM).

The correlation between the PM results determined with the PEMS instrumentation and that measured with the laboratory sampling systems was found to depend on the filter media employed. This was attributed to adsorption artefacts that become more important as the PM levels decrease. Teflo filters were found to be less susceptible to gas adsorption artefacts, but were difficult to handle yielding some times even negative masses. Even with Teflo filters, however, more than 99% of the PM at CRT out levels was OC which could not be detected by the real time aerosol instrumentation and therefore is expected to be adsorbed material. Furthermore, background PM levels at all candidate systems utilizing laboratory conditioned dilution air averaged at a level equivalent to 3 mg/kWh which is almost 1/3 of the Euro VI level. The background was even higher (equivalent to ~5 mg/kWh) for the PEMS system that employed ambient air (internally conditioned) for the dilution.

The study also evaluated the performance of the real time sensors employed in the different candidate systems using both engine exhaust aerosol and Poly(Alpha)-Olephin spherical particles. The results of these experiments revealed a number of issues related to the calibration of the instruments and cross sensitivities to non PM sources. These findings need to be addressed by the manufacturers as they are expected to significantly affect the accuracy of the measurements in PEMS applications.

How to obtain EU publications

Our priced publications are available from EU Bookshop (http://bookshop.europa.eu), where you can place an order with the sales agent of your choice.

The Publications Office has a worldwide network of sales agents. You can obtain their contact details by sending a fax to (352) 29 29-42758.

The mission of the JRC is to provide customer-driven scientific and technical support for the conception, development, implementation and monitoring of EU policies. As a service of the European Commission, the JRC functions as a reference centre of science and technology for the Union. Close to the policy-making process, it serves the common interest of the Member States, while being independent of special interests, whether private or national.

JRC
EUROPEAN COMMISSION

LB-NA-24793-EN-N

Publications Office

ISBN 978-92-79-19932-5

9 789279 199325